THE UNIVERSITY *of* EDINBURGH

International Master of Science in Fire Safety Engineering

# Experimental Investigation on the Thermal Behaviour of CLT-Steel Hybrid Connection

by

Deonisius Pradipta Aprisa

2023


HOST UNIVERSITY: The University of Edinburgh

FACULTY: College of Science & Engineering

DEPARTMENT: School of Engineering

Academic Year 2022-2023

# Experimental Investigation on the Thermal Behaviour of CLT-Steel Hybrid Connection

Deonisius Pradipta Aprisa

Supervisor: Prof. Luke Bisby

Master thesis submitted in the Erasmus+ Study Programme

**International Master of Science in Fire Safety Engineering**

# Declaration

This master's dissertation is submitted in partial fulfilment of the requirements for the degree of International Master of Science in Fire Safety Engineering (IMFSE). This master's dissertation has never been submitted for any degree or examination to any other University/programme. The author declares that this master's dissertation is original work except where stated. This declaration constitutes an assertion that full and accurate references and citations have been included for all material, directly included and indirectly contributing to the master's dissertation. The author gives permission to make this master's dissertation available for consultation and to copy parts of this master's dissertation for personal use. In the case of any other use, the limitations of the copyright have to be respected, in particular with regard to the obligation to state expressly the source when quoting results from this master's dissertation. The master's dissertation supervisors must be informed when data or results are used.

Read and approved,

*Deonisius Pradipta Aprisa*

11 May 2023

Word Count: 19570 words

This thesis was conducted under the supervision of Prof. Luke Bisby.

# Abstract

As the built environment's carbon footprint becomes increasingly scrutinised, the construction industry is moving towards greener construction methods. One common method is the replacement of conventional building materials with more sustainable materials, such as engineered timber. Cross-laminated timber (CLT) is one of the most common examples of engineered timber in the current market. The partial replacement of conventional materials (such as concrete slab) with CLT panel is called a hybrid solution which allows the construction of larger spans required in mid to high-rise buildings. Presently, knowledge of the thermal behaviour of the hybrid connection is limited. The structural performance of the connection at elevated temperatures depends on the performance of the CLT panel and the steel member, two different materials with distinct behaviours at elevated temperatures.

This study aimed to investigate the thermal behaviour of hybrid CLT-steel connections when exposed to fire condition. The influence of different coverage areas of epoxy intumescent coating as the passive fire protection for the steel beams was also studied to understand the most effective means of utilising it. The epoxy intumescent coating's dry film thickness (DFT) was determined from the manufacturer's data for a fire-resistance rating of 60 minutes and design temperature of 300°C. The interaction between CLT, steel beams, and the intumescent was investigated. To achieve the objectives, 6 test specimens (divided into 3 categories of protection coverage: unprotected, partially-protected, and fully-protected) were exposed to the ISO 834 fire curve for 60 minutes.

The temperatures on the different parts of the CLT panels and the steel beams were measured during the test. The highest temperatures on the CLT panels and the steel beams were observed from the unprotected steel beams. In this case, the unprotected steel flange slightly reduced the char rate on the adjacent CLT panels when compared to the CLT area directly exposed to the fire.

The study demonstrated that the epoxy intumescent coating greatly decreased the heat transferred to the steel beams and prevented charring on the adjacent CLT panels. However, the combustion of the intumescent coating also extended the char formation near the edge of the steel flange. The temperatures of the steel beam, especially on the bottom flange, were higher on the partially-protected steel beams than on the fully-protected steel beams. This is due to the combustion of CLT happening near the unprotected region of the bottom flange, resulting in more heat transferred to the bottom flange. Accordingly, the exposure area on the steel flange also increases as the char shrinks and regresses. While the partial protection couldn't fulfil its design criteria based on the manufacturer's data, the full protection achieved its design criteria.

# Abstrak (Bahasa Indonesia)

Sebagai usaha untuk mengurangi jejak karbon, industri konstruksi berpindah ke metode konstruksi hijau. Salah satu metode yang umum adalah mengganti bahan bangunan konvensional dengan bahan yang lebih ramah lingkungan, seperti *engineered timber*. Salah satu contoh umum *engineered timber* adalah *Cross Laminated Timber (CLT)*. Mengganti sebagian bahan bangunan konvensional dengan *CLT* dapat disebut sebagai solusi campuran. Saat ini, pengetahuan tentang perilaku termis dari koneksi campuran ini masih terbatas. Performa struktural koneksi ini pada kondisi suhu tinggi tergantung pada performa individu *CLT* dan anggota baja, dua bahan berbeda dengan perilaku yang juga berdeda.

Penelitian ini bertujuan untuk meneliti perilaku termis dari koneksi campuran *CLT*-baja dalam paparan api. Pengaruh dari perbedaan cakupan lapisan epoksi *intumescent* pada balok baja juga dipelajari untuk mengetahui cara paling efektif dalam penggunaannya. Ketebalan kering lapisan epoksi *intumescent* ditentukan dari data pabrikan untuk suhu kritis 300°C dan peringkat tahan api selama 60 menit. Interaksi antara *CLT*, balok baja, dan *intumescent* juga diselidiki. Untuk mencapai tujuan ini, 6 spesimen tes (dibagi dalam 3 kategori: tanpa proteksi, perlindungan sebagian, dan perlindungan penuh) dipaparkan pada kurva api ISO 834 selama 60 menit.

Suhu pada berbagai bagian dari panel *CLT* dan balok baja diukur selama tes berlangsung. Suhu tertinggi pada panel *CLT* dan balok baja diukur pada tes dengan balok baja tanpa proteksi. Pada kasus ini, flens baja hanya sedikit memperlambat laju pembentukan arang pada panel *CLT* yang bersebelahan dengan flens baja jika dibandingkan dengan daerah *CLT* yang terpapar api secara langsung.

Penelitian ini menunjukan bahwa lapisan epoksi *intumescent* sangat mampu menurunkan laju perpindahan panas ke balok baja dan mencegah pembentukan arang pada panel *CLT* yang bersebelahan dengan flens baja. Namun, pembakaran pada lapisan *intumescent* memperluas

area pembentukan arang dekat ujung flens baja. Suhu pada balok baja lebih tinggi pada balok baja dengan perlindungan sebagian dibandingkan perlindungan penuh, karena pembakaran dari *CLT* yang terjadi dekat daerah flens baja yang tidak terlindungi, mengakibatkan lebih banyak panas yang berpindah ke flens baja. Lalu, area yang terpapar pada flens baja bertambah ketika lapisan arang menyusut. Ketika perlindungan parsial tidak mampu memenuhi kriteria desainnya berdasarkan data pabrikan, perlindungan penuh terbukti mampu memenuhinya.

# Acknowledgements

First and foremost, I want to thank God for the chance to be here, wrapping up my thesis with this acknowledgement section. IMFSE has been a great 2 years of experience where I got to learn and teach, laugh and cry, find and lose, progress and regress, love and be loved, experience the highs and the lows of life, and most importantly: the opportunity for growth.

This thesis won't be possible without the knowledge and skills I have gained over these past 2 years, so I want to start by thanking every professor and IMFSE staff for the part they have played.

Special credit is dedicated to my thesis supervisors: Prof. Luke Bisby, Dr Ana Sauca, and Dr Ian Pope. It has been an immense pleasure to be able to work on my thesis under their guidance and supervision, which started in the summer of 2022. I began as someone who was super shy and anxious while interacting with my supervisors, the mere thought of a meeting would put me in an anxious state. But, they made sure to take their time with me so I could be comfortable working at my own pace and space. Without the discussions, suggestions, revisions, and meetings, I'm sure that I won't be able to complete this thesis.

I'm also grateful for the help given by Renaud (Stora Enso) and Holly (AkzoNobel) in securing the materials for this study and shaping this study. It was a stressful time to source the materials; however, they have always supported and accommodated our requests. I was lucky to be able to work on my thesis at DBI: where everyone, from my supervisors, Lennart, Alexandru, Poul, and others, was receptive and attentive to me and my thesis from the first time I stepped there until after I returned back to Edinburgh.

To my friends and colleagues in IMFSE: It's been a wild ride, hasn't it? Thank you for making the programme more colourful! Especially to Gizelle, thank you for listening to me and picking IMFSE over other programmes; If you didn't, I'd be stuck without my place to complain and vent my emotions & thoughts. We're a good duo capable of pushing each

other's to new heights, right?

For their unconditional support and love since the beginning of me: My family. Thank you, Ma & Pa, for always putting our education as the highest priority since we were kids. Thank you for the sacrifices and hardships you went through to provide for our family. For my sister: I know that we fought a lot, but I know we fought because we care and love each other. You taught me how to be persistent and genuinely kind to others regardless of the conditions. If the world ends tomorrow, know that the three of you are the loves of my life.

To Harry and Diandra, thank you for always being patient with me, although sometimes I can be painful to deal with. I'll never forget our (broke) trips to London, Barcelona, Copenhagen, and Edinburgh. Thank you for the constant support when I'm sick and especially for going the distance (literally and figuratively) to celebrate my birthday earlier in April. You guys know I'd be an emotional wreck on my birthday if it weren't for both of you. Cheers for future trips!

My friends back in Indonesia: terima kasih atas dukungannya selama ini! Sampai jumpa sebentar lagi, kalianlah salah satu alasan utamaku pulang ke Indonesia wkwk.

To the world, thank you for helping me grow to be a better person, for believing in me when I didn't even believe in myself, for not giving up on me on my hardest days, and for the patience to deal with and teach a naive and clueless youngster stuck inside a man's body. For giving me the warmth and comfort of home, the constant showering of love and the deepest tub of affection one could only think of receiving. I hope I could've given more of me to you, and I will never lose my hope in the world. You always say I'd do great, and it inspires me to do my best to live up to your words. I hope I make you proud.

To myself: My biggest kudos to you! Young Dito would've been so proud to see where you are right now, realizing your childhood dreams with your blood and tears. I know it has been hard and lonely, but thank you for always trying to give your best in everything. No need to be too hard on yourself, be patient, enjoy life and everything that you do, worry less, and you'll be where you're supposed to be. Surf the highs and the lows of life, trust yourself, find positives in everything, and just so you know: I'll always be there for you no matter what. If life treats you badly, sing with me: "*I'm not okay, but I know I'm gonna be*".

# Contents

# List of Figures

# List of Tables

# Abbreviations

**CaSi** Calcium Silicate.

**CLT** Cross Laminated Timber.

**CO** Carbon monoxide.

**$CO_2$** Carbon dioxide.

**DFT** Dry Film Thickness.

**ETA** European Technical Assessment.

**GHG** Greenhouse Gases.

**GLT** Glued Laminated Timber.

**H-TRIS** Heat-Transfer Rate Inducing System.

**MC** Moisture content.

**MUF** Melamine urea-formaldehyde.

**PUR** Polyurethane.

**TC** Thermocouples.

**Note:** Author abbreviations are shown in their corresponding reference entry.

# Chapter 1

# Introduction

## 1.1 Background

For the past century, the most common method of construction in mid-rise and high-rise buildings involves the usage of concrete and steel. However, the conventional construction method poses a real threat to the environment because the manufacturing processes of cement and steel release huge amounts of $CO_2$, which is a type of greenhouse gas (GHG) that causes global warming. Steel manufacture contributes to 8% of the global $CO_2$ emission [14], while the cement industry makes up another 8% of the $CO_2$ emission [15]. Global warming causes a long-term change in weather patterns and temperature, which then results in the melting of polar caps, an increase in the sea level, more frequent and intense extreme weather events, and other harmful effects.

On the other hand, the demand for built environments is ever-present. In addition to the rising rate of urbanization, the growth of the world's population will only further increase the demand for built environments. Thus, it is necessary to find ways to construct buildings while keeping the environmental consequences to a minimum. Presently, one of the most commonly adopted ways is to reduce the usage of conventional building materials e.g., steel and concrete, and replace them by using alternative 'greener' materials, such as engineered timber.

The popularity of engineered timber has risen because of its low environmental impact, ease of construction, as well as its aesthetic quality. Engineered timber consists of several types, such as GLT (Glued Laminated Timber) or Glulam, LVL (Laminated Veneer Lumber),

and CLT (Cross-laminated Timber). However, Cross-laminated Timber is one of the most common products that can be found in the current market. CLT is usually made of an uneven number of timber board layers, where an individual layer is glued to the adjacent layers at a right angle to ensure the stability and rigidity of the CLT. This configuration also gave CLT in-plane and out-of-plane load-bearing capacity. The CLT panels in the construction industry are commonly utilized as wall, floor and ceiling slabs.

Two structural solutions are present when incorporating CLT as a construction material, a pure CLT solution and a hybrid solution. A pure CLT solution will use little to no other construction materials but CLT for the walls, slabs, and roofs. In contrast, a hybrid solution means that other building materials, such as concrete or steel, will be used alongside the CLT panels to create composite structures. One advantage of a hybrid solution is that it enables the construction of bigger spans without the demand for thicker CLT slabs; thus, this solution is popular for the construction of mid to high-rise buildings. On the other hand, pure CLT construction is fit for low-rise constructions, such as schools and individual dwellings [16].

For the hybrid solution, CLT panels can be used as wall panels, floor slabs and roof decks. In the application of CLT as a floor slab, the CLT panel can be connected to and supported by a steel beam to form a hybrid connection. The loads applied to the CLT slab will then be transferred to the steel beam. This way, the advantages of both materials can be combined without sacrificing the performance of the building. However, introducing this hybrid connection will present a different fire risk to the building compared to the conventional connection since timber is an organic material that could burn, unlike steel or concrete.

The structural fire performance of CLT is greatly influenced by its charring behaviour, the heat transfer on the virgin timber layers, adhesive performance, and the exposed timber's contribution to the fire dynamics. In the event of a fire, the cross-section of CLT will decrease as it chars at approximately 300°C [17], causing the reduction of the element's load-bearing capacity. Furthermore, the strength of wood begins to decline significantly above 65°C [18], which is crucial during the cooling process and near the connections. The CLT panels must also retain their insulation capability and integrity within a structure. However, the solid char formed during the combustion of timber could protect the inner timber section because the char will act as a thermal insulator that reduces the thermal exposure to the underlying

timber layer. On the other hand, delamination could occur in fire conditions, in which one or more layers of the CLT panel separate from each other either partially or completely when the adhesive strength deteriorates in elevated temperature [19]. If this happens, the char formed will fall off and thus directly exposing the underlying timber to the fire, further reducing the load-bearing capacity of the timber and accelerating the formation of the char.

In the context of a hybrid CLT-steel connection, the structural fire performance of the connection will also depend on the load-bearing capacity of the steel beam at elevated temperatures. It is known that the mechanical properties of steel, such as the yield strength and modulus of elasticity, will gradually deteriorate as the steel element heats up [20]. Additionally, the high thermal conductivity of steel means that heat transfer occurs faster than in materials with lesser thermal conductivity, such as CLT. Steel members might lose their load-bearing capacity due to the decline in their strength and stiffness due to elevated temperatures, which could lead to the failure of the members.

Failure in the hybrid connection, either from the CLT or the steel beam, could cause catastrophic consequences such as the collapse of a part of or the whole building. In order to minimize the risk of failure in hybrid connection during a fire, it has become a common practice to provide a passive protection system to protect the steel with a non-reactive solution, e.g., board protection or reactive solution, such as intumescent coating. Currently, the intumescent coating is one of the most popular passive protection systems for steel structures. Nevertheless, the protection of steel by intumescent coating is complex, and its performance relies on many factors, such as the heating rate, the compositions, and the coating mixture [12][21][22].

Compared to conventional building materials, CLT is a relatively new material since it was first developed in the early 1990s in Austria [23]. Although its general acceptance and popularity have risen since then, there are many gaps in knowledge regarding the use of CLT in construction. Several studies have been conducted on the thermal behaviour of CLT solid panels, such as its fire and charring behaviour [24] [25], charring rate [26], delamination [27], and structural response [28][29], etc. Despite the efforts to conduct research and studies on CLT, limited research has been focused on the thermal behaviour of hybrid CLT–steel connections. One recent research in this subject was focused on the charring of steel-timber hybrid hollow beam section [30]. Moreover, there is limited knowledge on the subject of

protecting steel beams with intumescent coating on a hybrid CLT - steel connection. The current practice in the industry is to design the dry film thickness (DFT) following the manufacturer's data for the intended fire resistance time and critical temperature. However, the data is based on testing the individual steel member without considering the interaction between the different materials in a hybrid solution which could affect the effectiveness of the intumescent coating.

## 1.2 Purpose and objectives

This research aims to investigate the thermal behaviour of a hybrid CLT-steel connection when exposed to a standard fire curve. Furthermore, the effect of the provision of intumescent coating as a passive protection system for the steel beam on the hybrid connection will also be investigated.

The main objective is to conduct small-scaled experiments with the hybrid CLT-steel connection with different intumescent coating coverage in order to:

- Record and investigate the charring rate and charring behaviour of the CLT panel in the hybrid connection when exposed to the standard ISO 834 fire curve, specifically in the area directly exposed to the fire and the area protected by the bottom flange of the steel beam.
- Investigate and present the relation between the intumescent coating, the steel beam, and the CLT panel.
- Study the influence of different degrees of protection on the performance of the intumescent coating to protect the steel beam in the hybrid connection.
- Study the difference in charring behaviour of the CLT panel with different degrees of protection on the steel beams.
- Evaluate the appropriateness of manufacturer's data on intumescent coating thickness when being used to protect steel beam in hybrid CLT-steel connection.

By completing the study, the author expects the result to improve the general knowledge of hybrid CLT - steel connections in fire conditions. Additionally, the study could be used to

evaluate and improve the current practice of designing intumescent coating as a protection system for steel members in a hybrid CLT - steel connection.

# Chapter 2

# Literature review

The general objective of this chapter is to provide relevant information and recent research regarding the topic of the hybrid CLT-steel connection and its components.

To begin, the general characteristics of the timber will be presented, and a short summary of mechanical characteristics and the elevated-temperature behaviour of Cross-laminated Timber (CLT) will be discussed. Afterwards, the general characteristics of steel, its mechanical characteristics, and its behaviour in elevated temperatures will be explained. Furthermore, there will be a discussion regarding the hybrid connection of CLT and steel. To close the chapter, there will be a discussion regarding intumescent coating, the chosen passive protection system for the steel beams in this project.

## 2.1 General characteristics of timber

Wood has been a part of human life throughout history due to its availability and its characteristics, be it to construct structures, tools, fuel, and other uses. As a material, it has good mechanical strength in both compression and tension [31], and it possesses a high strength-to-weight ratio to add to its thermal insulating capacity and acoustical properties [32].

Wood comprises cellulose, lignin, hemicelluloses, and a small amount of other extraneous materials [33]. The physical properties of wood, such as its flexibility and hardness, are a product of the difference in the proportion of the components, cell structures, and cell characteristics [34]. Although there will be some differences in attributes of a single wood

species, in most cases, it's sufficient to sort out wood based on its species because the characteristics are relatively constant in a species [35].

The fibrous characteristic of wood comes from fibres, whose function is mainly to act as mechanical supporting cells for the tree [36]. These fibres grow perpendicularly to the long axis of the tree's growth. Consequently, wood is an orthotropic material, which means that it has independent properties in three axes of symmetry that are radial, longitudinal, and tangential, as shown in the figure 2.1 below [37]. Furthermore, the mechanical strength and density of wood are mostly affected by the thickness of the fibre cell wall, where species with thin-walled fibres will have lower density and strength when compared to other species with thicker fibre cell wall [1].

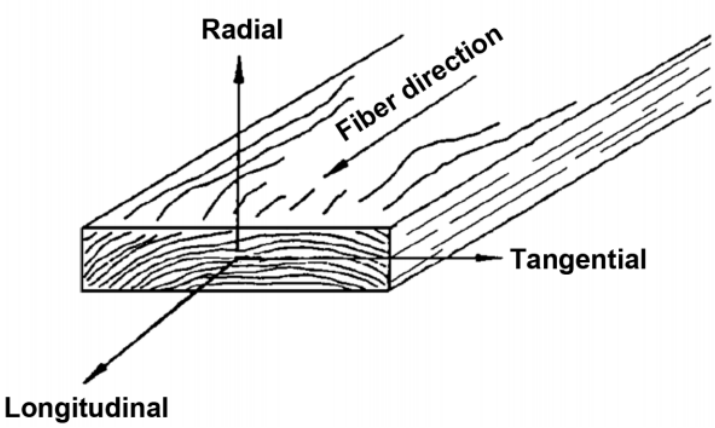


Figure 2.1: Three axes of wood with regards to the fibre direction [1]

Wood is one of the oldest construction materials utilized by the human race. While previously, the utilization of this material was mainly due to its manufacturing and lightness, nowadays, it is due to wood's sustainability, weight-to-strength ratio, availability and manufacturing options [38].

Modern techniques and equipment allowed the development of engineered timber, which can be defined as a wood product that combines timber or laminated product with other materials, such as timber boards or metal elements, to form a composite material. Engineered timber provides controlled properties, which can be adjusted to the customers' specific needs, and also opens the possibility of utilizing locally-defective wood elements, small-diameter timber, and forest residue [39]. Furthermore, the properties of engineered timber could better the properties of natural timber products when high-quality raw materials are combined with

proper processing variables [1]. Engineered timber has several advantages when compared to timber [40], namely:

- Economic advantage in engineered timber comes from the possibility of utilizing low-grade wood, as well as wood by-products and recycled materials. This also comes from the production of engineered timber panels without being limited by the log size.
- Uniform properties of the final product in terms of density, strength, and durability. This advantage practically minimizes the variability, which is one of the main disadvantages of using wood.
- Engineered properties for the timber can be made by using the proper materials and technique to produce timber with higher strength in the three axes, better resistance to insect attacks, and better fire resistance.

Engineered timber consists of several different products that require different materials and processing methods. Glued-laminated timber (Glulam), laminated veneer lumber (LVL), and cross-laminated timber (CLT) are three examples of commonly found engineered timber products in the market.

Figure 2.2: Glulam [2], LVL [3], and CLT[4]

As previously mentioned, the difference between each type of engineered timber is mostly from the materials and the production technique. Glued-laminated timber or glulam comprises several layers of laminated sawn lumber bonded with an adhesive with all the fibre or the grain of all the laminations running parallel to the longitudinal axis, making it strong in the longitudinal direction and weaker in the tangential direction [41]. Glulam is also manufactured with low moisture content to ensure its dimensional stability and prevent shrinkage and

swelling. In practice, glulam is frequently used as beams, truss members, joists, purlins, and columns.

Unlike glulam, laminated veneer lumber, or LVL, is made from carefully-selected wood veneers. The thin layers of veneers are then laminated to form a panel, and all the grain of the veneer has to run parallel to each other [1]. Compared to glulam, LVL is stronger but considered to be less attractive [42]. LVL is known to be a versatile construction material since it can be used for several structural applications such as beams, trusses, and I-joists.

Cross-laminated timber, or CLT, which will be one of the main components of the hybrid connection in this research, will be described in the next section.

## 2.2 Cross-laminated timber (CLT)

Cross-laminated timber, or CLT, is a type of engineered timber commonly found in the construction industry for load-bearing purposes. CLT is manufactured by joining individual layers of timber boards to the adjacent layers, with the grain orientation of each layer alternating at right angles, mostly in uneven numbers, using adhesive. The timber board, which is also known as lamellae or laminate, has a thickness of 20 – 60 mm and is commonly made from coniferous or deciduous timber. In Europe, the production of CLT has to comply with the performance characteristics set in EN 16351.

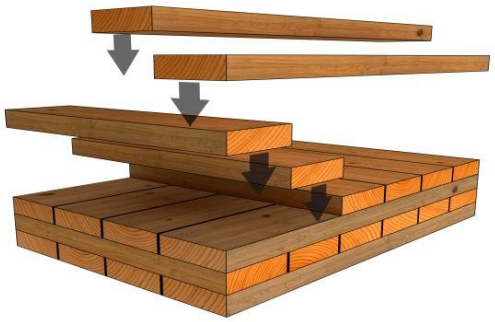

Figure 2.3: Conventional CLT layup, taken from [5]

CLT was first developed in the middle of the 1990s as a result of research between academia and industry [16]. Then, as the technology became more popular, the production and adoption of CLT also increased worldwide, especially in Europe. A recent study shows that in 2019, more than 80% of the world's CLT output came from Europe [43], and the production of CLT in Europe is increasing exponentially from 1996 as shown in Figure 2.4.

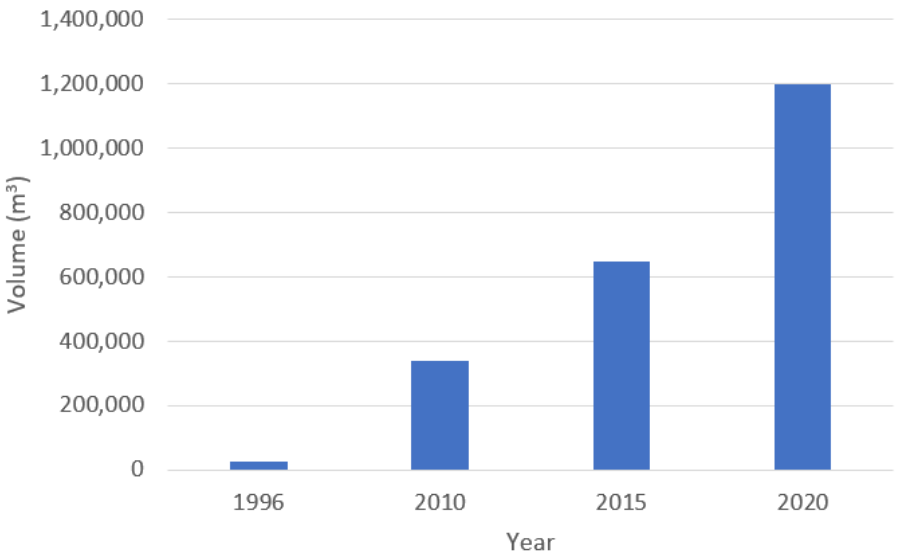


Figure 2.4: CLT production in Europe over the years, based on data from [6]

The cross-laminating process that differentiates CLT from glulam gives increased dimensional stability, which in return allows for a variety of board sizes to be produced up to the long and wide board used for floor slabs. Furthermore, another result of this process makes CLT have high in-plane and out-of-plane strength, enabling it to carry two-way actions similar to a reinforced concrete slab system.

In order to understand the characteristics of CLT, this section will focus on the general characteristics of CLT, along with its mechanical characteristics and its behaviour in elevated temperatures.

### 2.2.1 General characteristics of CLT

Cross-laminated timber has several key properties that appeal to the construction industry, such as its good thermal properties, aesthetical quality, as well as its seismic performance.

CLT has been shown to have good thermal properties due to its low thermal conductivity and high density. While concrete has a thermal conductivity of 1.15 – 2.5 W(m.K), CLT has a thermal conductivity value of 0.09 to 0.11 W(m.K), which is comparable to other timber-based construction materials [44]. With its lower thermal conductivity, adopting CLT can help reduce the heat transferred to the building envelope, consequently improving energy efficiency.

In terms of the seismic performance of CLT construction, a full-scaled study was carried

out involving a seven-storey structure on the SOFIE project by the Trees and Timber Institute of Italy [45]. The study proved that the structure could withstand major sustained vibration, which reached the strength of the Kobe earthquake in 1995 with a magnitude of 6.9, without significant damage. In the occurrence of an earthquake, the energy from the vibration is absorbed by CLT and its connection which act as a damper for the structure.

As previously stated, the performance of CLT produced in Europe has to comply with the European standard of EN 16351. Here, a few testing procedures for the material properties, such as compressive and rolling shear strength, dimensional stability, and bonding strength, are prescribed. The type and species of wood and adhesive families applicable are also given. However, the European standard lacks a uniform design procedure for CLT and reference values for the CLT elements. Finally, although there is a variety of wood species and adhesives, the most common material for CLT production in Europe is spruce (*Picea abies* L. Karst.) adjoined with polyurethane (PUR) adhesive based on literature review and interviews from several CLT producers [46].

### 2.2.2 Mechanical characteristic of CLT

As CLT is commonly adopted to replace conventional building materials, the mechanical characteristics of CLT are of high importance in designing and constructing structures. These mechanical characteristics are fundamental since CLT can be used for various structural purposes, such as floors, roofs, or walls. In any case, a structural member is expected to receive and carry several types of stress, such as compression, shear, bending, and tensile stress. In CLT, these stresses, forces, and moments are shown in Figure 2.5 below.

Figure 2.5 displays the loads applied on the CLT slab on three axes. Additionally, the resulting stresses are also demonstrated, and here, the complexity of cross-laminated timber can be shown in the stress diagrams on the cross-section of the CLT. This complexity arises because CLT comprises layers of timber panels adjoined at a right angle, combined with the orthotropic nature of wood itself. As a result, CLT has different strength properties when the loads are applied out-of-plane or in-plane of the CLT elements.

The bending strength in CLT for out-of-plane can be determined by a model which was based on experimental works done on CLT [8]. The foundation of this model is from a homogenous reference CLT section consisting of 5 layers of lamellae, as shown in Figure

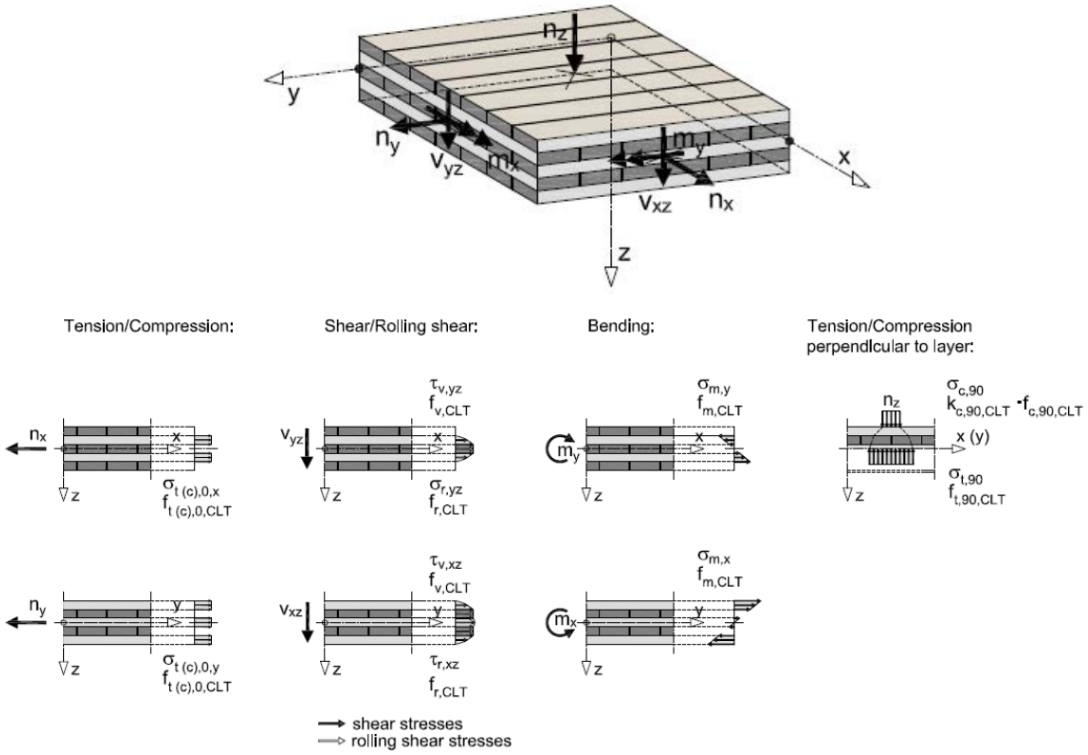


Figure 2.5: CLT with possible forces, moments, stresses, obtained from [7]

2.6. This model considers the reduction in variability of the mechanical characteristics of the whole element due to the homogenisation of the CLT's material properties. Additionally, the characteristic bending strength out-of-plane is translated from the characteristic tensile strength parallel to the grain with the consideration of four other influence factors to improve the model's validity.

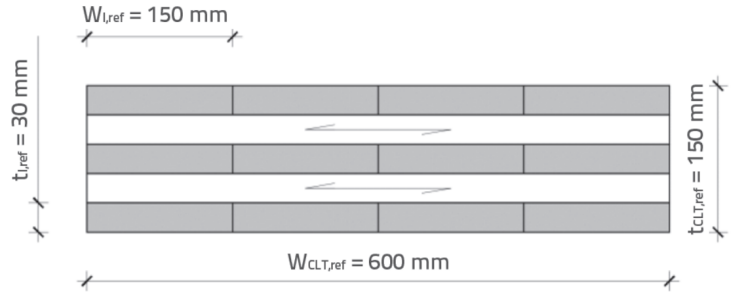


Figure 2.6: Dimension of the reference CLT section, from [8]

The bending load in an out-of-plane direction will result in two shear stresses:

- Shear stress in fibre direction in longitudinal layers.
- Shear stress at 90° to the fibre direction will occur in transerve layers.

The typical shear strength and the mean shear stiffness of CLT parallel to grain shall follow the basic material value in compliance with EN 14080, as per [47]. Studies have been conducted to determine the rolling shear strength and rolling shear stiffness perpendicular to the grain direction, and one study in particular involved more than 200 specimens. This study [48] proposed a bi-linear model to determine the rolling shear strength and stiffness with consideration of different types of wood, the geometry of lamellae with regards to the width-to-thickness ratio, and the type of lamellae with different distances from the heartwood.

For loading in-plane, the first thing that has to be checked is the three shear failure mechanisms for the CLT element, depicted in Figure 2.7 [9].

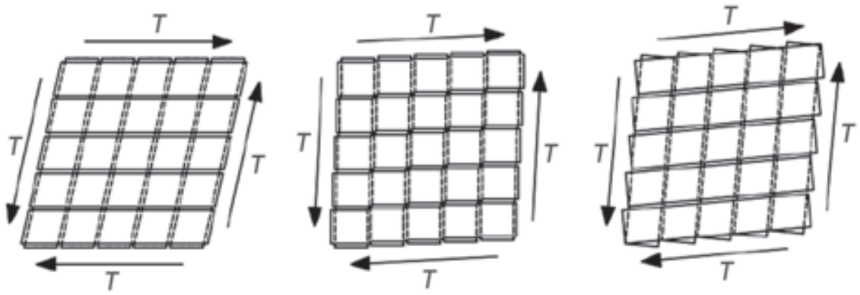


Figure 2.7: Shear failure mechanisms of CLT with an in-plane load [9]. FM I (left), FM II (middle), and FM III (right)

In failure mechanism (FM) I, the failure happens along the CLT's gross cross-section. In this case, it is recommended to follow EN 14080 and assume the typical shear strength of 3,5 N/mm$^2$ and mean shear modulus of 650 N/mm$^2$ to prove the carrying capacity.

However, in most cases, for CLT elements, the failure mechanism will be either FM II or FM III. FM II is the failure along the net cross-section of CLT, while FM III is the shear failure because of torsion and uniaxial shear stress at the point of contact between two glued lamellae. In CLT, FM II and FM III have to be investigated separately. The FM II and FM III can be determined from tests on small CLT specimens, while large CLT specimens are generally used only for determining FM II. The test results for FM II and FM III have been summarized in a study from 2018 [49].

One of the strength properties of CLT in an out-of-plane loading is the CLT tension strength perpendicular to the grain direction. Unfortunately, research on this topic is still insufficient. Thus, a study recommended using the tensile strength perpendicular to the grain from GLT, in accordance with EN 14080, because of the similarity between CLT and

GLT elements [49].

Similarly, the research on CLT tension strength parallel to grain direction is also lacking. One study proposed a model to calculate the characteristic tensile strength parallel to the grain of CLT [47]. This model considered the number of parallel-oriented longitudinal lamellae and the tensile strength variation parallel to the material's grain.

In order to determine the compression strength perpendicular to the grain direction of the CLT elements, experimental tests were conducted using small prismatic specimens, which were loaded on the surface with uniform stress. Several studies have been conducted to study this strength property, such as one conducted in 2010 by Salzmann [50], where various configurations of CLT were tested with different positions of point load and linear load. The study concluded that the lowest carrying capacity was found in the specimen subjected to corner load since the load can only be propagated to two sides of the specimen. Accordingly, the element with the highest carrying capacity was the element loaded in the centre since the load can be propagated to four sides of the specimen. Another research was done in 2014, where different parameters, such as the influence of moisture content on the strength and the influence of point, linear, and plane loading on CLT elements' behaviour, were explored [51]. From these experiments, the authors proposed a value for the characteristic compressive strength perpendicular to the grain to be 3.0 $N/mm^2$ and mean elastic modulus of 400 $N/mm^2$.

While there are several studies on the compression strength perpendicular to the grain of CLT, unfortunately, the compression strength parallel to the grain of CLT has not been sufficiently studied yet. Therefore, a conservative recommendation is given to use the out-of-plane bending strength of CLT as the compressive strength parallel to the grain [49].

### 2.2.3 Fire behaviour of CLT

Building materials' load-bearing capacity will decrease when exposed to elevated temperatures for a certain amount of time. This exposure will impact the structural stability of the affected member and, therefore, the whole structure. The ability to understand and predict the behaviour of structural elements in fire is important to ensure the design solution is sufficient for the safety of the people, the property, and the environment.

CLT is also no exception in this regard. Since CLT is made out of timber, it is com-

bustible, and the thermal degradation of CLT is similar to wood material. The thermal degradation of wood when exposed to elevated temperatures can be divided into several temperature regimes, as explained in [18]. When the temperature reaches 65°C, wood will experience a permanent strength reduction caused by depolymerization reactions. The extent of the reduction depends on several factors, such as moisture content, wood species, and exposure time. This is important, particularly in the cooling phase, since the thermal waves continue to travel through the section, which could further decrease the strength permanently. Consideration near the vicinity of screws/connections/joints is also important since the embedding strength of the screws/connections is reduced [52][53]. Then, above 100°C, the moisture content in the wood will evaporate while producing non-combustible gasses such as $CO_2$ and acetic acid. At 200 – 300°C, wood components begin to experience pyrolysis, and CO gas starts to be generated. Then, above 300°C, flammable volatiles are produced significantly. Finally, at this temperature, the char layer starts to form on the surface exposed to the fire. With its low thermal conductivity, the char layer will then protect the inner virgin timber from heat exposure [28]. However, at the same time, the formation of the char layer means a reduction in the timber's cross-section area. Based on the reduced-cross section method, this will decrease the shear and load-bearing capacity of the timber. Additionally, the reduction in the section area from the char formation could also decrease the efficiency of possible shear connectors between the timber and other building members, which plays an important role in the composite action for the structure [53].

Because of their combustible nature, CLT panels will contribute to the overall fire dynamics in a compartment as an additional source of fire load. Therefore, comprehending the fire dynamics in an enclosure with exposed CLT elements is necessary to create a fire-safe design. A study [54] was conducted to achieve this objective, where three configurations were tested to study the effect of different numbers of exposed CLT surfaces. The study discovered that auto-extinction happened when there were two exposed CLT surfaces; however, auto-extinction depended on the char fall-off phenomenon in the panels. Three exposed CLT surfaces, on the other hand, couldn't achieve auto-extinction due to the higher heat transfer preventing the critical auto-extinction heat flux from being achieved. Additionally, the enclosure's temperature was marginally affected by the exposed CLT surfaces (thus, the current prediction works well) while the total heat release rate (HRR) was found to be higher

than the prediction with the existing methodology.

The current practice of structural fire design for CLT panels involves standardized fire tests and several calculation methods and charring rates presented in standards and guidelines, such as the Eurocode 5: Design of timber structures (EN 1995-1-2) [55].

A. Frangi et al. conducted a study to study the fire behaviour of cross-laminated solid timber panels [24]. In this study, a finite-element thermal analysis was conducted to measure the charring of the CLT panel subjected to the ISO 834 fire curve. The study found that the fire behaviour of CLT timber depends on the behaviour of the individual layers. If the charred layers stay, the char will protect the virgin timber layers from heat exposure, thus reducing the charring rate. Meanwhile, if the charred layers fall off, the protection provided by the char will also be gone, resulting in an increased charring rate. CLT with thick layers behaves comparably to homogenous timber panels with one-dimensional charring. CLT with very thin layers, however, will behave akin to plywood. Additionally, horizontally-oriented CLT members also exhibit worse fire behaviour than vertical members. It was concluded that the fire behaviour of the CLT panel is influenced by the number and the thickness of single layers and the adhesives' performance in high temperatures.

In 2016, T. R. Moser et al. investigated the char rate of CLT exposed to the ISO 834 fire curve in an intermediate-scale furnace [26]. Ten tests were undertaken with heat exposure from the top side of the horizontally-oriented CLT panels. Two methods were used to measure the charring rate of the Radiata pine CLT panels, one with implanted thermocouples at different depths with the assumption that char temperature is defined at 300°C. Another method was to measure the actual thickness of the remaining timber after the test. Both methods produced similar results for the average char rate, at 0.83 ±0.2 mm/min and 0.83 ±0.074 mm/min for thermocouple and manual measurements.

As previously mentioned, the adhesive's performance of CLT also plays a vital role in its fire behaviour because of the possibility of delamination. Delamination is the separation of two bonded surfaces, and A. Colic studied this topic [27]. Three lamellae CLT blocks produced by three European CLT manufacturers were used on 30 small-scale tests. Two different adhesives were investigated, polyurethane (PUR) and melamine-urea formaldehyde (MUF). The samples were loaded with a shear stress of 0.15 and 0.20 MPa, and exposed to radiant heat flux of 50kW/m$^2$ from an H-TRIS apparatus. The tests show that the mean

delamination temperature ranges from 78°C for MUF adhesive to 235°C for PUR adhesive. Delamination is also affected by the amount of load applied to the samples, whereas in higher loads, the samples experienced delamination.

The structural response of loaded CLT beams exposed to a fire condition was studied by S. A. Lineham et al. [28]. Current industry practice in Europe (through Eurocode) treats the structural fire design of CLT as solid softwood timber. In this study, CLT beams were loaded with sustained flexural loading while exposed to heat from below (thus, one-sided fire exposure only). Then, a comparison of the structural fire response was made between the predictions from the Eurocode methods (The reduced cross-section and zero-strength layer thickness method) and the actual load-bearing capacities and time-history of deflection of the beams. The observations from the study found that the Eurocode methods aren't appropriate for predicting the structural response of CLT in elevated temperatures, especially for non-standard fire exposures.

Several novel studies on the fire behaviour of CLT, especially with regard to its structural performance, were conducted. The structural response of CLT compression element exposed to fire was studied in 2017 [56], followed by the rolling shear capacity of CLT at elevated temperatures in 2018 [57]. Furthermore, the study on structural capacity in fire of laminated timber elements in compartments with exposed timber surfaces [58] was published, followed by the effect of adhesive type and ply number on the compressive strength retention of CLT at elevated temperatures [59]

## 2.3 General characteristics of steel

Given its strength, durability, and versatility, steel is among the most widely used materials in the construction industry. Steel is an iron-carbon alloy with small amounts of other elements added to improve properties such as strength, corrosion resistance, and weldability. Steels are categorized based on their carbon content, from ultra-low carbon steel at less than 0.01%, up to carbon tool steels with a carbon percentage of 0.9-1.7%. The typical types of steel categorization based on the carbon content can be seen in Table 2.1.

Table 2.1: Typical properties and application of steel based on its carbon content, reproduced from [13]

| Type of Steel | Carbon content (%) | Alternative treatments | Properties | Applications |
|---|---|---|---|---|
| **Ultra low carbon steel** | <0.01 | Normalised, may be work hardened | Ductile<br>High formability<br>Weldable | Automotive sheets, wire mesh |
| **Extra low carbon steel** | <0.02 | Normalised | Ductile<br>Good formability<br>Weldable | Automotive sheets, pipes |
| **Low carbon steel** | 0.05-0.15 | Normalised | High strength<br>Ductile<br>Weldable | Offshore engineer--ing, pipes |
| **Mild steel** | 0.1-0.25 | Normalised | High strength<br>Ductile<br>Weldable | Structural rolled sections, tubes, plates, pipes, cast steel |
| **Medium carbon steel** | 0.25-0.5 | Quenched and tempered | High strength<br>High toughness<br>Difficult to weld<br>Brittle below room temperature | Machinery rails |
| **High carbon steel** | 0.5-0.9 | Quenched and tempered | High strength<br>Low ductility<br>Difficult to weld | Machinery |
| **Carbon tool steel** | 0.9-1.7 | Quenched and tempered | Very hard<br>Low toughness<br>Wear resistant<br>Cannot be welded<br>May be brittle | Machine tools dies, springs |

Steel is produced through a multiple-phase process, which starts with producing iron from iron ore in a blast furnace. Then, iron is transformed into steel through the basic oxygen or electric arc process. The molten steel will be cast, and the steel will be formed using the hot-rolling method. A further process to reduce the thickness of sheet steel is called the cold-rolling method.

In the field of construction, structural steels with a carbon content of 0.13-0.25% are most often used. Therefore, in this section and forward, the focus will be on structural steel. Steel is used in a variety of construction applications, including the construction of buildings, bridges, highways, and other structures. Steel can be used in various ways, including structural steel beams, columns, plates, and concrete reinforcing bars (rebar).

Steel's strength and durability are two of its primary advantages in construction. Steel structures can withstand severe weather, earthquakes, or other natural disasters better than other construction materials. Another advantage of steel in construction is its versatility. Steel is easily shaped and fabricated into a wide variety of sizes, forms, and properties, making it suitable for a wide range of applications. Steel structures can also be prefabricated

offsite and transported to the construction site for assembly, lowering costs and time.

The properties of steel are determined by its carbon content and the presence of the other alloying components. Generally, as the carbon content of the steel increases, the steel becomes harder and has higher strength; on the other hand, it also becomes more brittle and harder to weld.

Steel properties are commonly grouped into three categories: physical, chemical, and mechanical. While the physical properties of steel, such as its elasticity modulus and Poisson's ratio, are considered to be approximately constant for steel, steel's chemical and mechanical properties must be tested for every batch of steel produced due to the unavoidable variabilities in production [60].

### 2.3.1 Mechanical characteristic of steel

The popularity of steel as a construction material is mainly credited to its mechanical characteristics, which will define how the material responds to loads and forces. The mechanical characteristics of steel depend on various factors, such as its composition, treatments, formation methods, dimension, and steel grade. Some of the most common parameters to characterize the mechanical properties of steel are its modulus of elasticity, tensile and yield strength, elongation percentage (or ductility), reduction of area percentage, and hardness [60].

Modulus of elasticity, or also known as Young's modulus, is a measure of a material's capability to withstand deformation. The modulus of elasticity describes the deforming stress and the strain of the material in the elastic zone of the stress-strain curve [61]. A typical stress-strain curve for a ductile material, such as steel, is shown in Figure 2.8.

The tensile strength can be defined as the maximum amount of tensile (pulling) force that can be withstood by a material before it fails, expressed in the units of force per section unit area. Another common strength characteristic is the yield strength, which is the maximum force the steel can withstand before experiencing plastic, permanent deformation. The yield strength is also expressed in the same unit as tensile strength.

Elongation percentage is often tested during the tensile test of a material. It shows how much a material will elastically and plastically deform before breaking up. Then, the reduction of area percentage is the percentage reduction of the cross-section area of steel

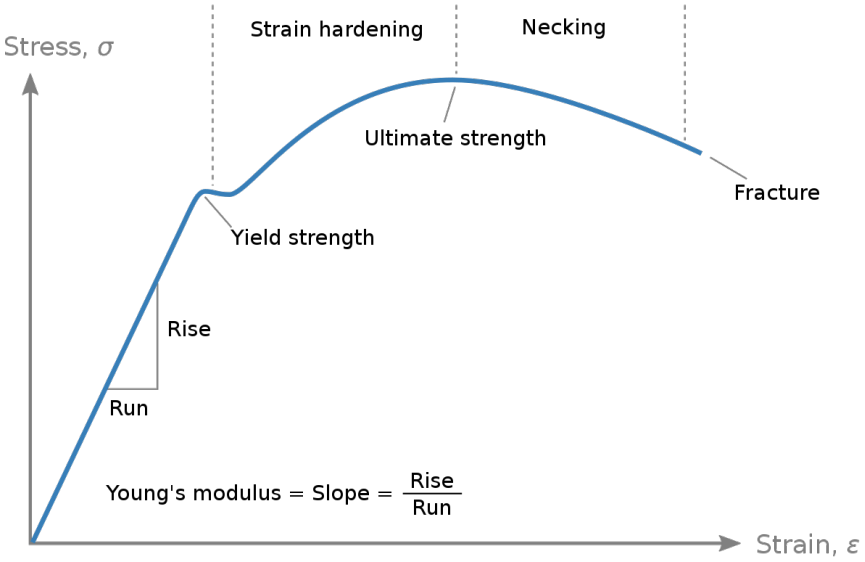


Figure 2.8: Typical stress-strain curve [10]

in the point of fracture and compared to its original cross-section area. As a rule of thumb, the material with high elongation percentage has the ability to experience bigger deformation before breaking up and is more ductile. Material with a high reduction of area percentage also exhibits similar characteristics.

The tensile strength, yield strength, elongation, and reduction of area percentage can be obtained through the tensile test. The tensile test is carried out by applying increasing stress or load on the standard test specimen, which is gripped between two screw-driven devices [60]. Then, the test results are obtained by measuring the load against the extension of the specimen.

The hardness of a material is the measure of a material's resistance to deformation. The hardness test can be done by the Brinell test and the Rockwell test, which both attempt to cause an indentation on the flat surface of a material. The hardness value is helpful in demonstrating several other properties of the steel, such as softness, resistance to deformation, wear and scratch resistance, and bendability [60].

### 2.3.2 Fire behaviour of steel

Unlike timber, steel is a non-combustible construction material that will not contribute to fire when exposed to high temperatures. However, exposure to high temperatures will deteriorate

the mechanical properties of steel as it heats up. Another major difference between these two materials is their thermal conductivity. While timber has a very low thermal conductivity, between 0.09 – 0.11 W(m.K) as previously described in 2.2.1, steel's thermal conductivity is much greater in comparison with values ranging from 51.9 – 62.8 W(m.K) at 20°C for different grades of steel as compiled in [62]. An additional factor that influences the rate of rise of steel temperature is the specific heat capacity of steel, which is between 0.465 – 0.486 kJ/kg.°C, depending on the carbon content. The specific heat of steel is considerably lower compared to other construction materials, such as wood (between 2.4 – 2.8 kJ/kg.°C) or even concrete (0.88 kJ/kg.°C) [61]. Understanding the mechanical properties of steel in high temperatures is necessary to predict the performance of individual members and the structure as a whole and to make fire resistance design of the structure.

Multiple studies have been conducted to learn about the change in steel's properties at elevated temperatures. The changes in the properties at elevated temperatures are often shown in the percentage of the properties in ambient temperature as a reduction factor. One example of such a study was conducted in 2013 by Wang, et al. [11], where the authors investigated the mechanical properties of high-strength steel (Q460 class) at elevated temperatures. High-strength steel is chosen because of its increasing application for high-rise buildings and excellent mechanical properties. Two test setups, one for elastic modulus and one for tensile strength, were employed to evaluate the mechanical properties of the steel between the 20-800°C, which were then used to derive the strength and elastic modulus of the steel.

The main observations from the research are shown in figure 2.9, where three parameters are compared between the Q460 steel with two types of mild steel (SM31 and Q235) and another type of high-strength steel (BISPLATE 80). It can be seen that the yield strength of the Q460 steel initially reduced when the temperature increased up to 100°C, but then the yield strength increased to be higher than at room temperature. When the temperature keeps on increasing, however, the yield strength begins to decrease. Above 450°C, the yield strength decreases rapidly. Compared to other steels in this study, the Q460 steel shows higher yield strength retention.

In the ultimate strength property, the Q460 steel shows a similar trend as the other tested high-strength steel, the BISPLATE 80. These two high-strength steel shows a higher

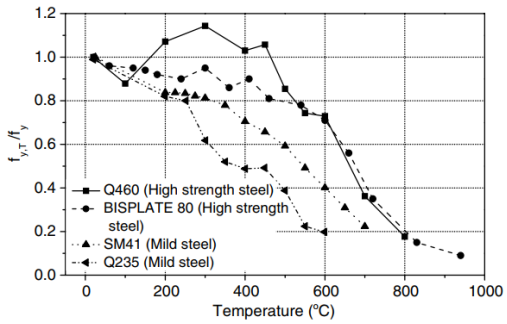


((a)) Yield strength

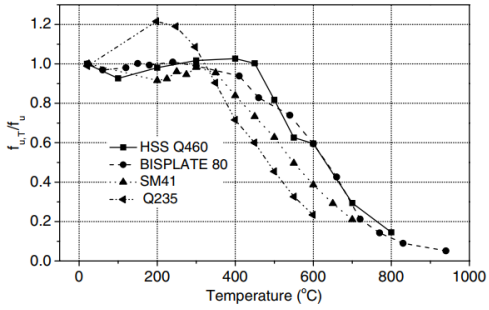


((b)) Ultimate strength

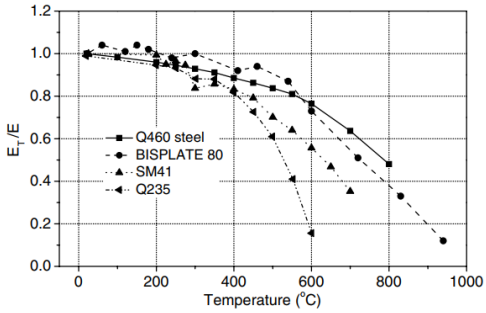


((c)) Elastic modulus

Figure 2.9: Mechanical properties of Q460 at elevated temperatures, compared to other steel types [11]

reduction factor of the ultimate strength when compared with the mild steels. The same trend can be observed for the elastic modulus, where the reduction factor for the Q460 steel compares well with BISPLATE 80, and their reduction factors are higher than the mild steels. The better performance of the Q460 steel at elevated temperatures is accredited to the difference in composition of the steel, where Q460 contains more alloys which help with the fire resistance of the steel, compared to the other steels.

An extensive review of recent research on mechanical properties of steel in elevated temperature was completed in [20], where the authors compiled results from 8 research with different steel classes. The research conducted had proven that the mechanical properties of steel would reduce as it heats up, thus affecting the stability of the member and the structure as a whole. Since the fire resistance of structural members is of high importance in the design and operation of a building, passive fire protection systems are often used to increase the fire resistance or decrease the effect of elevated temperatures on the strength loss of the structural members.

## 2.4 Hybrid structure of CLT and steel

The construction industry often uses hybrid structures consisting of two or more different materials to form a structural system. A hybrid structure gives the designers more flexibility and provides each material's best properties while simultaneously reducing its weaknesses. While previously hybrid construction may only consist of steel and concrete, nowadays, engineered timber products are commonly used in the field. Additionally, incorporating hybrid timber structures with steel and/or concrete will enable the construction of taller and bigger buildings in comparison with pure CLT structures. In turn, this construction solution could help increase cost efficiency, reduce construction time (especially with prefabricated engineered timber), and reduce the structure's carbon footprint.

One of the commonly found examples of a hybrid timber-steel structure is the replacement of concrete slabs with engineered timber panels, such as CLT, while maintaining the use of a steel frame for the structure. In this type of construction, different types of assembly are possible to be used depending on the type of steel beams and the needs of the buildings. Three examples of the assemblies are shown in Figure 2.10.

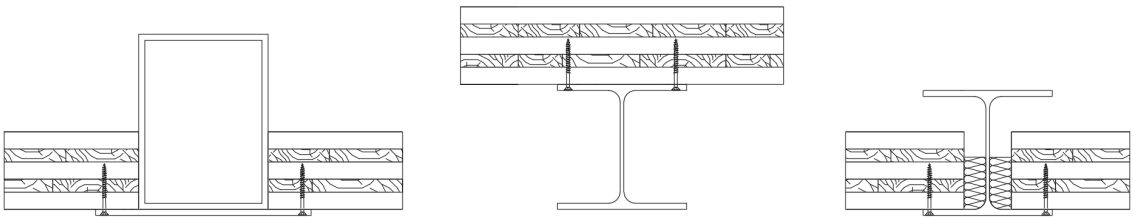

Figure 2.10: Cross-sectional examples of CLT-steel structure assemblies

On the leftmost of Figure 2.10, the CLT slabs rest on top of a steel plate welded to a steel hollow section (SHS). The CLT slabs are installed on the steel plate with screws. In the middle of the figure, the assembly shows a CLT slab that rests on top of the top flange of an H-steel beam and is fixed to the beam with screws. Another possible assembly is shown on the rightmost of the figure above, where the CLT slabs are resting on the bottom flange of the steel beam and fixed using screws.

One important consideration while using the hybrid structure of CLT and steel is their behaviour at elevated temperatures. Since the structure is made of two very different materials, each of the materials will have a different reaction and behaviour when exposed to elevated

temperatures. When combined, the interactions between the materials produce completely different reactions compared to each of the material's reactions to elevated temperature.

Steel isn't combustible, while CLT is. However, steel has a higher thermal conductivity value compared to CLT. While exposed to elevated temperatures, the steel beam protects the CLT panel from direct exposure. This could slow down the charring from the CLT in this area; however, the steel will also transfer heat through conduction to the CLT area in contact with the steel. Unfortunately, the study on this subject is still scarce, although of its importance with the current trend of CLT adoption in construction.

A study was recently conducted on the charring rate on steel-timber hybrid beam section, especially on a slim-floor construction [30]. The temperatures in CLT and the steel section were investigated through two full-scaled fire tests, one without protection on the steel beam and another with fire protection by intumescent coating on the steel beam. The measurement of temperatures in CLT and steel was done with the help of thermocouples, and char depth measurements were conducted using actual char layer measurement after the test and thermocouple measurements on the CLT with 300°C isotherm method. These two tests showed that the steel bottom plate did not reduce charring on the CLT behind the unprotected plate, while the protected plate managed to reduce the char on the adjacent CLT. Numerical simulations for the two tests were also conducted using SAFIR [63], and the results showed a good agreement between the experimental work and numerical modeling.

Another study focused on using thermal modelling to investigate the connectivity and structural capacity of hybrid steel beam to CLT connection under fire condition [53]. For the thermal modelling, two-dimensional finite element modelling was carried out. Unlike the previous study, here, a wide flange beam was used. The main assessment of this study was to investigate the failure due to the weakening of the CLT due to heat transfer, which will result in the top flange being unable to be restrained by the screw. The steel beams were also modelled to have an intumescent coating around the exposed area. The study concluded that the failure of the steel beam could occur because of the loss of lateral torsional bracing before the required fire resistance period. While intumescent coating did the job of protecting the steel beam, the thermal transfer of heat into the steel made its way to the screw, which then lost its capacity to provide the lateral torsional bracing for the beam.

## 2.5 Intumescent coating

Intumescent coating is a commonly available reactive passive fire protection solution in the market that can be applied to structural members such as timber, concrete, and steel to provide localized protection through thermal insulation capability. Compared to non-reactive passive fire protection, the intumescent coating has several advantages, boosting its adoption in the construction industry. Those advantages are faster speed of construction, corrosion protection, the flexibility of both on-site and off-site applications, better quality control, cost-efficient, and better aesthetical looks.

Intumescent coatings can be categorized into two major groups: thin intumescent coating (with a dry film thickness in the order of 1–3 mm), either solvent-based or water-based, and thick intumescent coating (dry film thickness of a few centimetres), typically epoxy-based, which is a combination of two components. The thick intumescent coating was originally developed to protect structural members from hydrocarbon fire, which is considered more severe than cellulosic fire. However, manufacturers have modified and manufactured thick intumescent coating as protection from cellulosic fire.

The dry film thickness (DFT) of the thin and the thick intumescent coating will depend on several factors. Firstly, it will depend on the protected member's maximum allowable or limiting temperature. Then, the duration of the protection, or the fire rating of the protected member. The section factor, or the ratio between the surface area of the member exposed to the fire and the volume of the member, will be another important factor. Finally, the type and shape of the member will also be decisive in determining the dry film thickness.

Intumescent coating is made out of several key ingredients with a specific function for each of them, as explained in literature [22]. The components are:

1. An inorganic acid
2. Polyhydric compound or carbonific
3. An organic amine or spumific
4. Halogenated organic material or blowing agent
5. Synthetic resin or binder

6. Additives, such as fibers, thickeners, solvents, etc.

Based on [22], the activation of intumescent coating could be divided into several phases. The coating starts to work when it reaches its critical temperature due to heat exposure, typically at approximately 250°C. Then, the inorganic acid will be thermally decomposed, melting and turning into fluid with a viscous consistency. The spumific and the blowing agent will then decompose at different temperatures, forming a substantial amount of gases through an endothermic reaction which absorbs heat from the substrate. The gas bubbles are trapped in the carbon mass of the coating from the carbonific ingredient to produce a thick layer of thermally insulating char. Later, the char will oxidise and release $CO_2$ while transforming into a brittle foam structure at the surface. The binder ensures the mass has a uniform and continuous foam structure. While different ingredients, mixtures, and heating conditions will affect the phases and behaviour of the intumescent process. Generally, the process can be divided into four stages, as shown in Figure 2.11 below. A more thorough explanation of the intumescent process can be found in the literature.

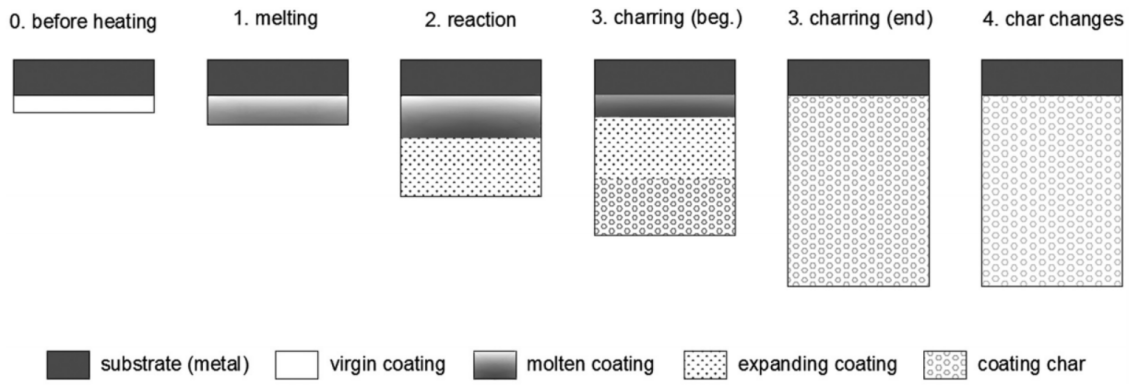


Figure 2.11: Four stages of intumescent process [12]

Multiple studies have been conducted to investigate intumescent coating and its behaviour. A review of the recent development and studies on intumescent coating to protect steel members was done by Lucherini [12]. Additionally, Lucherini conducted a novel investigation on the application of intumescent coating to protect timber elements [64].

As previously stated, different ingredients and mixtures of chemical components would influence different aspects of intumescent behaviour as studied by Bourbigot [65] and Le Bras [66]. Lucherini [21] conducted an experimental study to study the performance of two different types of intumescent coating (solvent-based and water-based) when exposed to different

heating conditions and heating rates. The experiments were carried out in three different experimental setups and highlighted the shortcomings of the current procedure for designing intumescent coatings based on the standard fire resistance test. Other notable studies from recent years which investigated the performance of intumescent coatings exposed to different fire conditions, such as hydrocarbon fire [67] and external heat flux [68], can be found in the literature.

# Chapter 3

# Methodology

Since the nature of the study is experimental, the following chapter will describe the methodology and procedures taken to prepare the specimens and the instrumentations required to achieve the objectives of the study. The preparations are done based on the test matrix shown below in Table 3.1. The complete experimental methodology is also summarized later in this chapter. Furthermore, the information on the pieces of equipment and the materials are also described.

## 3.1 Test matrix

The test matrix of the study is presented in Table 3.1.

Table 3.1: Test matrix of the experimental study

| Test name | Protection method | Protection coverage | Protection design criteria | | Fire curve |
|---|---|---|---|---|---|
| | | | Temperature | Resistance time | |
| 1.A | Unprotected | - | - | - | ISO 834 |
| 1.B | Unprotected | - | - | - | ISO 834 |
| 2.A | Epoxy intumescent coating | Partial (Bottom flange) | 300°C | 60 minutes | ISO 834 |
| 2.B | Epoxy intumescent coating | Partial (Bottom flange) | 300°C | 60 minutes | ISO 834 |
| 3.A | Epoxy intumescent coating | Full (Whole surface) | 300°C | 60 minutes | ISO 834 |
| 3.B | Epoxy intumescent coating | Full (Whole surface) | 300°C | 60 minutes | ISO 834 |

As shown, two tests were performed for each of the different protection coverage. In

total, 6 tests were conducted in this study.

## 3.2 Flow chart of the study

The methodology of the experimental research is summarized and displayed in Figure 3.1.


Figure 3.1: Flowchart of the methodology in this research

## 3.3 Equipments employed

Several equipments were employed in this experimental study, with the mobile furnace as the main piece of equipment employed. Another notable equipment was the oven used to dry the small cylindrical cuts from each of the CLTs. Further information on each equipment is given below.

### 3.3.1 The mobile furnace

The mobile furnace was designed and developed by DBI (The Danish Institute of Fire and Security Technology) to conduct small-scale tests. The furnace is powered by multiple electrical heating elements located on the bottom of the furnace enclosure. The power of the furnace is controlled automatically through four thermocouples installed on all four sides of the furnace, approximately 10 cm from the furnace opening. The temperature readings from each thermocouple are averaged and compared against the chosen fire curve. If the average temperature of the furnace is less than the expected temperature of the fire curve, the furnace will supply more power to heat up the heating elements. On the other hand, if the actual temperature exceeds the expected temperature, the furnace will automatically lessen the energy supplied to the heating elements. The control of the furnace is done through an in-house software installed on a computer connected to the furnace.

The mobile furnace has a horizontal opening with the size of 50 $\times$ 50 cm to place and thermally expose the specimen to the desired fire curve. The boundary of the opening is made from thermally insulating mineral stone to minimize the heat transfer from the furnace to the unexposed specimen. Different fire curves, either standard or custom-made, are possible to be carried out in the mobile furnace. However, a 15-minute pre-heating on the bottom chamber of the furnace, separated from the upper chamber by a removable CaSi board, needs to be done before the actual test to ensure that the furnace will be able to follow the ISO 834 fire curve. The mobile furnace is illustrated in Figure 3.2.

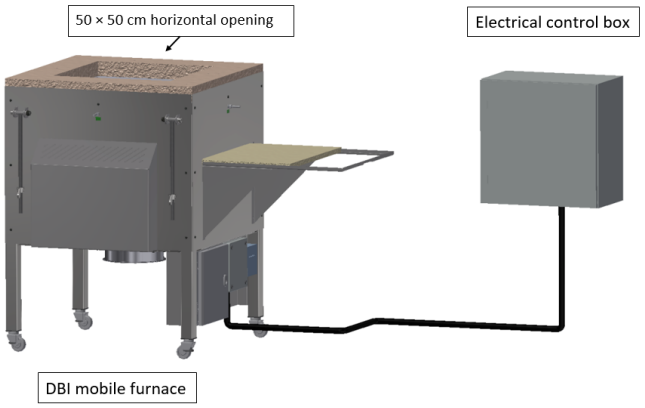


Figure 3.2: The mobile furnace

### 3.3.2 Oven

The main function of the oven is to dry the samples taken out of each CLT panel. Specifically, the oven is BINDER Model E 28, specifically made for drying and heating by BINDER. The maximum nominal temperature to be reached by the oven is 230°C. One of the key benefits of the oven is the identical test conditions all over the chamber interior, regardless of the sample size and quantity. The oven employed in this experiment is shown in Figure 3.3.


Figure 3.3: The BINDER E28 oven

## 3.4 Sample preparation

This experimental study utilized three main materials for each test: CLT panels, steel beams, and mineral wool insulation. Current industry practice employs mineral wool for better and more consistent placement of the CLT panels because of the curved internal corners on the

steel beam. The acoustic performance of the connection is also improved with the installation of mineral wool insulation. Additionally, several of the tested steel beams were protected with intumescent coatings in different coverage areas. The materials were set up together to form one assembled sample, as shown in Figure 3.4.

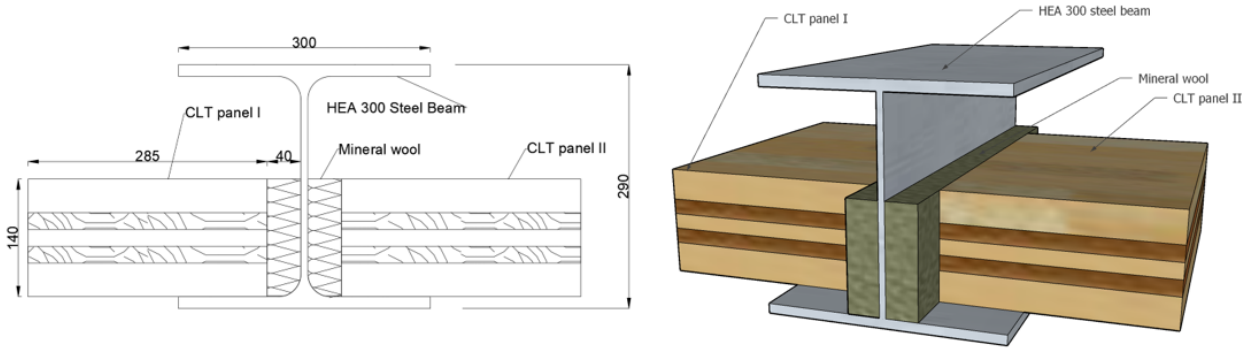


Figure 3.4: The assembled test sample: Front view (left) and 3D illustration (right)

### 3.4.1 CLT panels preparation and instrumentation

Stora Enso provided the CLT panels in this study. The initial dimension of the CLT panel is 2000 mm (length) by 450 mm (width) by 140 mm (height). The CLT panels consisted of 5 layers, adjoined by polyurethane (PUR) adhesive. The thickness of the outermost layers is 40 mm, while each of the three layers sandwiched between them has a thickness of 20 mm. The strength class of the timber used for the CLT is C24, with a maximum of 10% of timber with C16 strength class according to ETA. The timber used comes from spruce wood (*Picea Abies*). Since the surface quality of the CLT is not an important parameter of the study, the CLT panels chosen have a non-visual quality classification. Finally, the CLT panels have a density of 490 kg/m$^3$.

The CLT panel was cut and divided into seven equal parts. Each part had a length of 450 mm, a width of 285 mm, and a height of 140 mm. The newly cut CLT panel is illustrated in Figure 3.5.

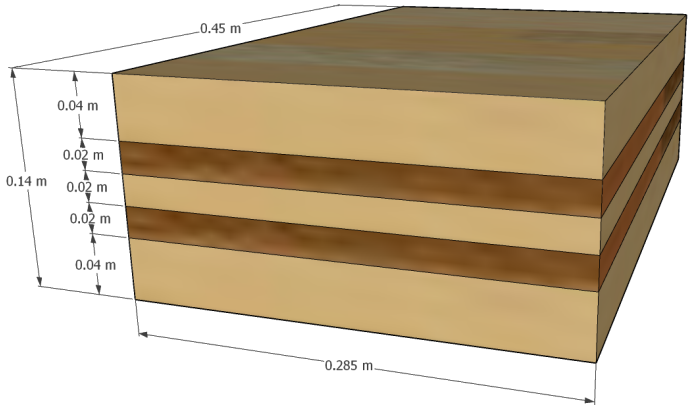


Figure 3.5: The CLT panel

Two CLT panels were used on each side of the steel beam in one experiment, as shown in Figure 3.4. The CLT panels were labelled CLT as I and CLT II. There was no difference between CLT I and CLT II; however, all the instrumentations required in the study were installed on CLT I. Additionally, CLT II was drilled vertically along its height to fit the copper chimney. The installation of the copper chimney was required as an extraction system to remove the combustible products from inside the furnace.

**CLT panel I**

In CLT I, 12 thermocouples (TC) were installed inside the CLT to monitor the CLT temperature. Two additional thermocouples, TC 13 and TC 14, were installed on the side of the CLT to measure the surface temperatures between the CLT and the mineral wool insulation at a distance of 30 mm and 60 mm from the bottom surface. The thermocouples installed at the CLT were manufactured by Guenther Polska, with the type 92-30205015-GG.V3. The thermocouples used the type K cable, with a size of 2 x 0.50 mm. The cables were covered with fiberglass and braided with another layer of fiberglass. These thermocouples were divided into two groups, as described in Table 3.2 below.

The first group of thermocouples required drilling holes from the side of the CLT with a diameter of 2 mm, similar to the diameter of the thermocouples. The holes were drilled at the middle length of the CLT panel at a depth of 50 mm from the side surface using a drill-press machine. The thermocouples were installed from the sides, parallel to the thermal wave in the CLT panels, to reduce the thermal disturbance error, which could negatively

Table 3.2: Location of thermocouples in CLT I

| **TC group** | **TC number** | **Distance (from CLT bottom surface)** | **Exposure** |
|---|---|---|---|
| First group | TC 1 | 5 mm | Protected by steel flange |
| | TC 2 | 10 mm | Protected by steel flange |
| | TC 3 | 20 mm | Protected by steel flange |
| | TC 4 | 30 mm | Protected by steel flange |
| | TC 5 | 45 mm | Protected by steel flange |
| | TC 6 | 60 mm | Protected by steel flange |
| Second group | TC 7 | 5 mm | Direct exposure |
| | TC 8 | 10 mm | Direct exposure |
| | TC 9 | 20 mm | Direct exposure |
| | TC 10 | 30 mm | Direct exposure |
| | TC 11 | 45 mm | Direct exposure |
| | TC 12 | 60 mm | Direct exposure |

affect the accuracy of the thermocouples [69][70][71]. The 50 mm depth was chosen for several reasons: First, to avoid the corner-rounding effect of the CLT if there is insufficient depth. Then, to avoid excessive error in the placement of the thermocouples if the holes were too deep. Finally, by providing enough length of the thermocouple wires parallel to the heated surface, errors caused by thermal disturbance near the tip of the thermocouples can be avoided.

After drilling, the thermocouples were inserted into the holes. The placements of the first group of thermocouples and the additional two thermocouples on the surface of the CLT panel's side can be observed below in Figure 3.6 and Figure 3.7.

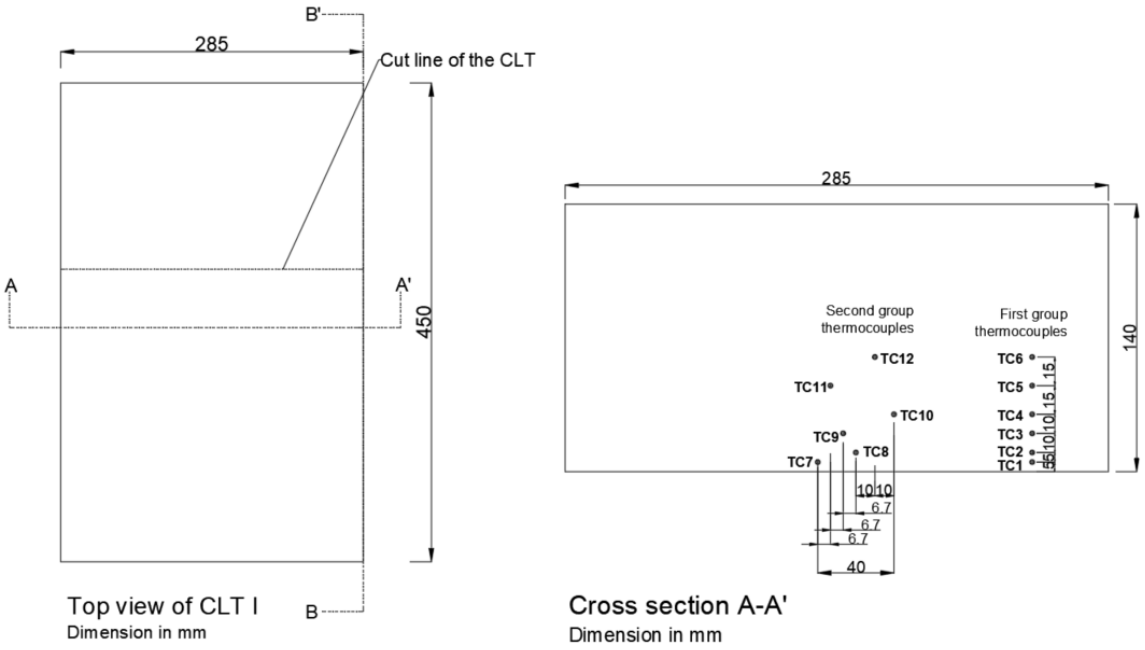


Figure 3.6: The top view (left) and cross-section A-A' (right) of CLT I

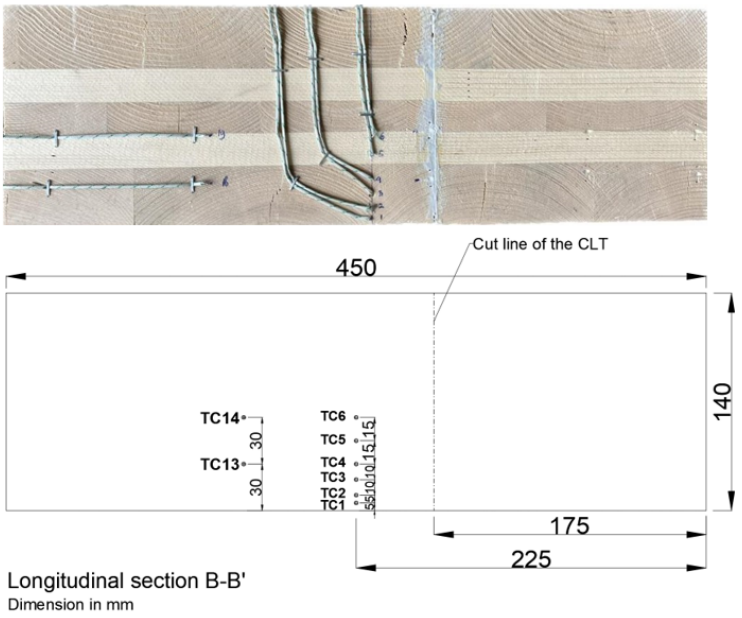


Figure 3.7: The thermocouples placement from longitudinal section B-B' of CLT I

The installation of the second group thermocouples required more steps to be taken due to their locations. The thermocouple placement of the second group is also seen in Figure 3.6. First, the CLT slab is cut using a bench saw along the cut line seen in Figure 3.6 and 3.7. Then, the holes were drilled with a depth of 50 mm to be along the same plane as the thermocouples from the first group. Grooves with the size of the thermocouple

cable had to be made using a chisel to ensure that the two pieces of CLT could be adjoined without a significant gap. Because of the grooves, the second group of thermocouples had to be distributed to minimize the loss of timber in the same vertical plane and to avoid the creation of a dense cluster of thermocouples which could impact the temperature profiles due to its highly conductive nature. Afterwards, the thermocouples from the second group could be installed according to their designated locations. The 3D illustrations to demonstrate the location of the cut on the CLT I and its look after the installation of the second group thermocouples can be seen below in Figure 3.8. After the second group of thermocouples was installed, fireproof cement was applied to the surface, as seen in Figure 3.9. The fireproof cement's function is to ensure there was no air gap that could affect the thermocouple readings. Then, the two pieces of CLT are clasped together with a steel clamp.

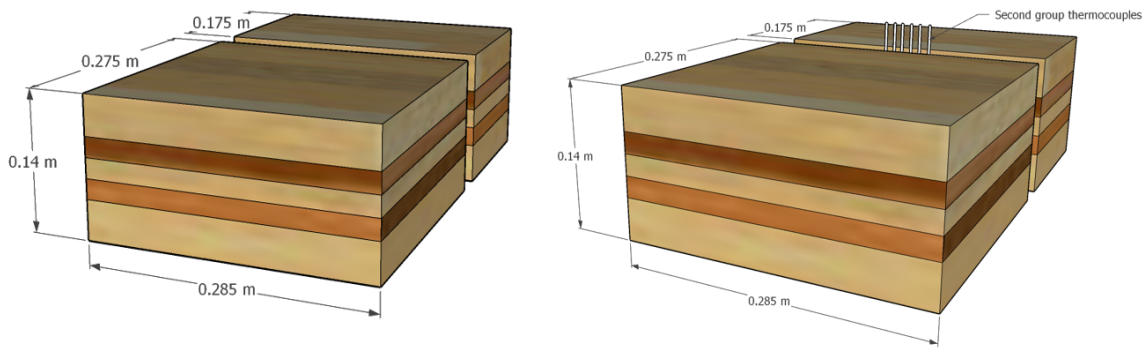


Figure 3.8: Illustrated CLT I with the cut (left), and after installation of the second group thermocouples

Figure 3.9: Installation of second group thermocouples (left), and application of fireproof cement

**CLT panel II**

The preparation of CLT panel II only required drilling vertically to fit a copper chimney. The copper chimney has a diameter of 52 mm with a length of 650 mm, as seen in Figure 3.10. After completing the preparation on CLT panels I and II, the CLT panels were stored in a conditioning room. The conditioning room had a relative humidity of 50 $\pm$ 5 % and a temperature of 23 $\pm$ 2°C. The CLT panels were stored for at least 24 hours before performing the test to ensure that the panels had a uniform moisture content.

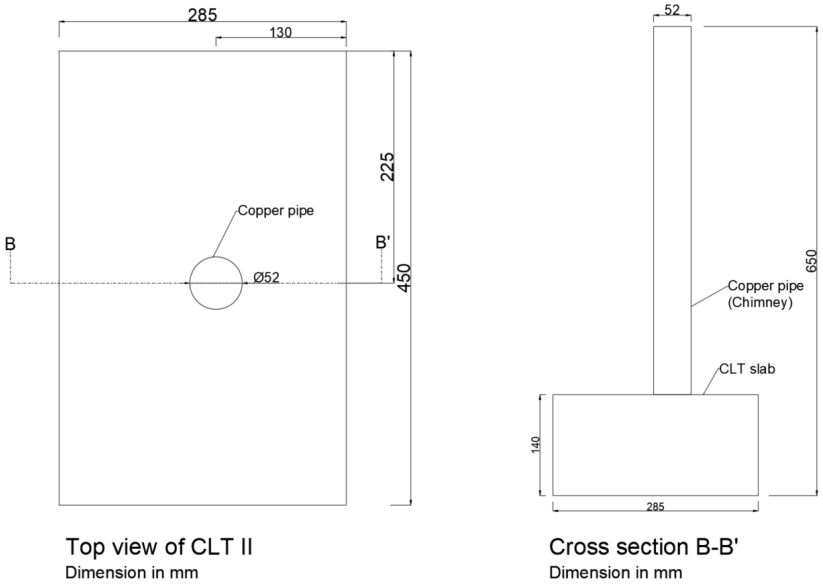


Figure 3.10: The top view (left) and cross-section B-B' (right) of CLT II

### 3.4.2 Steel beams preparation and instrumentation

The current experimental study required 6 steel beams, as previously shown in the test matrix (Table 3.1). The beams used were HEA 300 steel beams with an individual length of 600 mm. Compared to the I steel beam of similar size and class, the H beam has a thicker web and wider flanges, enabling it to carry a higher load.

The steel beams preparation started with the application process of epoxy intumescent coating. The epoxy intumescent coating will be referred to as Product A, which was applied professionally and provided by AkzoNobel along with the steel beams. Therefore, the steel beams preparation and instrumentation were conducted by AkzoNobel at their facility.

Although Product A is an epoxy intumescent coating, it was specifically designed for cel-

lulosic fire. In the construction industry, the intumescent coating's dry film thickness (DFT) is designed based on the steel's section factor, the number of exposed sides, the desired fire resistance period and limiting temperature. This data, however, was developed based on furnace tests of the individual steel member. Since the interaction between materials in the hybrid connection wasn't considered, the provided data by the manufacturer might be too conservative or insufficient to protect the steel. Additionally, several types of configurations of the hybrid connection would limit the exposed sides of the steel beam. For example, the chosen setup for the test sample (Figure 3.4) limits the fire exposure to only the bottom flange of the steel. Because of the limitations on research and knowledge, the steel will be fully covered with the intumescent coating as a standard procedure, although the exposure is limited. This procedure could potentially increase the project's price for the redundancy in the intumescent coating.

The main variable in this experimental study is the protection coverage of the intumescent coating. In test 1, the steel beams were unprotected, beams in test 2 were partially protected, and in test 3, the beams were fully protected. As previously explained, one of this study's objectives is to investigate the effect of different protection coverage on the hybrid connection. Regardless of the protection coverage, all six steel beams underwent surface preparation and primer application process. Prior to the application of the intumescent coating, the thermocouples on the steel were installed.

For test 1.A-B, there were 20 thermocouples installed on the steel beams. The layout of the thermocouples for test 1.A-1.B can be seen in Figure 3.11 Meanwhile, there were 24 thermocouples installed on each of the steel beams for test 2.A-B and 3.A-B. The layout is seen in Figure 3.12. For the steel beams, the type of thermocouples used were type-K Inconel sheathed thermocouples with a diameter of 2 mm.

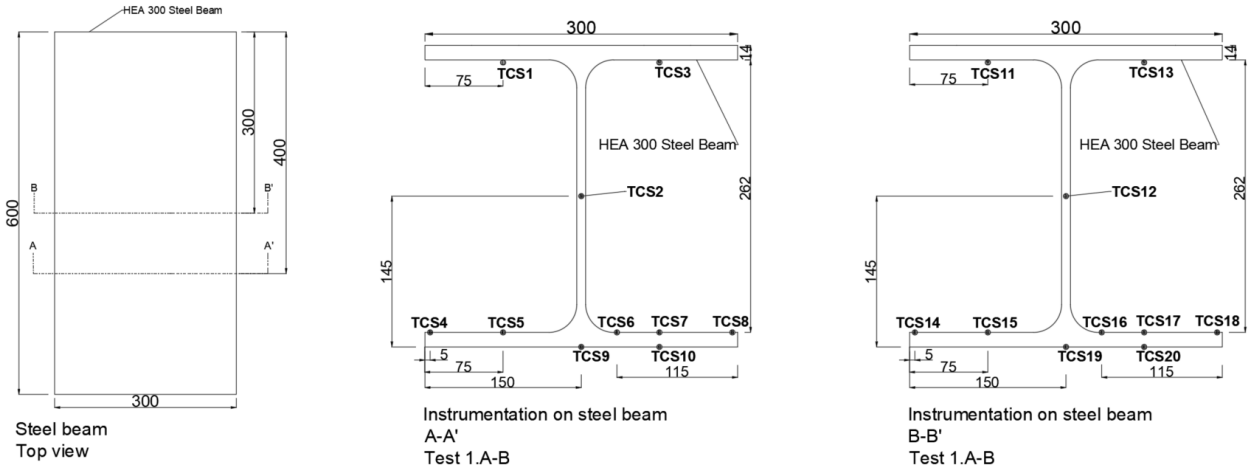


Figure 3.11: The top view of the beam (left), cross-section A-A' (centre), and B-B' (right) of test 1

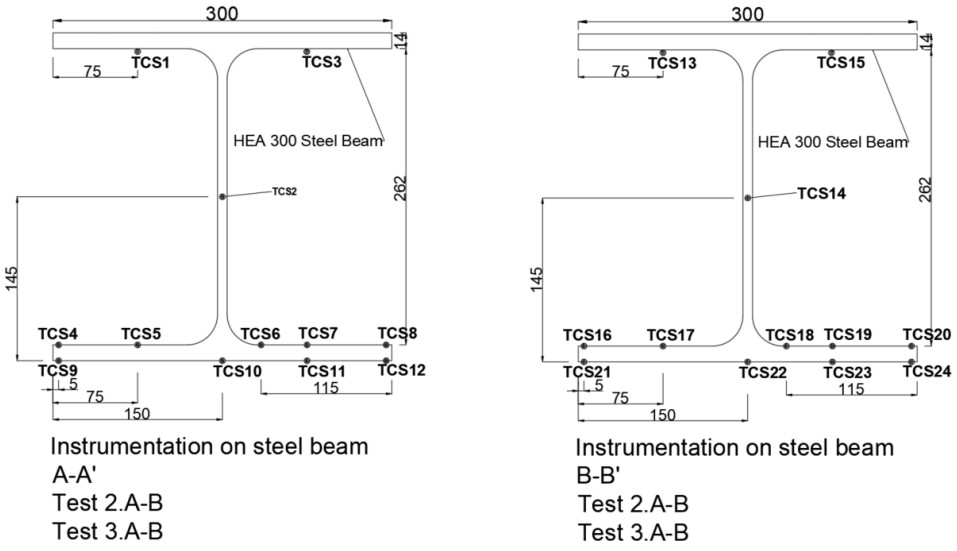


Figure 3.12: The cross-section A-A' (left) and B-B' (right) of tests 2 and 3

Once the thermocouples were installed, the epoxy intumescent coating was applied to the steel beams according to the different protection coverage (refer to Table 3.1). The epoxy intumescent coating's dry film thickness (DFT) on the steel beams was calculated based on a 3-sided exposure with a section factor of 126 $m^{-1}$ for a limiting temperature of 300°C and fire resistance period of 60 minutes. The same dry film thickness was applied on the steel beams, regardless of the coverage area. Figure 3.13 below illustrates the difference between the protection coverage.

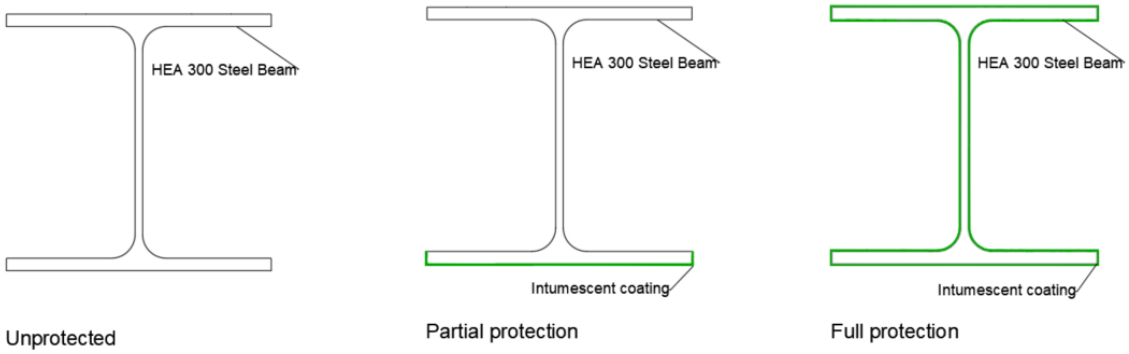


Figure 3.13: The different protection coverage on the steel beams

After the preparation of the steel beams was finished, the steel beams were then sent to DBI, where the test would take place.

## 3.5 Experimental procedures

This section describes the experimental procedures performed on the previously described samples using the testing equipments.

### 3.5.1 Moisture content test

The procedure in testing the moisture content of the CLT samples followed the ASTM D4442 standard: Method B. Six samples, one from each test, were weighed before each test in order to measure the original weight ($A$) and then oven-dried at a temperature of 103°C. Once dried, the samples were then weighed again to obtain the oven-dry mass ($B$). The moisture contents were then calculated as:

$$MC(\%) = (A - B) \div B \times 100 \tag{3.1}$$

### 3.5.2 Mobile furnace test

Before running the mobile furnace test, several preparations must be conducted. The preparation steps taken are:

1. Remove the CLT panels to be tested from the conditioning room to the testing room 2 hours before the test

2. Install the copper chimney on CLT panel II
3. Install mineral wool insulation on all four sides of the CLT panels to avoid fire spreading to the side surfaces of the panels
4. Connect thermocouples on the CLT panel and in the steel beam to the data logger
5. Install mineral wool insulation on the furnace opening boundaries to ensure there was no open gap between the furnace and the specimen

The test procedure started with turning on the smoke extraction system in the testing hall. Then, the mobile furnace was turned on, and the appropriate fire curve was loaded into the software. The next step taken was to turn on the data logger and check whether there were any irregularities in the thermocouple readings, which could be caused by either a bad connection to the data logger or damaged thermocouples. Next, the mobile furnace was preheated for a minimum time of 15 minutes. After finishing the preheat, the mobile furnace's top and bottom chamber, where the heating elements are located, are separated by a CaSi board. The top chamber is cooled down with the help of a fan to a temperature below 50°C to minimize the effect of elevated temperature on the sample prior to starting the test. Afterwards, the specimen was put on top of the steel furnace, starting with the steel beam and then the CLT panels. Adjustment of the specimen's placement was made, the CaSi board was then removed, and the furnace test could be started.

The fire curve chosen for the test was the ISO 834 fire curve, a standard time-temperature curve commonly used in fire resistance tests for building materials and structural elements representing cellulosic fire [72]. Additionally, ISO 834 fire curve is also used in Eurocode 5 [55], where two calculation methods were presented to generate the fire design of timber structures exposed to the fire curve. The timber char depth exposed to ISO 834 fire curve could also be predicted by the reduced cross-section method from Eurocode 5.

The ISO 834 fire curve is described through the following equation:

$$\Delta\theta(t) = T_o + 345 \times \log_{10}(8t + 1) \tag{3.2}$$

where the $\triangle\theta(t)$ is the furnace temperature at time $t$ in °C, $T_o$ represent the initial furnace temperature, and $t$ is the time in minutes.

The tests lasted for 60 minutes, which corresponded to the designed fire resistance time for the epoxy intumescent coating. Figure 3.14 shows an example of the test. Once the test had finished, the furnace and the data logger were turned off, the CaSi board was put back inside the furnace to stop the heat exposure to the sample, and the CLT panels were removed and extinguished by water. Once the panels were quenched, the char layer from CLT panel I was removed carefully not to damage the remaining timber. Finally, the remaining timber thickness was measured for every centimeter of the CLT panel's width.

The remaining timber thickness would be used to calculate the charring rate and depth for the area directly exposed to fire and the area protected by steel flange. The calculations from the actual measurement will be compared with the charring rate and depth from thermocouple measurements. With this method, the char-line position is determined based on the 300°C isotherm, based on [55].

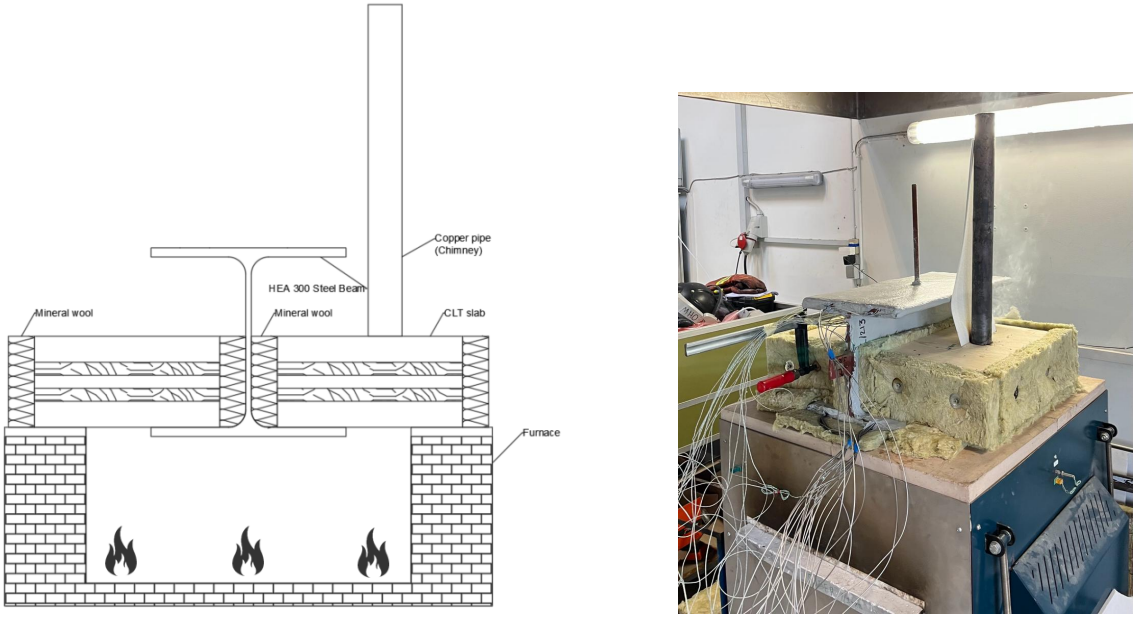


((a)) Vertical cross-section of the test rig and specimen

((b)) Furnace test (Example test 3.B)

Figure 3.14: The mobile furnace test

# Chapter 4

# Results and discussion

## 4.1 CLT moisture content

Before the start of each test, a small section is taken out from the CLT panel to be tested for moisture content (MC). The moisture content of CLT is important to the dimensional stability (CLT panel expands when MC increases and contracts when MC decreases), durability (higher MC increases CLT panel's susceptibility to mould growth), and the strength and stiffness of the CLT (higher MC reduces the strength of CLT panel) [23]. On the other hand, higher moisture content helps with the fire resistance of the CLT panel since the moisture will help to absorb the heat during a fire. The result of the moisture content measurement of the CLT panels can be seen in Table 4.1.

Table 4.1: The moisture content in the six tests

| Test | 1.A | 1.B | 2.A | 2.B | 3.A | 3.B |
|---|---|---|---|---|---|---|
| Intial weight (gr) | 23.17 | 24.41 | 24.76 | 18.86 | 25.15 | 26.02 |
| Dried weight (gr) | 20.9 | 22.12 | 22.28 | 17.03 | 22.7 | 23.49 |
| Moisture content (%) | 10.86 | 10.35 | 11.13 | 10.75 | 10.79 | 10.77 |

The table shows that the values of the moisture content fall between 10.35 – 11.13%, consistent with the data provided by the manufacturer of the CLT panels, where the MC should be between 6 – 15% according to EN13183-2.

## 4.2 Furnace temperature

The main experimental tests on the furnace were conducted with the ISO 834 standard fire curve. However, furnace temperature differences are still expected from test to test; thus, it is important to evaluate and compare the furnace temperature evolution of each test with the ISO 834 fire curve. The comparison is presented in Figure 4.1.

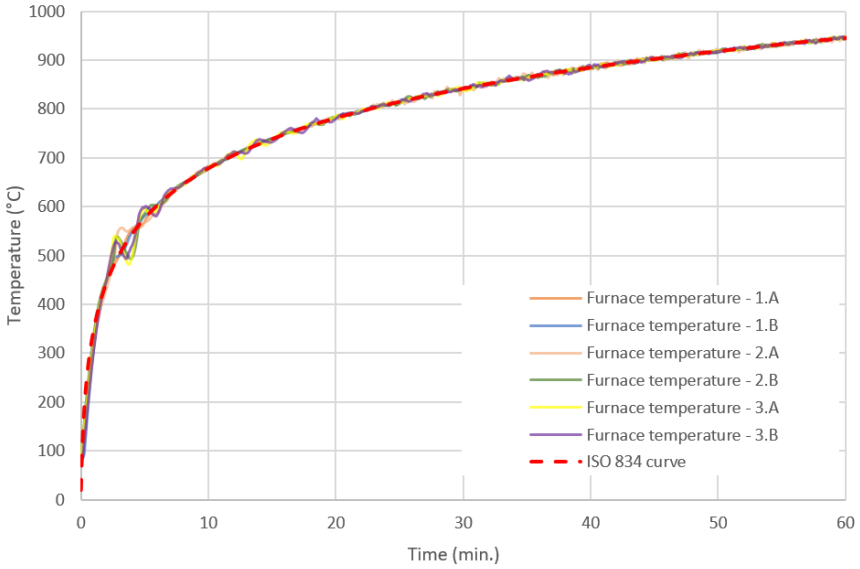


Figure 4.1: The furnace exposure in the six tests

From the figure, it can be observed that the furnace temperatures in all six tests were able to follow the ISO 834 fire curve closely. Additionally, fluctuations in the furnace temperatures started to be seen when the furnace temperature was between 400°C – 600°C, which was caused by the significant increase in pyrolysis gases production from the pyrolysis [73]. The abundance of pyrolysis gases resulted in a sudden increase in the combustion intensity. Due to the sharp increase in temperature, the furnace automatically reduced the energy supplied to the heating elements to prevent further offset from the fire curve, explaining the drop in temperature after the sharp increase. The furnace showed a good capability to compensate for the increase in the temperatures from the contribution of the CLT panels to the fire dynamics during the test, keeping the difference in temperatures to be less than 10%. Furthermore, a closer inspection revealed that the fluctuations lasted for less than five minutes; thus, the impact of the fluctuations on the overall results should be insignificant.

## 4.3 CLT panels temperature

### 4.3.1 Test 1

The temperature evolution for test 1, where the steel beams were unprotected, is presented in Figure 4.2 below. Figure 4.2(a) and 4.2(b) shows the temperature evolution from the area directly exposed to fire and from the area protected by the steel flange. Each color represents a CLT depth, corresponding to Table 3.2. Additionally, the results from test 1.A is shown in the solid lines, while the result from test 1.B is presented in the dashed lines.

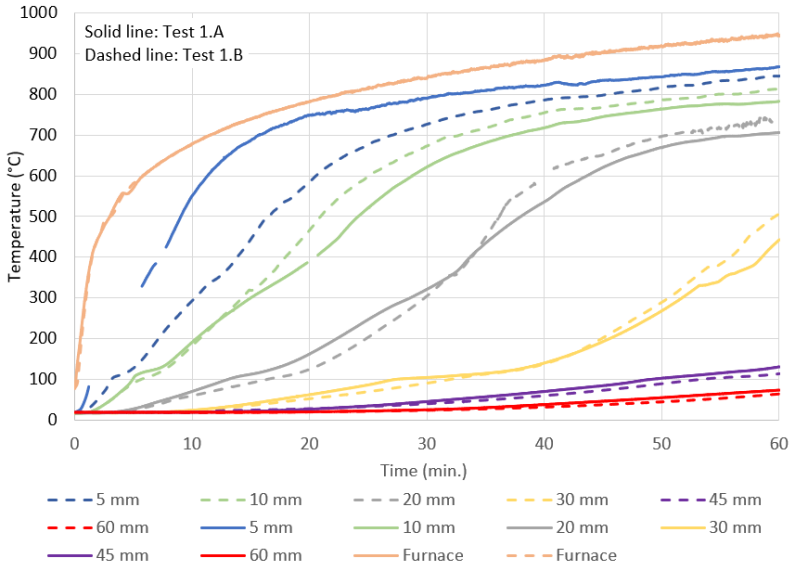


((a)) Directly exposed to fire

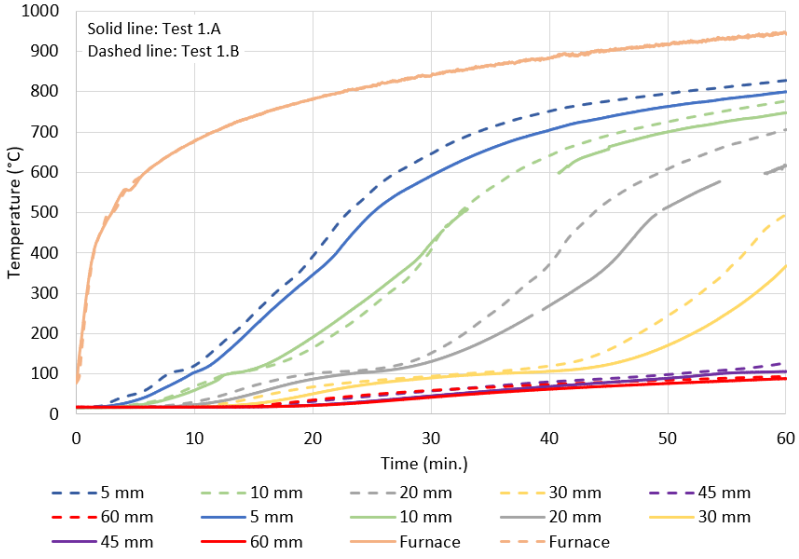


((b)) Protected by steel flange

Figure 4.2: CLT temperature evolution from test 1

During the test, the thermocouples could produce bad readings when the connections between the two metal wires experienced disturbance. Therefore, these data were erased, explaining the existence of empty gaps in a particular line.

Looking at the two graphs, Figure 4.2(a) shows temperature evolution from the area directly exposed to fire, while Figure 4.2(b) displays the temperature evolution from the area protected by steel flange.

Additionally, there is minimal difference in the actual furnace time-temperature curve between test 1.A and test 1.B. However, differences could be observed in the CLT temperature readings on Test 1.A and test 1.B, especially in the first 30 minutes of the tests in Figure 4.2(a). The maximum difference between test 1.A and 1.B was seen in minute 16 on the 5 mm depth, where the temperature was recorded at 710°C and 498°C for test 1.A and test 1.B consecutively. As the tests progressed, the difference became smaller, and by the end of the tests, the difference between the two tests was only 23°C, a stark contrast from the maximum difference at 212°C. The natural variation in each test caused the differences, such as the crack formation on the char layer. Another possible source of discrepancies came from errors in drilling the holes for the thermocouples. However, comparing the result from test 1.A and 1.B showed the same trend of temperature evolution in all depths.

An alternative presentation of the temperature evolution in the CLT panels can be found in Appendix A, where the data is presented as a temperature vs depth profile.

Figure 4.3 consists of two graphs comparing the temperature evolution of the CLT in the area directly exposed to the fire with the area protected by the steel flange for test 1.A and test 1.B. The two graphs below show small differences in the final temperatures after 60 minutes for equal depth. Still, the difference in the temperature increase rate is more evident. This can be noticed from the steeper incline in the temperatures from the graphs. In the CLT area protected by the steel flange, the temperature evolution at a depth of 5 mm and 10 mm was shown to be similar to the temperature evolution at a depth of 10 mm and 20 mm from the area directly exposed to the fire. Therefore, the graphs show that the unprotected steel flange contributed to reducing the heat transferred to the CLT panels adjacent to it.

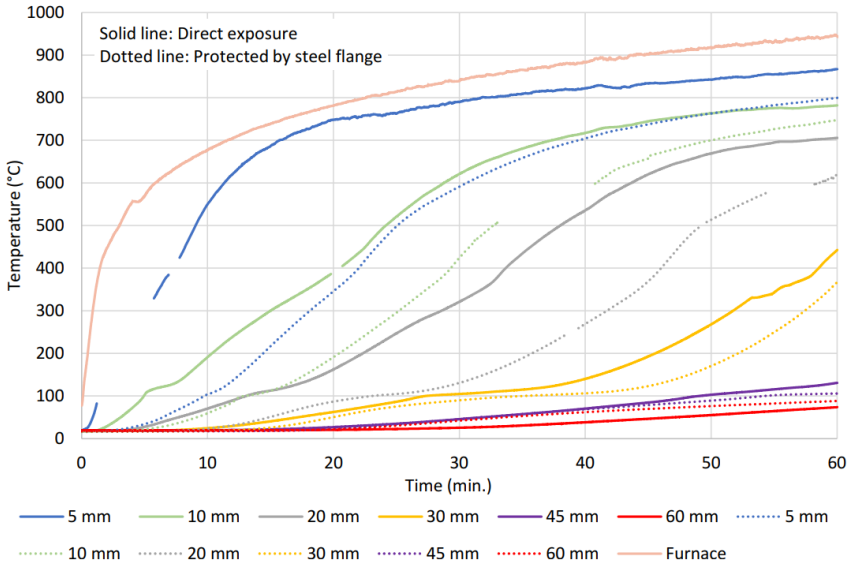


((a)) Test 1.A

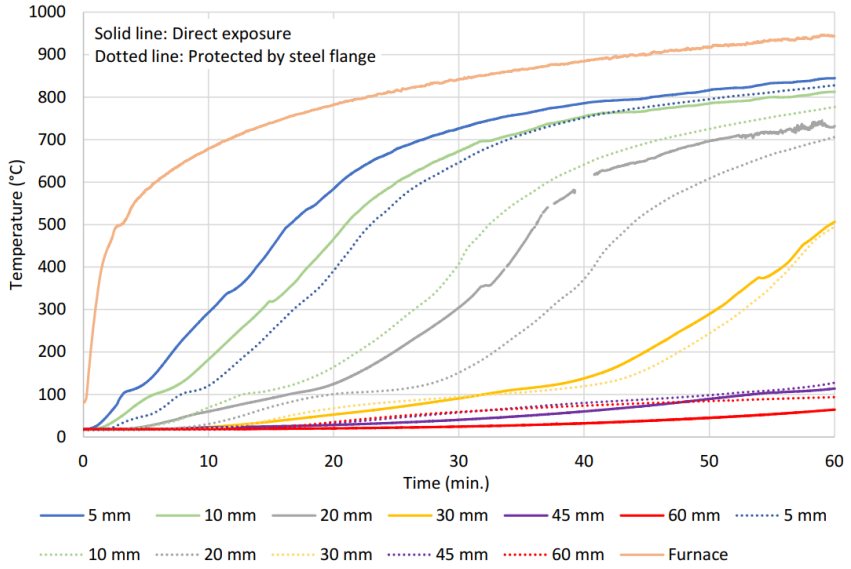


((b)) Test 1.B

Figure 4.3: CLT temperature evolution comparison between the area directly exposed and the area protected by flange

### 4.3.2 Test 2

Figure 4.4 displays the temperature evolution of the CLT from test 2, where the bottom flange of the steel beams was protected with the epoxy intumescent coating. Figure 4.4(a) shows the reading results from the area directly exposed to fire, while Figure 4.4(b) shows the reading results from the area protected by steel flange. Solid lines represent the results from test 2.A, and dashed lines from test 2.B.

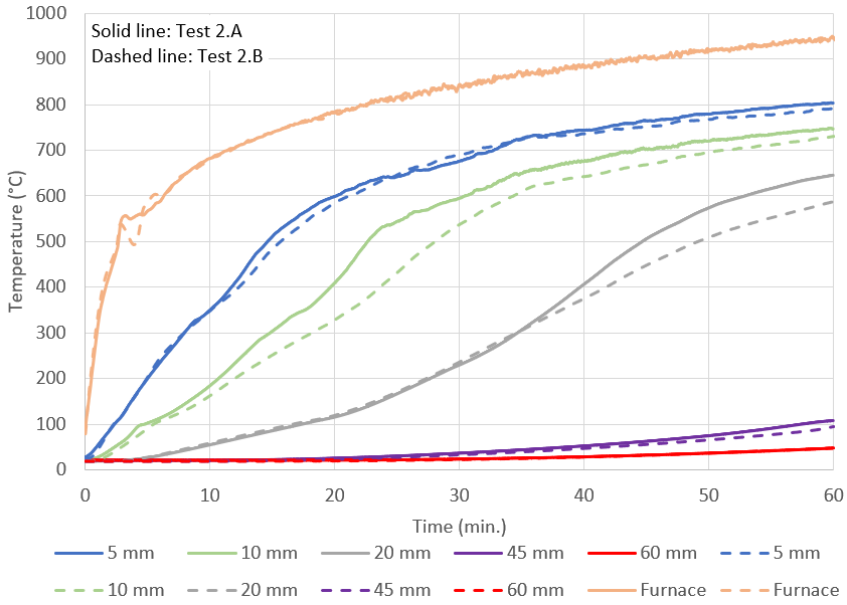


((a)) Directly exposed to fire

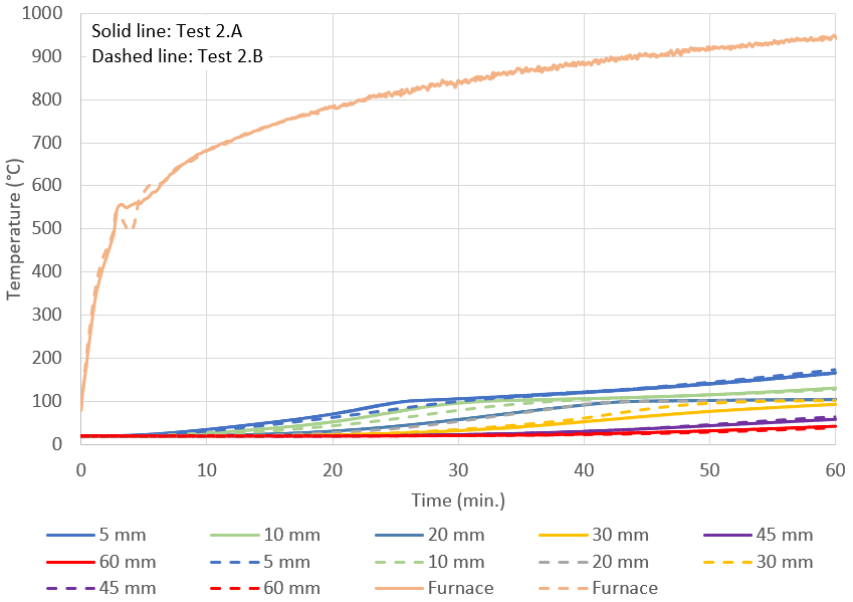


((b)) Protected by steel flange

Figure 4.4: CLT temperature evolution from test 2

All around, the results from test 2.A and test 2.B showed good agreement with minor discrepancies, which can be seen in Figure 4.4(a) on the 10 mm and 20 mm depth. The discrepancies were to be expected because of the natural variations in the experiment.

In Figure 4.4(b), we can see that the increase in temperature of the CLT plateaued at 100°C before increasing again after a period of time. At 100°C, the heat transferred is used to evaporate the moisture content of the CLT; thus, the temperature increase was halted. Once the moisture had been evaporated and the CLT dried, the heat transferred would be

used to heat up the CLT and increase its temperature.

In Figure 4.4(a), the data set from the depth of 30 mm were removed because the placement of the thermocouples was too close to the steel flange border, resulting in data that weren't deemed to be representative of the area directly exposed to the fire. This is illustrated in Figure 4.5 below.

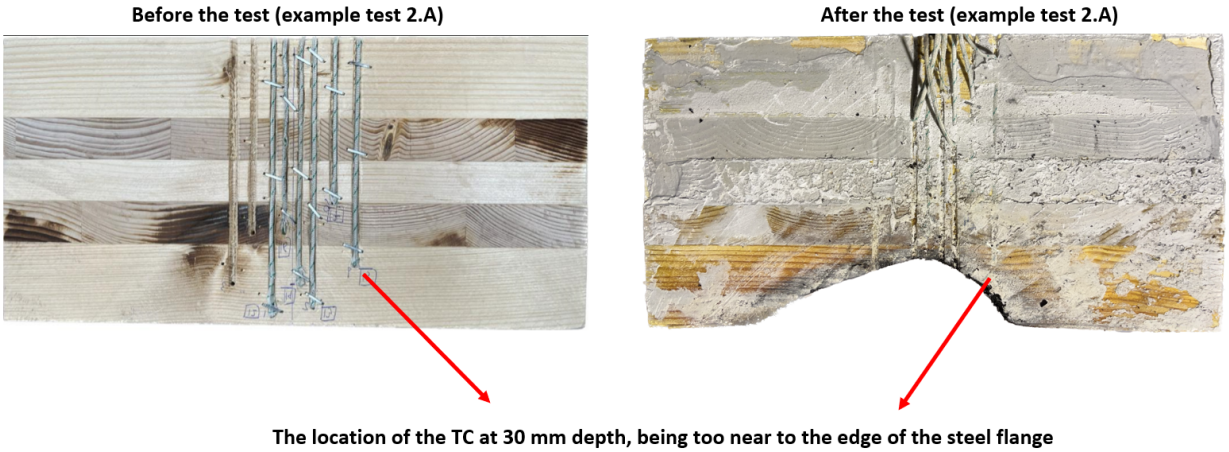


Figure 4.5: The placement of the thermocouple at 30 mm depth (direct exposure)

An alternative presentation of the temperature evolution in the CLT panels can be found in Appendix A, where the data is presented as a temperature vs depth profile.

In Figure 4.6, the two graphs show the temperature evolution comparison between the CLT area directly exposed to the fire and the CLT area protected by the steel flange. Figure 4.6(a) shows the comparison from test 2.A, while Figure 4.6(b) displays the comparison from test 2.B.

Unlike the result from test 1, in 4.3.1, the temperatures in the area of CLT protected by steel flange are substantially lower compared to the area directly exposed to fire. The graphs below in Figure 4.6 show that in the CLT area protected by the steel flange (represented by the dotted lines), none of the temperature readings reached 300°C, which means there is no charring at the depth measured. The graphs demonstrated that partial protection on the bottom flange of the steel flange with intumescent coating helped to prevent the charring on the adjacent CLT panels. This is consistent with the observation of the actual CLT panel after the test.

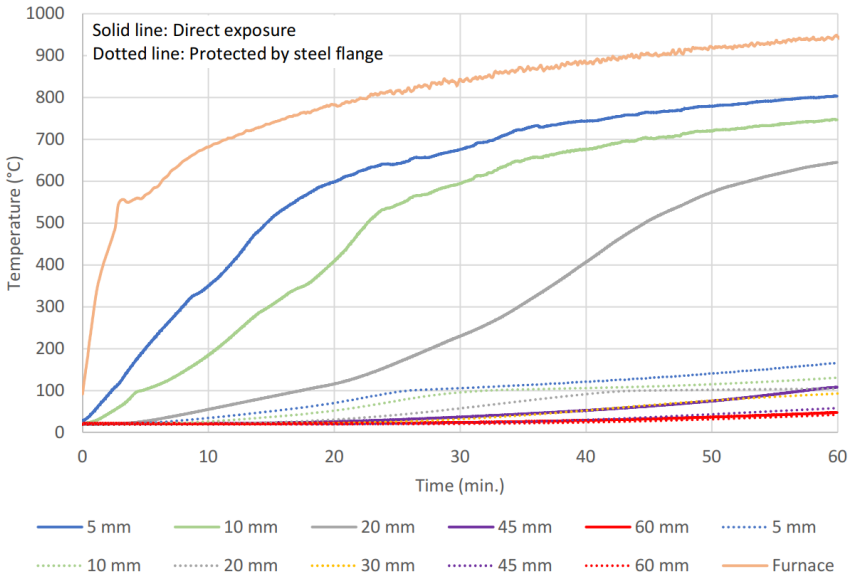


((a)) Test 2.A

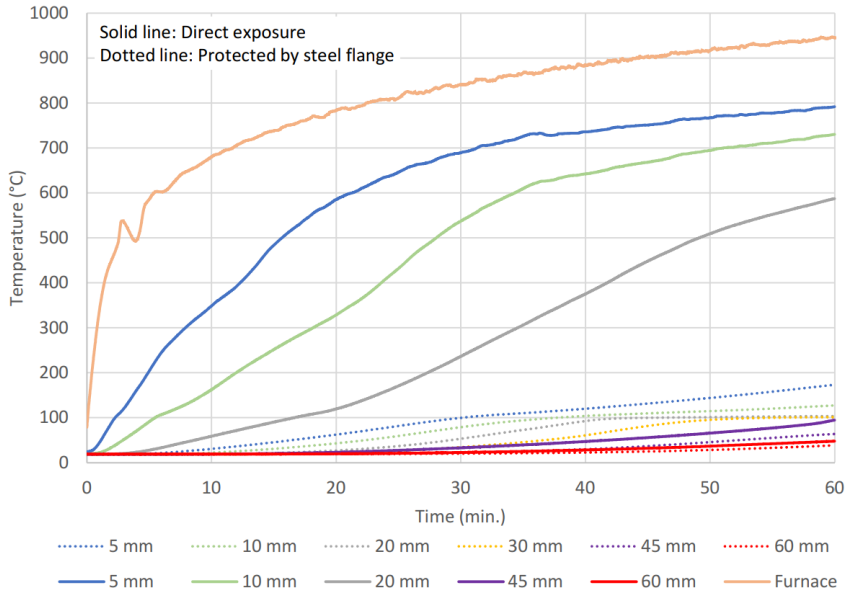


((b)) Test 2.B

Figure 4.6: CLT temperature evolution comparison between the area directly exposed and the area protected by flange

### 4.3.3 Test 3

The temperature evolutions of the CLT from test 3 are displayed in Figure 4.7 below. Figure 4.7(a) shows the temperature evolution from test 3.A and 3.B from the CLT area directly exposed to the fire, while Figure 4.7(b) depicts the temperature evolution from test 3.A and 3.B from the CLT area protected by the steel flange. In test 3, the steel beams were completely covered by the epoxy intumescent coating. Similarly to Test 2, Figure 4.7(a)

excluded the readings from the thermocouples at 30 mm depth due to their placement not being deemed to be representative of the CLT area directly exposed to the fire. Solid lines in the graphs depict the result from test 3.A, and the dashed line from test 3.B.

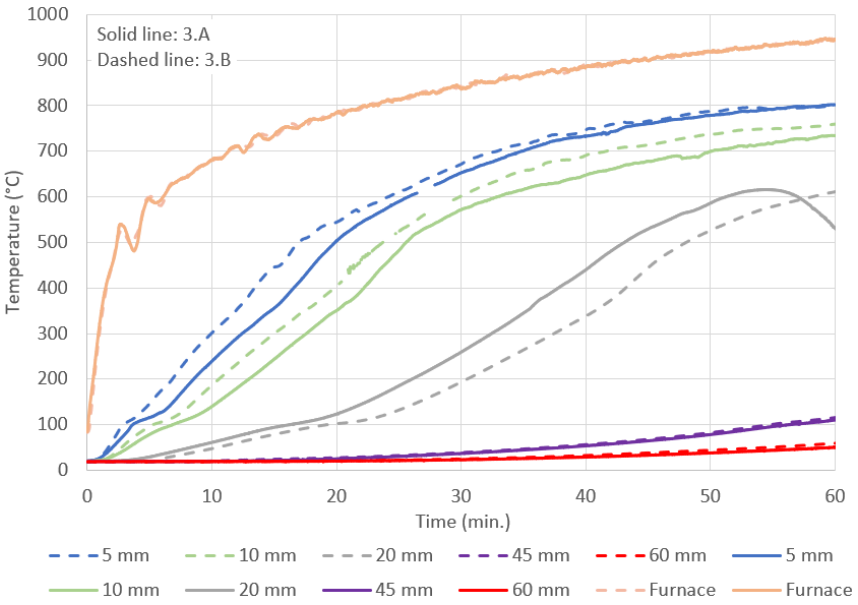


((a)) Directly exposed to fire

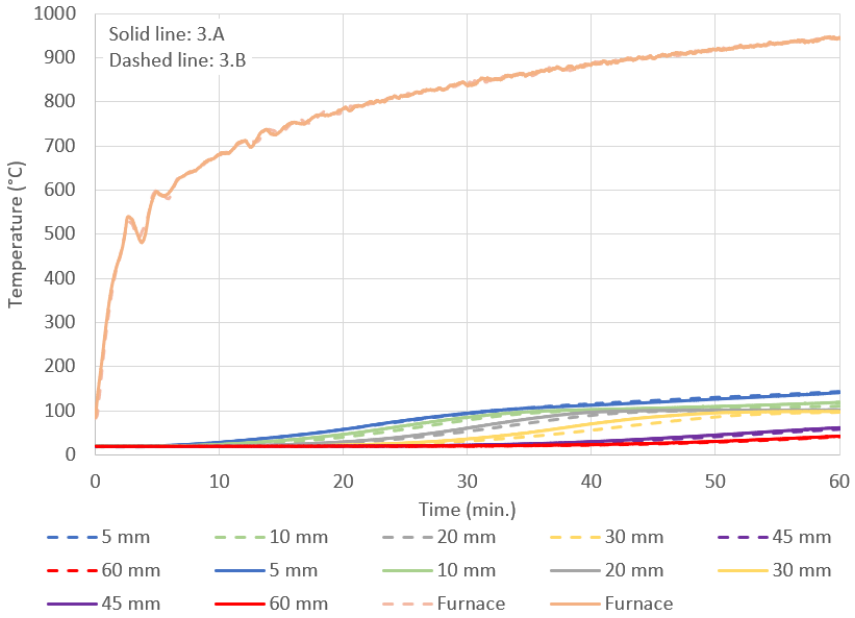


((b)) Protected by steel flange

Figure 4.7: CLT temperature evolution from test 3

Based on the figures above, small differences were found between test 3.A and 3.B. In Figure 4.7(a), the minor discrepancies could be seen at the temperature readings on 5 mm, 10 mm, and 20 mm depth. The minor differences could be caused by the difference in moisture

content of the CLT panels and the size of air gap between the specimen and furnace, which affect the oxygen availability for the combustion. Figure 4.7(b) revealed smaller differences between test 3.A and 3.B.

Figure 4.8 displays the two graphs comparing the temperature evolution from the CLT area directly exposed to the fire and the CLT area protected by the steel flange. Figure 4.8(a) portrays the comparison from test 3.A, while Figure 4.8(b) illustrates the comparison from test 3.B.

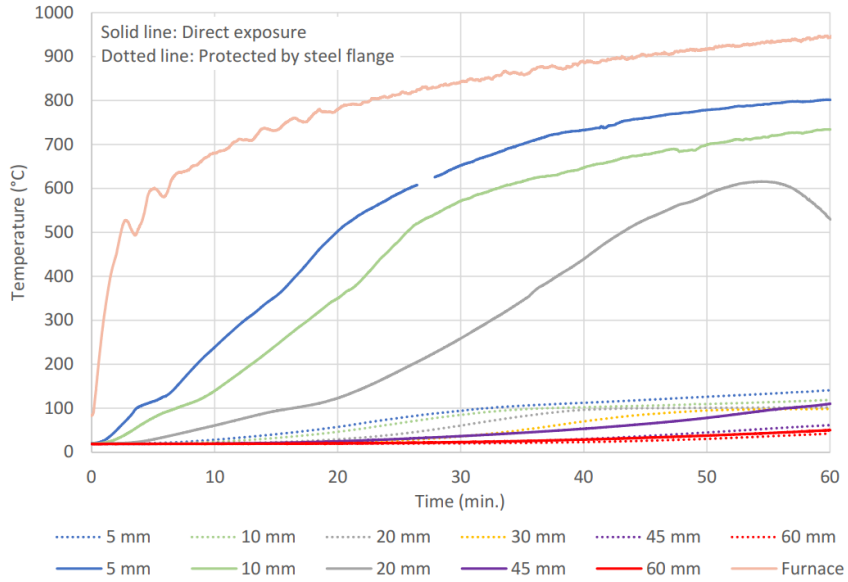


((a)) Test 3.A

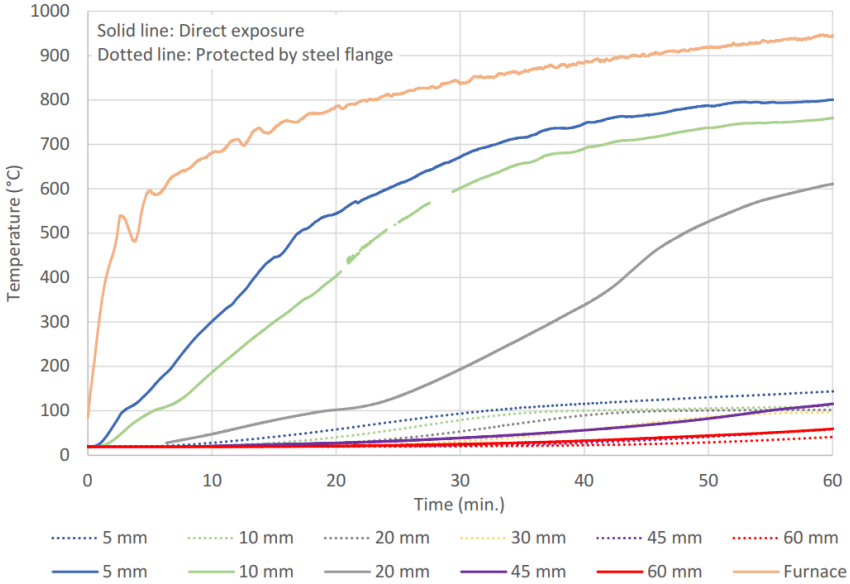


((b)) Test 3.B

Figure 4.8: CLT temperature evolution comparison between the area directly exposed and the area protected by flange

From the two graphs in Figure 4.8, we can see that the temperatures in the CLT area protected by the steel flange are greatly lower than in the area directly exposed to the fire, much like in test 2. For comparison, the temperature at 5 mm depth on test 3.A and 3.B for the area directly exposed to the fire reached 800°C after 60 minutes, while for the same depth, the area protected by steel flange stayed below 150°C. Full protection of the steel beam with intumescent coating was proven to be effective in preventing charring on the adjacent CLT.

An alternative presentation of the temperature evolution in the CLT panels can be found in Appendix A, where the data is presented as a temperature vs depth profile.

### 4.3.4 Further comparison and discussion

#### CLT area directly exposed to the fire

From the previous discussion, we saw that there are slight differences in the CLT temperature of the area directly exposed to the fire, depending on the protection coverage on the steel beams. The differences can be seen in Figure 4.9 below, which compares the CLT temperatures from this area from test 1.B, test 2.B, and test 3.B.

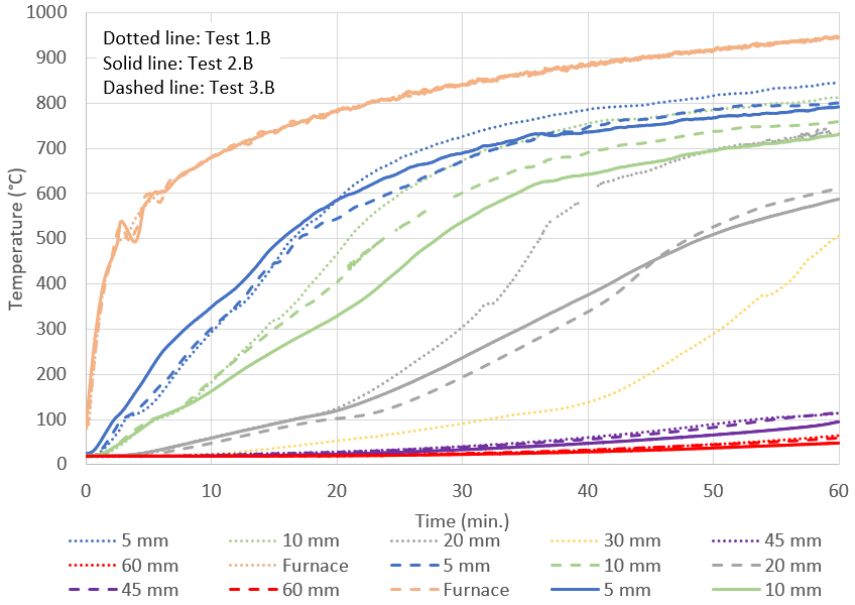


Figure 4.9: The CLT temperature evolution (direct exposure) for test 1.B, 2.B, and 3.B

The result from test 1.B is shown in dotted lines, while test 2.B is in solid lines, and test 3.B in dashed lines. While the results from test 2.B and test 3.B are similar, the differences

could be noticed when comparing the results to test 1.B. The overall temperatures are lower in tests 2 and 3 compared to test 1 in the area directly exposed to fire.

This could be explained because, in test 1, the thermocouples on the directly exposed area were placed close to the unprotected steel flange. Therefore, the CLT and subsequently the thermocouples absorbed more heat from the heated steel flange. In tests 2 and 3, intumescent coating on the bottom flange of the steel beam managed to limit the temperature of the steel flange and heat transfer to the CLT, limiting the heat transferred from the steel flange to the thermocouples on the CLT area with direct exposure.

### CLT area protected by steel flange

For the CLT area protected by steel flange, the obvious difference lies in test 1 compared to test 2 and test 3. Since there was no protection on the steel beam of test 1, the heat absorbed by the steel flange is then conducted to the adjoined CLT. As a consequence, the CLT was then ignited and burned. The stark difference is shown in Figure 4.10 below.

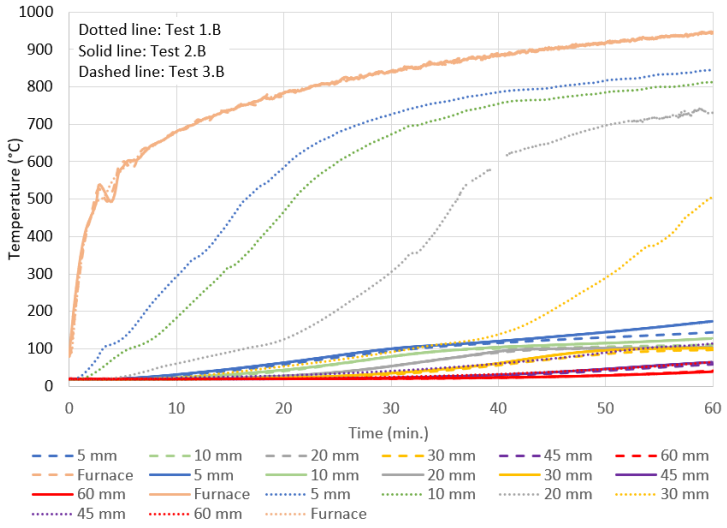


Figure 4.10: The CLT temperature evolution (protected by flange) for test 1.B, 2.B, and 3.B

The temperature evolution from test 3 follows a similar trend as the result from test 2. As the bottom steel flange was protected with epoxy intumescent coating in test 2 and test 3, the heat absorbed by the bottom flange was limited. Hence, the heat conducted to the CLT also became lower. Upon closer inspection, displayed in Figure 4.11, reveals that compared to test 3, the overall temperature at the area of CLT protected by steel flange is

higher in test 2 by a maximum of 20% found on the 5 mm depth. The temperature evolution is similar on all depths until the temperature reaches 100°C. In test 2, the moisture content evaporation is quicker than in test 3, resulting in a steeper inclination past the 100°C. This is caused by the application of epoxy intumescent on the top part of the bottom flange in test 3, thus further reducing the heat transferred through conduction from the steel to the CLT panel.

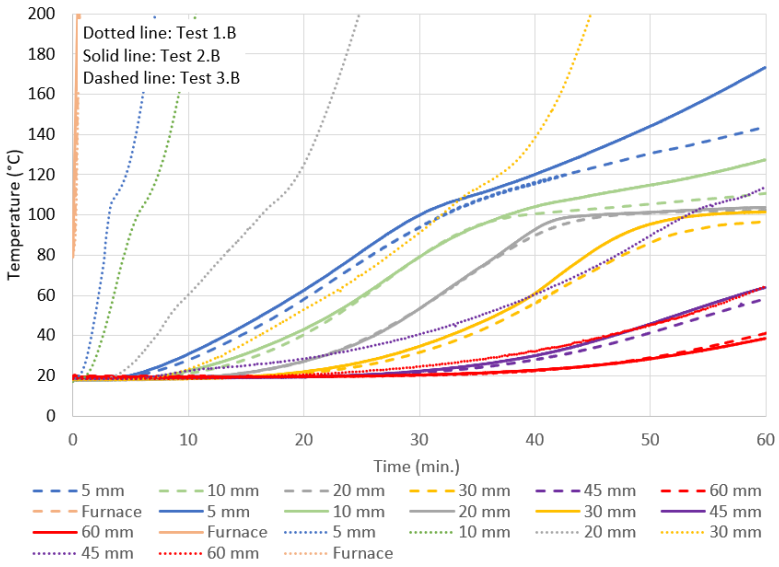


Figure 4.11: The CLT temperature evolution (protected by flange) for test 1.B, 2.B, and 3.B

## 4.4 CLT-insulation temperature

As previously explained in 3.4.1, two thermocouples were installed on the surface of the CLT to record the temperature evolution between the CLT and the mineral wool insulation. The thermocouples were placed at 30 mm and 60 mm from the bottom surface of the CLT. The temperature evolution from these thermocouples was compared and presented in Figure 4.12 below. For the purpose of demonstration, only results from test A were used.

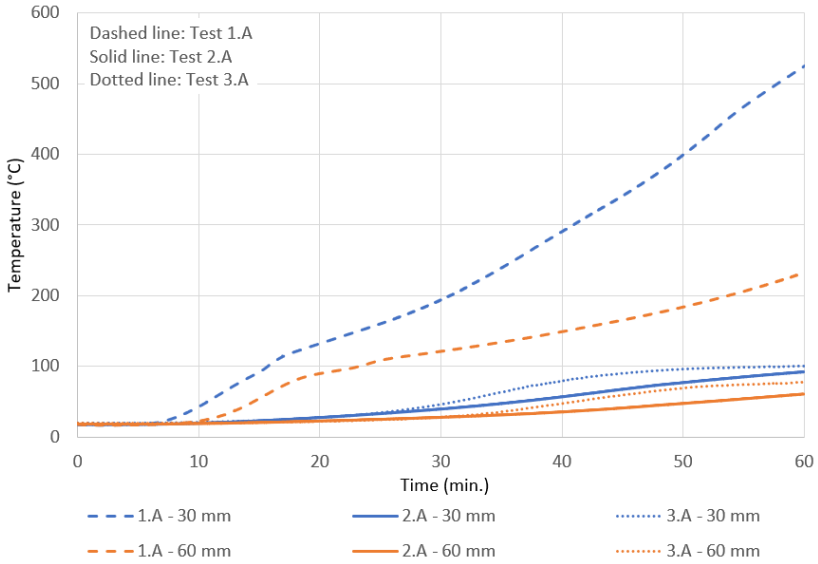


Figure 4.12: The CLT-insulation temperature

As expected, the thermocouples recorded higher temperatures on test 1, exceeding 300°C at a depth of 30 mm at approximately 40 minutes of the test. This contrasts with the results from test 2 and test 3, where the final temperatures didn't exceed 100°C after 60 minutes of the tests. The graph further strengthens the result from 4.3 that in test 1, the CLT panels in the area protected by the steel flange were charred, unlike in tests 2 and 3.

## 4.5 Steel beams temperature

As a structural member, the steel beams' temperatures are important to assess the load-bearing capacity at elevated temperatures. This section will present the temperature evolution graphs from the three categories. However, only several thermocouples were chosen to be displayed in the graphs below. The thermocouples were chosen to represent the temperatures on the bottom flange, web, and top flange of the steel beams. The thermocouple layout is shown below in Figure 4.13.

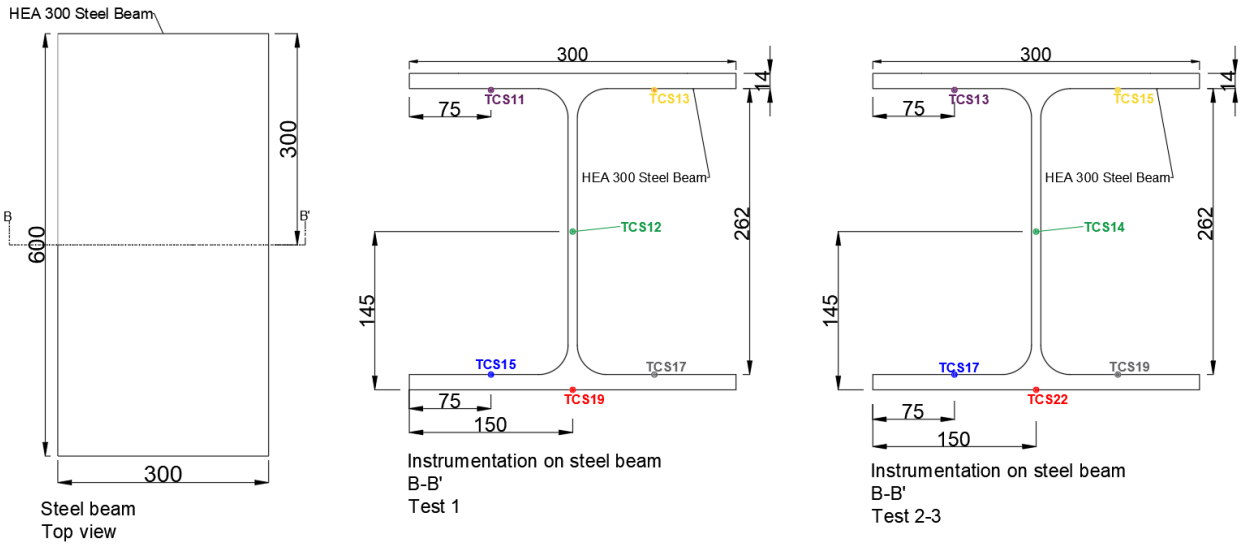


Figure 4.13: The top view of the beam (left), cross-section B-B' of test 1 (center) and test 2-3 (right)

### 4.5.1 Test 1

The temperature evolution graph of the steel beam in test 1 is shown below as Figure 4.14. The readings from test 1.A is shown in the solid lines, while the dashed lines represent the readings of test 1.B. The results from the two tests showed a good agreement with no significant dissimilarity. The graph shows that the thermocouple readings are divided into three main groups based on its location: temperature of the bottom flange, web, and top flange.

Being directly exposed to the fire, the thermocouples on the bottom flange recorded the highest rate of temperature increase. The temperature readings from this group show a logarithmic growth, similar to the ISO 834 standard fire curve. By the 10th minute of the test, the bottom flange reached an approximate temperature of 300°C. The bottom flange temperature doubled by the 20th minute of the tests, where it rose to 600°C. By the end of the test, the final temperature was recorded at approximately 900°C. TCS 15, located on top of the bottom flange, recorded the highest temperature because of its close proximity to the combustion of the CLT panel. Additionally, TCS 19 recorded the lowest temperature among the thermocouples located on the bottom flange because the heat from the vicinity of TCS 19 was transferred through the steel web, which acted as a thermal bridge.

The rate of increase in temperature of the steel web is slower than the bottom flange,

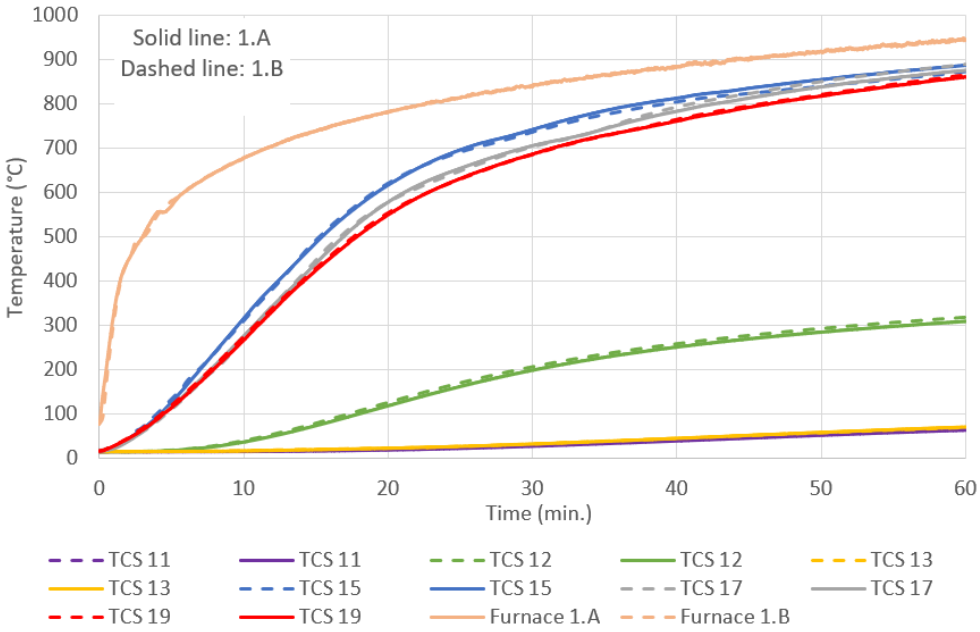


Figure 4.14: The steel beam's temperature evolution (test 1)

where the increase started to be noticed near the 10th minute of the tests. At the bottom of the graph, the readings from the top flange of the beams could be found. The increase in temperature in the top flange is minor when compared to the bottom flange, where the final temperature after 60 minutes didn't reach 100°C.

### 4.5.2 Test 2

Figure 4.15 represents the temperature evolution of the partially protected steel beams. The solid line in the graph shows the result from test 2.A. Meanwhile, the dashed line shows the result from test 2.B. Based on the graph, it can be seen that the readings were divided into three groups based on the location of the thermocouples: bottom flange, web, and top flange. Observation revealed that the results from test 2.A and 2.B were similar, except for the readings of TCS 22 from test 2.A. Unlike test 1, however, the differences in temperature between the groups are lesser. Additionally, the rate of increase in temperatures was lesser, consequently creating a linear increase for the lines.

After 60 minutes of the test, the temperature of the bottom flange didn't exceed 300°C except for the readings from TCS 22, which reached 360°C. On the steel web, the temperature reached approximately 100°C, and the top flange temperatures were below 30°C. This shows that partially protecting the steel beam with intumescent coating immensely helped

to keep the steel beam's temperature low at elevated temperatures.

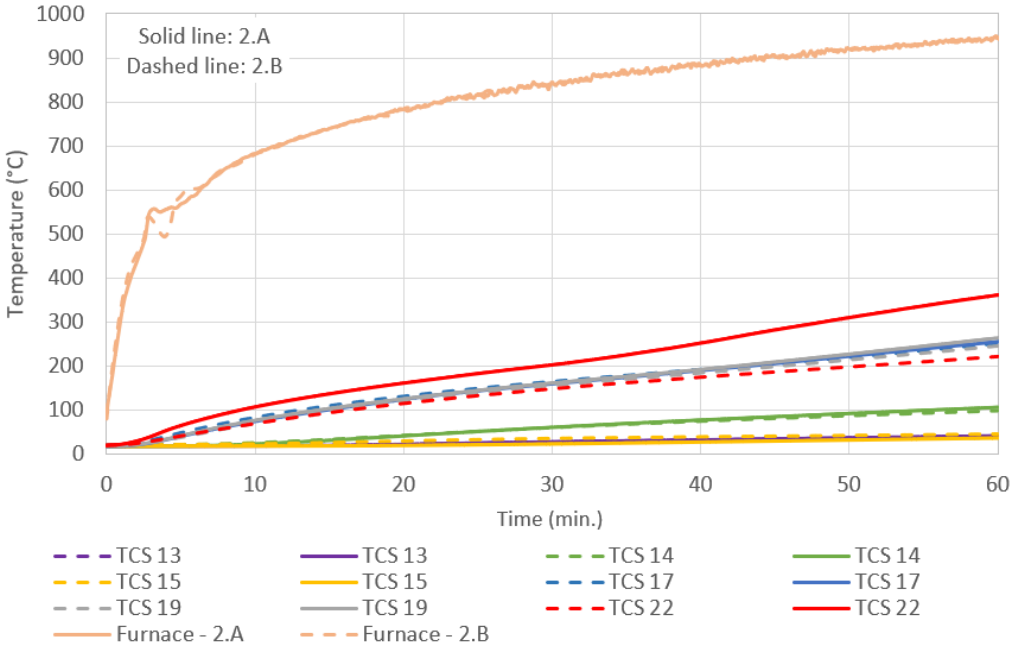


Figure 4.15: The steel beam's temperature evolution (test 2)

### 4.5.3 Test 3

The temperature evolution of the fully protected steel beam from test 3 is shown in Figure 4.16. Solid lines represent results from test 3.A, while the dashed lines represent results from test 3.B. Similarly to test 1 and test 2, the readings could be divided into three groups based on the location of the thermocouples.

The overall result from test 3 is similar to test 2, where the lines formed a linear growth. However, further examination shows that the temperatures on test 3 are slightly lower than in test 2. By the 60th minutes of the test, the temperature on the bottom flange was at approximately 200°C, while the temperature on the web and the top flange stayed well below 100°C and 30°C.

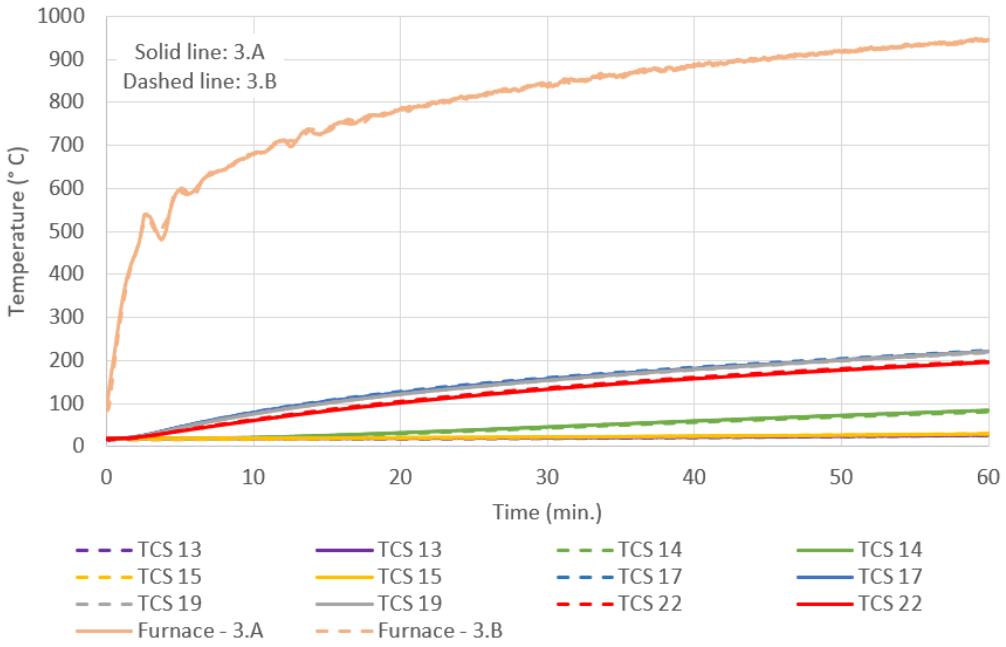


Figure 4.16: The steel beam's temperature evolution (test 3)

### 4.5.4 Further comparison and discussion

Based on the available information in the previous subsection, it was concluded that there are only slight differences in temperature between test 2 and test 3. Therefore, for the purpose of comparison with test 1, only the result from test 2 will be used as a representation. The comparison is shown in Figure 4.17 below.

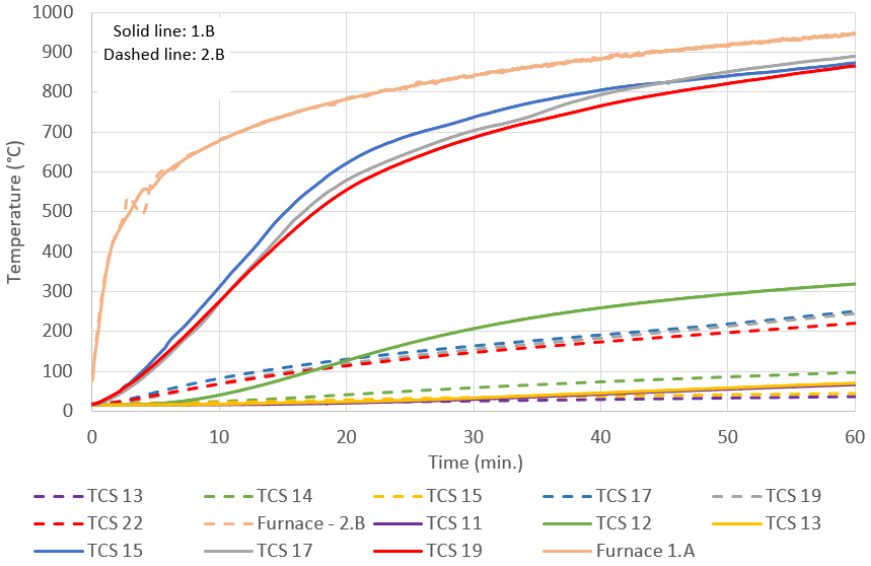


Figure 4.17: The steel beam's temperature evolution comparison (test 1.B and 2.B)

From the graph above, we can observe that the thermocouples on the bottom flange of test 1.B (TCS 15, 17, and 19) recorded significantly higher temperatures than test 2.B on the same location (TCS 17, 19, and 22). The same case can also be said for the temperature of the web between test 1.B (TCS 12) and test 2.B (TCS 14). However, a comparison of the top flange temperatures revealed negligible differences of less than 5°C.

Furthermore, this subsection takes a deeper look into the temperature of the bottom flange of test 2 and test 3 based on more thermocouple readings located on the bottom flange of the steel beams. The thermocouple layout for the comparison is shown in Figure 4.18.

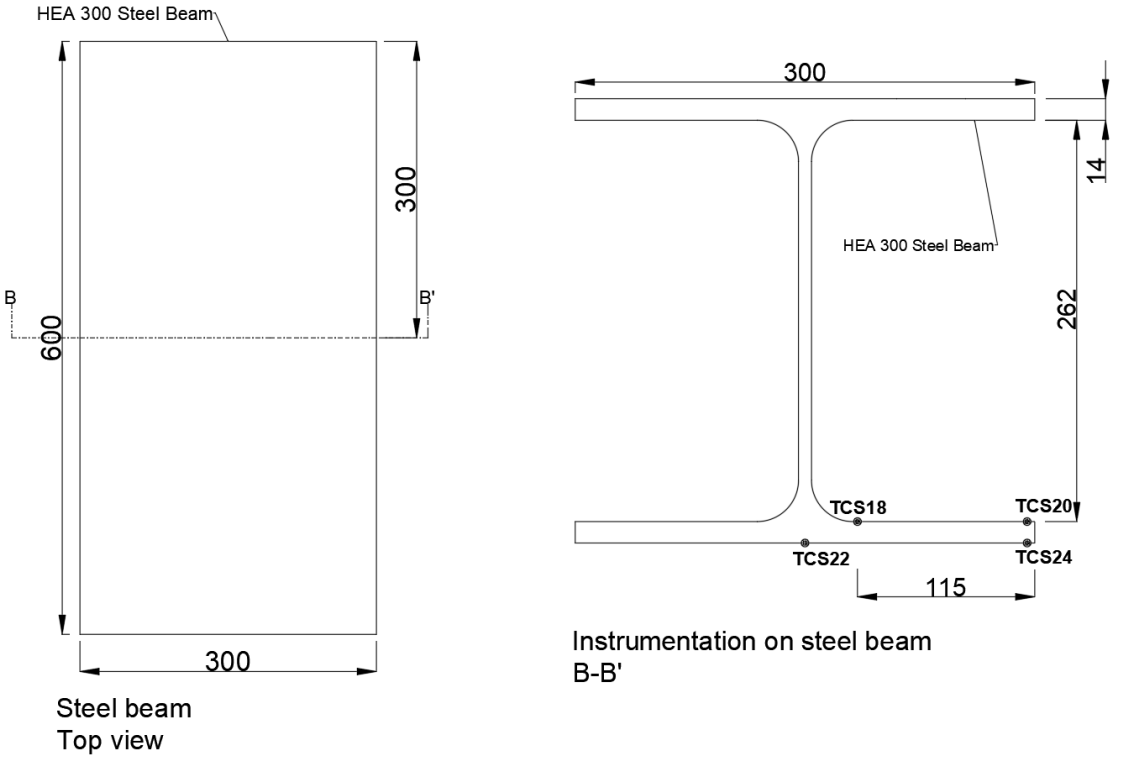


Figure 4.18: The top view of the beam (left), and cross-section B-B' of test 2 and 3 (right)

The temperature evolution of the steel beams' bottom flange from test 2 and test 3 is shown in Figure 4.19.

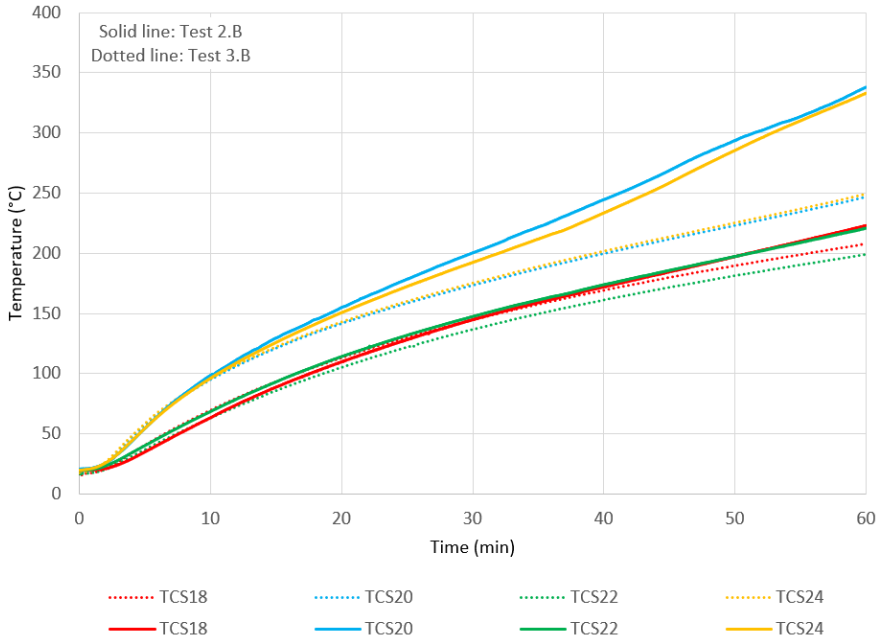


Figure 4.19: The steel beam's temperature evolution comparison (test 2.B and 3.B)

In Figure 4.19, we can see that the highest temperatures from both tests came from TCS 20 and 24. These two thermocouples were installed on the edge of the bottom flange of the steel beams. However, these thermocouples' readings reached a maximum temperature of 332°C on test 2.B, while the readings of the same thermocouples had final temperatures of 249°C on test 3.B. Since the intumescent coating didn't cover the top part of the beam's bottom flange in test 2, this area became susceptible to heat transfer from the CLT panel's combustion process. On the other hand, this area was covered with epoxy intumescent coating on test 3, inhibiting the heat transfer to the bottom flange of the beam.

The thermocouples on the edge of the steel beams also recorded higher temperatures (Maximum difference of 33% on the partially-protected steel beam and 11% on the fully-protected steel beam) than the other thermocouples, TCS 18 and TCS 22, located further away from the flange. The lower temperatures were due to the location of TCS 18 and TCS 22 further from the combustion of the CLT near the edge of the flange and the heat transferred through the steel web.

Based on this comparison, we can conclude that partial protection of the steel flange with the epoxy intumescent coating couldn't fulfil the objective of keeping the steel temperature below 300°C for 60 minutes. On the other hand, full protection of the steel beam with epoxy intumescent coating fulfilled the objective according to the design criteria.

## 4.6 CLT Charring

Another important aspect of the CLT-steel hybrid connection's thermal behaviour is the charring behaviour of the CLT. The charring of the CLT will determine the reduction factor in the CLT's loadbearing capacity. In this study, two methods were employed to evaluate the char thickness of the char layer: the 300°C isotherm method from the thermocouple readings in the CLT and the actual measurement of the remaining CLT thickness after the test. Therefore, this section will present the results from each of the abovementioned methods. The results from the two methods were then compared and presented below.

### 4.6.1 300°C isotherm method

The char layer thickness was determined from the readings of the thermocouples with temperature profile graphs. For the sake of simplicity in the comparison, the temperature profile graphs were made with the final temperature measured by each thermocouple at 60 minutes or at the completion of the furnace test. Two graphs were made, one to represent the area of CLT directly exposed to the fire (Figure 4.20), and another representing the area of CLT protected by the steel flange (Figure 4.21).

#### Direct exposure to fire

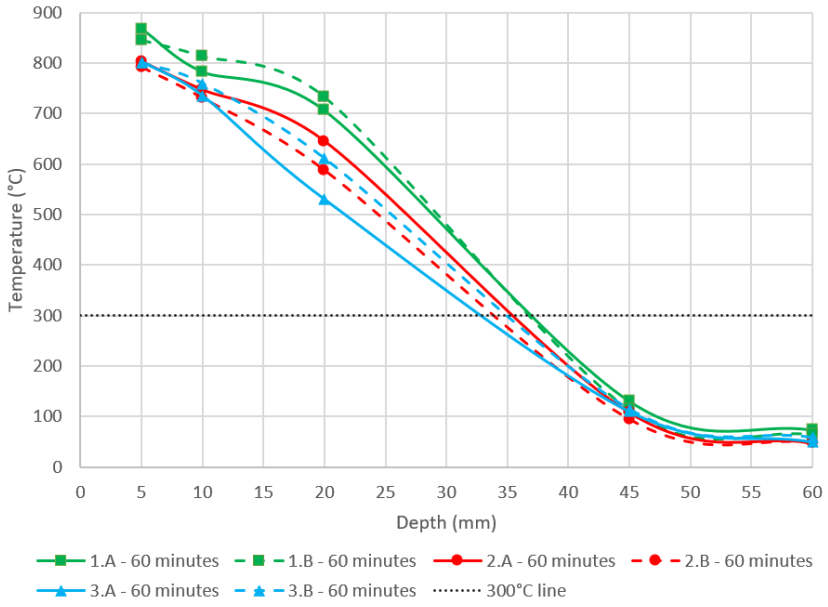


Figure 4.20: The temperature profile of CLT directly exposed to fire

In Figure 4.20, the y-axis depicts the temperature from the thermocouple readings, and the x-axis represents the depth of the CLT from the bottom of the CLT surface. The result from test 1 is shown with the green lines, while test 2 and test 3 are represented by red and blue lines consecutively. Each line colour consists of two type of lines: solid line (represent test A), and dashed line (represent test B). Because the positioning of thermocouples at 30 mm depth isn't representative of the directly exposed area, the readings from this depth were removed, as explained before in 4.3.2. Therefore, spline interpolation from the nearest depths (20 mm and 45 mm) was used to fill the gap. We can observe that a charred layer was formed in each test because certain depths' final temperatures exceeded 300°C. Then, the char depth from each test could be determined based on the 300°C isotherm method and the temperature profile graph. The char depths from Figure 4.20 are summarized in Table 4.2. Additionally, the table contains the charring rates from each test, which were calculated by dividing the char depth by the test duration of 60 minutes.

Table 4.2: Char depth and charring rate of CLT directly exposed to fire

| **Protection** | **Test no.** | **Char depth (mm)** | **Char rate (mm/min)** |
|---|---|---|---|
| Unprotected | 1.A | 37 | 0.62 |
| | 1.B | 37 | 0.62 |
| Partial protection | 2.A | 35.5 | 0.59 |
| | 2.B | 33.5 | 0.56 |
| Full protection | 3.A | 33 | 0.55 |
| | 3.B | 35 | 0.58 |

**Protected by steel flange**

Figure 4.21 shows the temperature profile of the CLT from the area protected by the steel flange. The representation of the axis, color, and type of lines are the same as in Figure 4.20. From test 1, we see that a char layer was formed on test 1.A and test 1.B. However, we can observe from Figure 4.21 that none of the thermocouples from tests 2 and 3 recorded a temperature above 300°C. Based on the 300°C isotherm method, this means that there was no charring present on the CLT where it was protected by steel flange on tests 2 and 3.

The char depth and char rate from Figure 4.21 are shown below in Table 4.3.

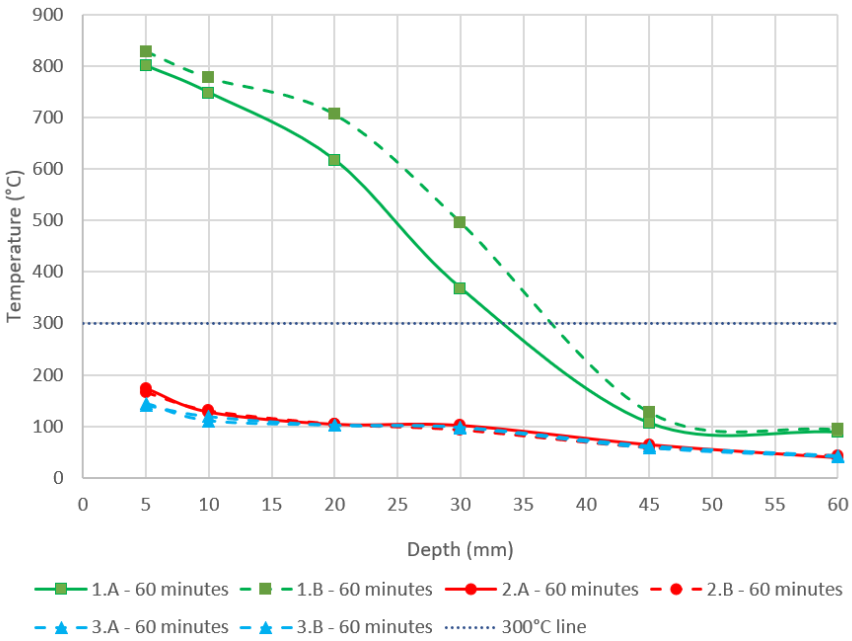


Figure 4.21: The temperature profile of CLT protected by steel flange

Table 4.3: Char depth and charring rate of CLT protected by steel flange

| Protection | Test no. | Char depth (mm) | Char rate (mm/min) |
|---|---|---|---|
| Unprotected | 1.A | 33.5 | 0.56 |
| | 1.B | 37 | 0.62 |
| Partial protection | 2.A | - | - |
| | 2.B | - | - |
| Full protection | 3.A | - | - |
| | 3.B | - | - |

### 4.6.2 Manual measurement method

The remaining thickness of the timber from each CLT was measured using a calliper. The distance between measurement points was decided at 1 cm to ensure sufficient accuracy in representing the actual char layer. A graph from each test was then made to represent the char layer, and the graph was then placed on top of the actual photo of the CLT layer and the drawing of the sample.

#### Test 1 - Unprotected steel beams

The result from the manual measurement from test 1 is shown in Figure 4.22(a) for test 1.A, and 4.22(b) for test 1.B. The measurement result matched the photo of the remaining

timber thickness taken after the measurement.

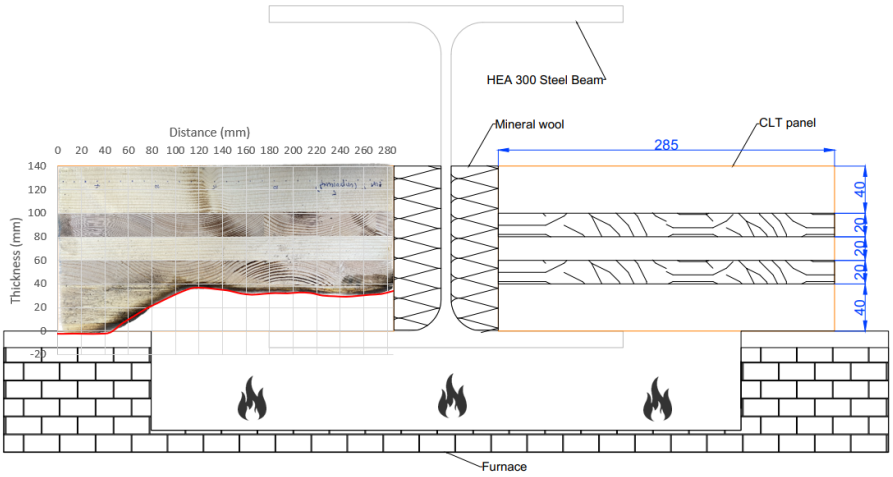


((a)) Test 1.A

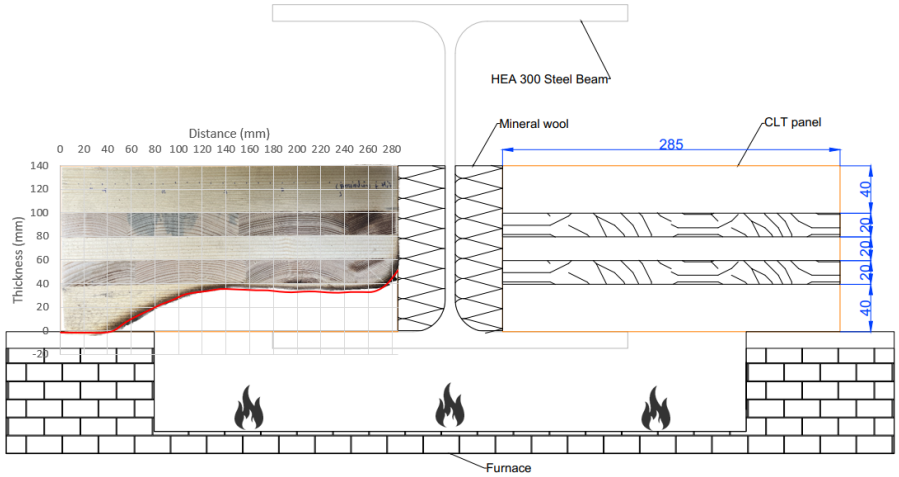


((b)) Test 1.B

Figure 4.22: Manual CLT char measurement from test 1

We can also observe that in all of the tests, the effective exposure area, that is the area of the CLT directly exposed to the fire, had a width of 100 mm (which started at 80 mm and ended at 180 mm on the x-axis). As the CLT got closer to the furnace boundary, the char thickness was found to be lesser and lesser. However, it is also apparent that the char formation extended to approximately 20 mm from the furnace boundary.

Additionally, the bottom flange of the unprotected steel beams has a slight effect on protecting the CLT from charring. We can also see that there is a corner rounding effect on the edge of the CLT from test 1 (width of 280 - 285 mm), although the effect is bigger on test 1.B.

The charring depth and thickness data from test 1 is shown in Table 4.4 below. The

charring depth on the area directly exposed is chosen as the highest char thickness from between 80 mm to 180 mm. Consequently, the depth of the area protected by the steel flange is chosen from 180 mm to 270 mm (to avoid the result with the corner rounding effect). It can be observed from the table that the charring depth on the area directly exposed to the fire is slightly higher compared to the area protected by the steel flange. The steel flange, albeit without intumescent coating, managed to slightly reduce the severity of the charring on the adjoined CLT consistent with the CLT temperatures measurement in the area protected by the steel flange on test 1. This observation shows agreement between the 300°C isotherm method and the manual measurement.

Table 4.4: Summary of test 1 manual char measurement

| | | Direct exposure | | Protected by flange | |
|---|---|---|---|---|---|
| Protection | Test no. | Char depth (mm) | Char rate (mm/min) | Char depth (mm) | Char rate (mm/min) |
| Unprotected | 1.A | 36.8 | 0.61 | 32.9 | 0.55 |
| | 1.B | 35.4 | 0.59 | 33.3 | 0.56 |

**Test 2 - Partially protected steel beams**

The manual measurement result of the remaining timber thickness from test 2.A is shown in Figure 4.23(a) and test 2.B is shown in Figure 4.23(b). As previously seen in test 1, the char formation became less and less nearing the furnace boundary, and a char layer formed extending beyond the furnace boundary.

In test 2, the provision of intumescent coating on the bottom steel flange managed to reduce the bottom steel flange temperature (as seen in section 4.3.2). Consequently, the heat transferred to the CLT is also reduced, resulting in no observed charring in the CLT area protected by the steel flange. A minor extension of the char formation is still seen between the CLT width of 180 mm to 200 mm. However, the formation resulted from the fire's horizontal spread from the area directly exposed to the fire.

The numerical charring data from test 2 is displayed in Table 4.5. The data selection for the area with direct exposure and the area protected by flange is the same as in test 1. However, the minor charring extension on the area protected by the steel flange isn't considered due to its nature as a local phenomenon.

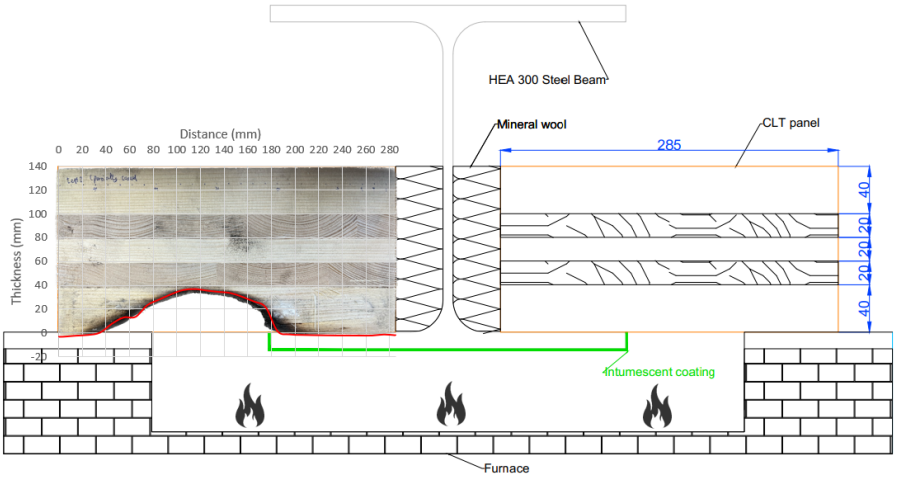


((a)) Test 2.A

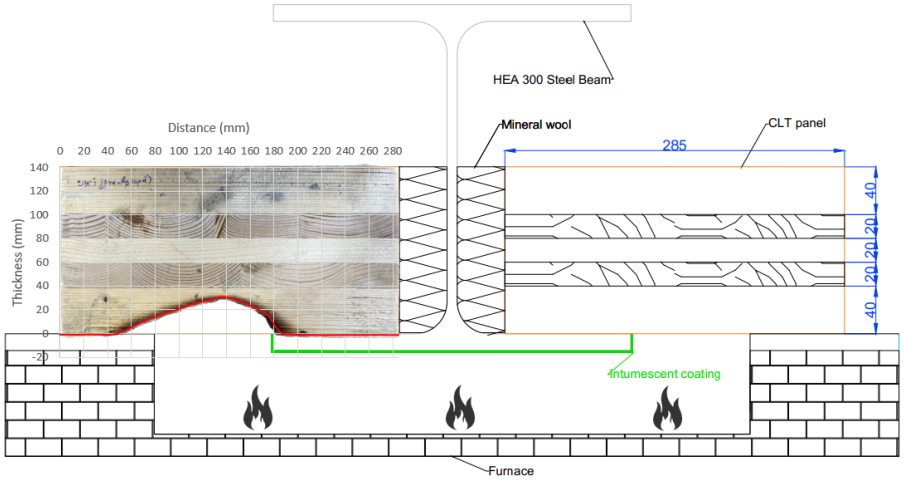


((b)) Test 2.B

Figure 4.23: Manual CLT char measurement from test 2

Table 4.5: Summary of test 2 manual char measurement

| | | Direct exposure | | Protected by flange | |
|---|---|---|---|---|---|
| Protection | Test no. | Char depth (mm) | Char rate (mm/min) | Char depth (mm) | Char rate (mm/min) |
| Partial protection | 2.A | 37.1 | 0.62 | - | - |
| | 2.B | 30.0 | 0.50 | - | - |

### Test 3 - Fully protected steel beams

The manual timber thickness measurement results are shown in Figure 4.24(a) for test 3.A, and Figure 4.24(b) for test 3.B. As observed, the results from test 3 are similar to the results from test 2.

There is an extension of char formation beyond the furnace boundary. The provision of

intumescent coating on all the surface area of the steel beams also ensured that only a minor extension of the charring which can be noticed in the CLT width of 180 mm to 200 mm.

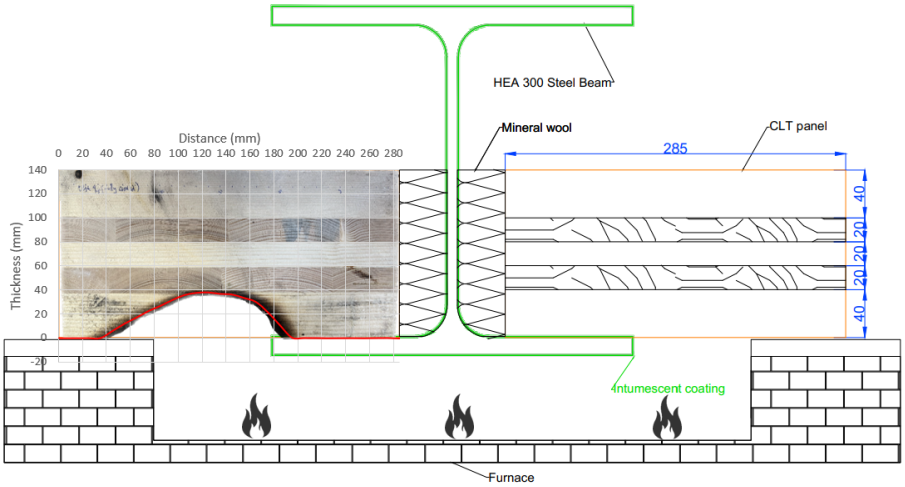


((a)) Test 3.A

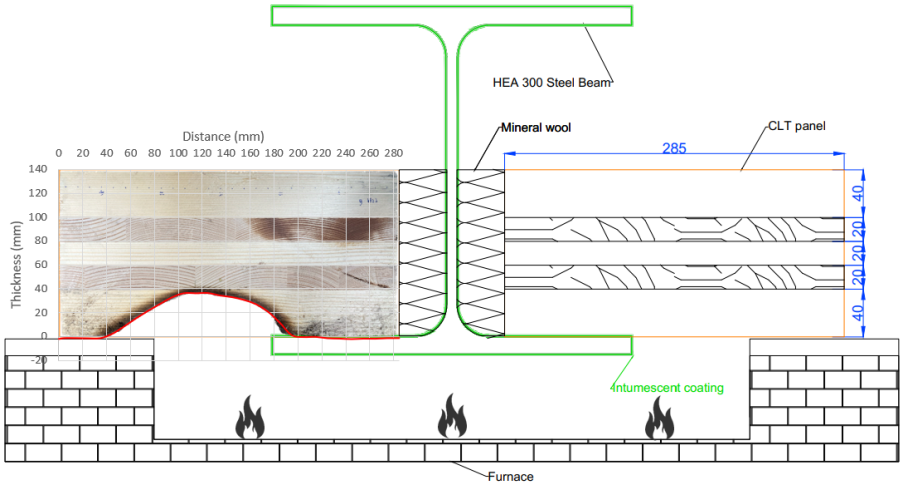


((b)) Test 3.B

Figure 4.24: Manual CLT char measurement from test 3

The data from the manual CLT char thickness of test 3 is displayed in Table 4.6. The data selection of the CLT area with direct exposure and protected by the steel flange is the same as in test 2. The provision of the intumescent coating on all the surfaces of the steel beams proved to be effective in protecting the CLT adjoining the bottom steel flange.

Table 4.6: Summary of test 3 manual char measurement

| | | Direct exposure | | Protected by flange | |
|---|---|---|---|---|---|
| Protection | Test no. | Char depth (mm) | Char rate (mm/min) | Char depth (mm) | Char rate (mm/min) |
| Full protection | 3.A | 37.7 | 0.63 | - | - |
| | 3.B | 36.4 | 0.61 | - | - |

**Comparison on manual measurement results**

Previously, the manual measurement results of each test were shown individually, along with a picture of the specimen where the measurements were taken. In this subsection, a graph showing each test's char-line will be displayed to compare and discuss the results from the tests conducted. The graph is shown in Figure 4.25.

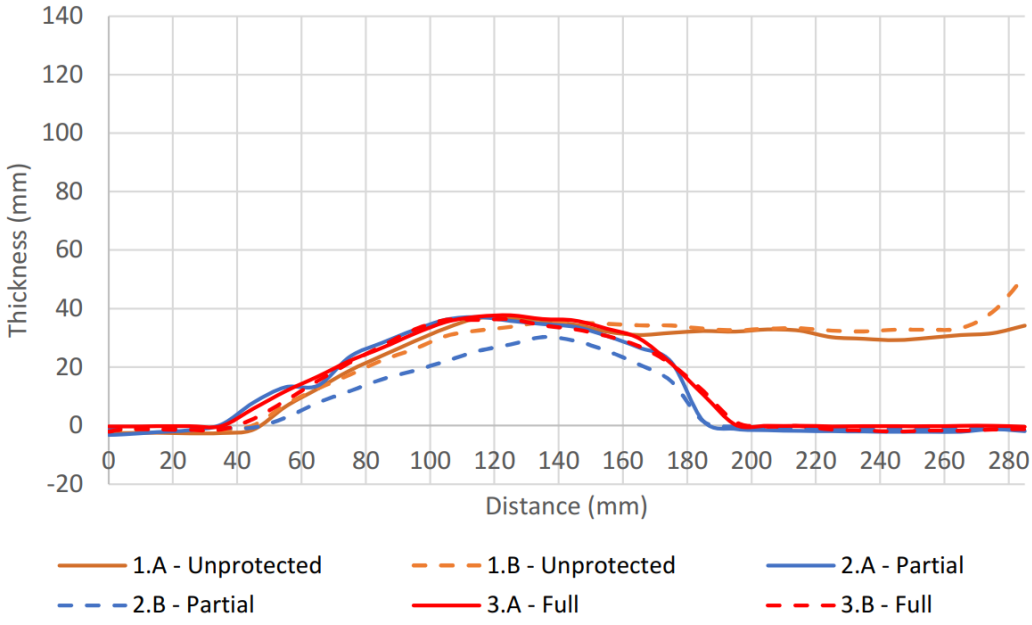


Figure 4.25: The char-line of the CLT panels tested

We can observe that from test 1 to 3, the char formation extended beyond the furnace boundary. While the effective exposure area is only from 80 mm – 180 mm on the x-axis, charring started from approximately 40 mm on all the tests. However, the charring lines formed slopes with the peaks located in the effective exposure area.

Moving closer to the boundary between the effective exposure area and the steel flange at 180 mm on the x-axis, the char lines formed steeper slopes than the previous ones on the

furnace boundary. Here, the most obvious difference is observed between test 1 and test 2-3. Although the charring formation on test 1 extended all the way to the edge of the CLT in the area protected by the steel flange, only minor char formations were observed on test 2 and test 3.

Albeit tests 2 and 3 produced similar results, a difference can be noticed near the boundary of the effective exposure area and the steel flange upon closer inspection. The char formation on test 3 extended deeper when compared to the formation on test 2. The difference in the char formation is caused by the variance in the protection coverage of test 2 and test 3. While in test 2, the top of the bottom steel flange is unprotected, the same area is protected by intumescent coating in test 3. Examination after the furnace test on test 3 shows that during the activation process of the intumescent coating, the event caused small flaming combustion, which helped the char formation to extend further. The combustion on the intumescent coating can be seen in Figure 4.26(a), and the boundary of the intumescent coating activation is seen in Figure 4.26(b).

((a)) Combustion on the intumescent coating ((b)) Boundary of the intumescent activation

Figure 4.26: Intumescent activation on the edge of bottom steel flange (Test 3)

Another explanation for the char expansion difference between these two tests is that in test 2, as the CLT burns, the heat is transferred to the steel beam through the unprotected

top part of the bottom flange. Therefore, the steel flange acted as a heat sink. In test 3, since the top part of the bottom flange was coated with the intumescent coating, the heat from the combustion wasn't dissipated to the steel flange.

### 4.6.3 Comparison of char depth and char rate

A table that compares the char depth of the experiments based on the 300°C isotherm method and the manual measurement is established in Table 4.7, and the char rate is shown in Table 4.8.

Table 4.7: Char depth comparison between the two methods

| | | **Char depth (mm)** | | | |
|---|---|---|---|---|---|
| | | **Direct exposure** | | **Protected by flange** | |
| **Protection type** | **Test no.** | **300°C isotherm** | **Actual measurement** | **300°C isotherm** | **Actual measurement** |
| Unprotected | 1.A | 37 | 36.8 | 33.5 | 32.9 |
| | 1.B | 37 | 35.4 | 37 | 33.3 |
| Partial coating | 2.A | 35.5 | 37.1 | - | - |
| | 2.B | 33.5 | 30.0 | - | - |
| Full coating | 3.A | 33 | 37.7 | - | - |
| | 3.B | 35 | 36.4 | - | - |

The table above presents the char depth results from three types of protection (unprotected, partial coating, and full coating) for CLT in direct exposure and protected by steel flange area. Two tests were conducted for each test, named A and B. Two char-line determination methods were used, the 300°C isotherm and the actual measurement. The char depth is shown in millimetres.

The two methods showed good agreement on the char depth values, although slight differences were anticipated. The contrasts could be credited to errors during the manual measurement, different points of measurement between the two methods, errors from the char depth interpolation on the 300°C isotherm method, and errors from the placement of the thermocouples due to the drilling process.

Another important observation from the char depth displayed that none of the char depth values exceeded 40 mm, which is the thickness of the bottom timber layer of the CLT panel. Therefore, the charring in the experiment could be characterized by the behaviour of only the bottom layer, acting similarly to a homogenous timber panel.

The discrepancies from the char depth values also affected the char rate values shown in

Table 4.8. Since the charring could be assumed as a charring on a homogenous timber panel, the experimental char rate values can be compared to the char rate value from Eurocode 5 [55] of 0.65 mm/min for softwood timber with a density of 290 $\geq$ kg/m$^3$.

Table 4.8: Char rate comparison between the two methods

| | | **Char rate (mm/min)** | | | |
|---|---|---|---|---|---|
| | | **Direct exposure** | | **Protected by flange** | |
| **Protection type** | **Test no.** | **300°C isotherm** | **Actual measurement** | **300°C isotherm** | **Actual measurement** |
| Unprotected | 1.A | 0.62 | 0.61 | 0.56 | 0.55 |
| | 1.B | 0.62 | 0.59 | 0.62 | 0.56 |
| Partial coating | 2.A | 0.59 | 0.62 | - | - |
| | 2.B | 0.56 | 0.50 | - | - |
| Full coating | 3.A | 0.55 | 0.63 | - | - |
| | 3.B | 0.58 | 0.61 | - | - |

Directly comparing the values from Table 4.8 to the Eurocode 5 value of 0.65 mm/min, we can see the char rate values from the CLT area directly exposed (with an average value of 0.59 $\pm$ 0.04 mm/min for 300°C isotherm method, and average value of 0.59 $\pm$ 0.09 mm/min for actual measurement method) are slightly lesser compared to the Eurocode value. However, test 2.B was an exception, with a char rate value of 0.50 mm/min based on the actual measurement method. In this experimental study, the char rate given by Eurocode 5 is shown to be conservative.

The lower charring rate when compared to the Eurocode value could be explained by the limited amount of oxygen inside the mobile furnace during the test. Hence, the combustion process became underventilated, reducing the intensity. If greater supply of oxygen were to be provided, it could allow for more internal combustion near the timber and regression of the char layer.

# Chapter 5

# Conclusion and future recommendation

## 5.1 Conclusion

The experimental study investigated the thermal behaviour of hybrid CLT-steel connection. The main variable in the study was the different protection coverage of epoxy intumescent coating on the steel beam. Six tests were conducted in the study, where the specimens were exposed to the ISO 834 standard fire curve using DBI's mobile furnace. The six tests were divided into three categories: Unprotected steel beams, partially protected (only on the bottom flange) steel beams, and fully protected (on the whole surface area) steel beams. The results and discussion of the experiment were presented in Chapter 4. From the experimental study, the subsequent conclusions were drawn:

- The furnace temperatures in all six tests were able to follow the ISO 834 fire curve, except for fluctuations in furnace temperature between the second to the sixth minute of the test due to a sudden increase in pyrolysis gas production. The deviation in temperatures due to the fluctuation was found to be less than 10% of the ISO 834 fire curve.

- In general, the presence of the steel flange slowed down the heat transfer to the adjacent CLT regardless of the protection coverage. However, the epoxy intumescent coating on the steel beam was proven to be effective in containing the temperature on

the adjacent CLT panel below 300°C. This prevents the charring and, consequently, combustion on the adjacent CLT.

- The partially-protected steel beam transferred more heat to the adjacent CLT than the fully-protected steel beam, resulting in slightly higher temperatures on the CLT panel. Based on the thermocouple readings, the maximum difference was found to be 20% higher compared to the CLT adjacent to the fully-protected steel beam.
- The partially-protected steel beam was found to be susceptible to heat transfer from the combustion of the CLT to the unprotected region on top of the bottom flange. By the end of the test at 60 minutes, the temperature on top of the partially-protected bottom flange reached 332°C, while full protection of the beam kept the temperature at 221°C.
- The temperatures on the edge of the steel beam's bottom flange were found to be higher than the region further from the edge (maximum of 33% on the partially-protected steel beams and 11% on the fully-protected steel beams). This is caused by the CLT panel combustion happening near the steel flange's edge and the heat being transferred along the steel web acting as a thermal bridge.
- Partially protecting the steel beam (only on the bottom flange) failed to achieve the design criteria based on the manufacturer's data on the intumescent coating dry film thickness (DFT). However, full protection on all the surfaces of the steel beam managed to fulfil the design criteria.
- With an increase in protection coverage from partial to full coverage, the char formation zone extended further horizontally by an average of 8.5 mm. The combustion of the intumescent coating is the most probable cause the extension.
- The charring rate of the exposed CLT area had shown to be lower compared to the Eurocode 5 value of 0.65 mm/min, regardless of the method of measurement. The lack of oxygen supply to the mobile furnace could be the main reason why this is the case.
- The insertion of thermocouples parallel to the isotherms was proven to be a credible method to measure the char layer progression during the test accurately.

In general, the study demonstrated in the absence of protection (in the form of epoxy intumescent coating) on the steel, the steel temperature exceeded 800°C. Consequently, extensive charring occurred on the CLT panel adjacent to the steel flange. With only partial protection of the steel beam (intumescent coating only on the bottom flange), the study showed that intumescent had massively reduced the temperature of the steel beam and the CLT panel adjacent to the flange, avoiding charring. However, the design criteria of the critical temperature and fire resistance time were only achieved with full protection of the steel beams.

## 5.2 Future research recommendation

Because of the novelty of the research topic, further research is required to strengthen the result and the knowledge obtained from this experimental study. Additionally, the variability of the hybrid CLT-steel connection configuration and protection materials might produce diverse results, which should also be accounted for. Therefore, the recommendation for further studies are:

- The utilization of a larger scale test to better capture the char profile on the CLT. Since this experimental study was conducted using a small-scaled furnace, the exposed area of the CLT was limited, thus, the effect of the furnace boundary was apparent even on the fully exposed area.

- The application of different types of intumescent coating since many types and brands are available on the market. Since thin intumescent coating is more popular for usage in the construction of building, it will be beneficial to do research using the said type of intumescent coating.

- The effect of loading on the structural element (either the CLT, steel beam, or both) will be important to be investigated to observe the difference in thermal behaviour and subsequent mechanical properties.

- A thermal and structural modelling of the hybrid connection shall be done to validate the current and future research results.

- The use of Inconel sheathed thermocouples, especially for the measurement of temperatures inside the CLT, is recommended because it was proven to provide better reliability than the fibreglass thermocouples.

- Since ISO 834 is not an accurate representation of an actual fire, future studies could use a variety of different fire exposures to better understand the behaviour of the hybrid connection. Furthermore, the inclusion of the cooling phase and the contribution of the combustible surfaces of the CLT to the fire dynamics could be investigated.

# References


[1] Forest Products Laboratory, *Wood handbook: Wood as an engineering material*. U.S. Department of Agriculture, Forest Service, Forest Products Laboratory, 2021.

[2] Kallesoe Machinery, "GLT - Glue Laminated Timber - Kallesoe Machinery." Accessed on 2023-02-10.

[3] Apple Plywoods, "Laminated Veneer Lumber - Apple Plywoods." Accessed on 2023-02-10.

[4] Mass Timber Services Ltd, "Cross Laminated Timber (CLT) - Mass Timber Services." Accessed on 2023-02-10.

[5] D. Buck, X. A. Wang, O. Hagman, and A. Gustafsson, "Further Development of Cross-Laminated Timber (CLT): Mechanical Tests on 45° Alternating Layers," in *World Conference on Timber Engineering (WCTE 2016)*, 2016.

[6] A. Sandoli, C. D'Ambara, C. Ceraldi, B. Calderoni, and A. Prota, "Sustainable cross-laminated timber structures in a seismic area: Overview and future trends," *Applied Sciences*, vol. 11, 20178, 2021.

[7] T. Wiegand, "Current status of European product and design standards for Cross-Laminated Timber," in *Proceedings of the Joint Conference of COST Actions FP1402 FP1404*, pp. 33 – 41, 2016.

[8] R. Jöbstl, T. Bogensperger, T. Moosbrugger, and G. Schickhofer, "A Contribution to the Design and System Effect of Cross Laminated Timber," in *CIB W18, 39th Meeting*, 2006.

[9] M. Flaig and H. J. Blaß, "Shear strength and shear stiffness of CLT-beams loaded in plane," in *Proceedings of 46th CIB-W18 Meeting*, 2013.

[10] Nicoguaro, "Typical stress vs. strain diagram for a ductile material (e.g. steel).," 2020. File: LambdaPlaques.jpg.

[11] W. Y. Wang, B. Liu, and V. Kodur, ''Effect of temperature on strength and elastic modulus of high-strength steel,'' *Journal of Materials in Civil Engineering*, vol. 25, 2013.

[12] A. Lucherini and C. Maluk, ''Intumescent coatings used for the fire-safe design of steel structures: A review,'' *Journal of Constructional Steel Research*, vol. 162, 2019.

[13] M. Forde, *ICE manual of Construction Materials*. Thomas Telford Ltd, 2009.

[14] C. Hoffmann, M. V. Hoey, and B. Zeumer, ''Decarbonization Challenge for Steel,'' tech. rep., 2020.

[15] ''Concrete needs to lose its colossal carbon footprint,'' *Nature 597*, pp. 593--594, 2021. https://doi.org/10.1038/d41586-021-02612-5.

[16] Waugh Thisleton Architects, *100 Projects UK CLT*. 2018.

[17] R. H. White, *Analytical Methods for Determining Fire Resistance of Timber Members*, pp. 1979--2011. New York, NY: Springer New York, 2016.

[18] R. H. White and M. Dietenberger, ''Wood products: thermal degradation and fire,'' in *Encyclopedia of materials: science and technology*, pp. 9712--9716, 2001.

[19] R. Emberley and J. T. Cullen, ''Cross-laminated timber failure modes for fire conditions,'' *Proceedings of the Second International Conference on Performance-Based and Life-Cycle Strutural Engineering, School of Civil Engineering, The University of Queensland*, pp. 1023--1030, 2015.

[20] W. Wang, and V. Kodur, *Material Properties of Steel in Fire Conditions*. Elsevier, 2020.

[21] A. Lucherini, L. Giuliani, and G. Jomaas, ‘‘Experimental study of the performance of intumescent coatings exposed to standard and non-standard fire conditions,’’ *Fire Safety Journal*, vol. 95, pp. 42--50, 2018.

[22] ‘‘Intumescent coating systems, their development and chemistry,’’ *Journal of fire sciences*, vol. 2, 1971.

[23] The Swedish Forest Industries Federation, *The CLT Handbook*. Sweden: Skogsindustrierna Svenskt Trä, 2019.

[24] A. Frangi, M. Fontana, M. Knobloch, and G. Bochicchio, ‘‘Fire behaviour of cross-laminated solid timber panels,’’ *Fire Safety Science*, vol. 9, pp. 1279--1290, 2008.

[25] J. McTavish and C. Palmer, ‘‘Charring behaviour of New Zealand cross-laminated timber,’’ Presented at the Civil and Natural Resources Engineering Research Conference, Christchurch, New Zealand, October 2013.

[26] T. Moser, M. Aitken, and M. Spearpoint, ‘‘Measuring the char rate of cross-laminated timber in an intermediate-scale furnace,’’ *New Zealand Timber Design*, vol. 24, 2016.

[27] A. Colic, ‘‘Study of the char fall-off phenomenon in cross-laminated timber under fire conditions,’’ Master’s thesis, The University of Edinburgh, Edinburgh, 2021.

[28] S. A. Lineham, D. Thomson, A. I. Bartlett, L. A. Bisby, and R. M. Hadden, ‘‘Structural response of fire-exposed cross-laminated timber beams under sustained loads,’’ *Fire Safety Journal*, vol. 85, pp. 23--34, 2016.

[29] F. Wiesner, *Structural Behaviour of Cross-laminated Timber Elements in Fires*. University of Edinburgh, 2019.

[30] ‘‘Charring of steel-timber hybrid beam section,’’ 11 2022.

[31] Giovanna Concu, *Timber buildings and sustainability*. London, UK: InTechOpen, 2019.

[32] F. Asdrubali, B. Ferracuti, L. Lombardi, C. Guattari, L. Evangelisti, and G. Grazieschi, ‘‘A review of structural, thermo-physical, acoustical, and environmental properties of wooden material for building application,’’ *Building and Environment*, vol. 114, pp. 307--332, 2016.

[33] W. Hillis, ‘‘Heartwood and tree exudates,’’ *Springer Series in Wood Science*, vol. 4, 1987.

[34] H. Pereira, J. Graça, and J. Rodrigues, ‘‘Wood chemistry in relation to quality,’’ *Cheminform*, vol. 35, 11 2004.

[35] M. C. Wiemann *et al.*, ‘‘Characteristics and availability of commercially important woods,’’ *Forest Products Laboratory. Wood handbook: wood as an engineering material. Madison: United States Department of Agriculture: Forest Service*, 2021.

[36] A. Wiedenhoeft and T. L. Eberhards, ‘‘Structure and function of wood,’’ *Forest Products Laboratory. Wood handbook: wood as an engineering material. Madison: United States Department of Agriculture: Forest Service*, 2021.

[37] C. A. Senalik and B. Farber, ‘‘Mechanical properties of wood,’’ *Forest Products Laboratory. Wood handbook: wood as an engineering material. Madison: United States Department of Agriculture: Forest Service*, 2021.

[38] D. Breyer, K. Fridley, D. Pollock, and K. Cobeen, *Design of Wood Structures-ASD/LRFD*. McGraw Hill LLC, 2014.

[39] M. A. Irle *et al.*, ‘‘Wood composites,’’ 2021.

[40] R. M. Rowell, *Handbook of wood chemistry and wood composites: Second edition*. Florida, US: CRC Press, 2013.

[41] C. A. Issa and Z. Kmeid, ‘‘Advanced wood engineering: glulam beams,’’ *Construction and Building Materials*, vol. 19, pp. 99--106, 2004.

[42] J. Coulson, *A handbook for the sustainable use of timber in construction*. Hoboken, New Jersey: Wiley Blackwell, 2021.

[43] L. Muszynski, P. Larasatie, J. E. M. Guerrero, R. Albee, and E. N. Hansen, ‘‘Global clt industry in 2020: Growth beyond the alpine region,’’ *Proceedings of the 63rd International Convention of Society of Wood Science and Technology*, 2020.

[44] B. Shan, B. Chen, J. Wen, and Y. Xiao, ‘‘Thermal performance of cross-laminated timber (clt) and cross-laminated bamboo and timber (clbt) panels,’’ *Architectural engineering and design management*, 2022.

[45] A. Ceccotti, C. Sandhaas, M. Okabe, M. Yasumura, C. Minowa, and N. Kawai, ‘‘Sofie project { 3d shaking table test on a seven-storey full-scale cross-laminated timber building,’’ *Earthquake Engineering & structural Dynamics*, vol. 41, 2013.

[46] M. Torneport, ‘‘Industrial requirements for cross-laminated timber manufacturing,’’ bachelor’s thesis, Linnaeus University, Sweden, 2021.

[47] H. Unterwieser and G. Schickhofer, ‘‘Characteristic values and test configurations of CLT with focus on selected properties,’’ in *Focus solid timber solutions - European conference on cross laminated timber (CLT)*, pp. 53--73, 2013.

[48] T. Ehrhart, R. Brandner, G. Schickhofer, and A. Frangi, ‘‘Rolling shear properties of some european timber species with focus on cross

laminated timber (CLT): Test configuration and parameter study,'' in *Proceedings of 2nd INTER-Meeting*, 2015.

[49] M. Jelec, D. Varevac, and V. Rajcic, ‘‘Cross-laminated timber (clt) { a state of the art report,'' *Gradevinar*, vol. 70, 2018.

[50] C. Salzmann, ‘‘Ermittlung von querdruckkenngrößen für brettsperrholz (bsp),'' Master's thesis, Graz University of Technology, Graz, Austria, 2010.

[51] R. Brandner and G. Schickhofer, ‘‘Properties of cross laminated timber (CLT) in compression perpendicular to grain,'' in *Proceedings of 1st INTER-Meeting*, 2014.

[52] J. Velasquez, ‘‘Performance of joints for glued laminated timber exposed to the iso fire temperature curve,'' Master's thesis, Lund University, Lund, 2021.

[53] D. Barber, A. Roy-Poirier, and L. Wingo, ‘‘Modelling the fire performance of steel beam to CLT connections for hybrid construction,'' in *12th Asia-Oceania Symposium on Fire Science and Technology)*, 2020.

[54] R. M. Hadden, A. I. Bartlett, J. P. Hidalgo, S. Santamaria, F. Wiesner, L. A. Bisby, S. Deeny, and B. Lane, ‘‘Effects of exposed cross laminated timber on compartment fire dynamics,'' *Fire Safety Journal*, vol. 91, pp. 480--489, 2017. Fire Safety Science: Proceedings of the 12th International Symposium.

[55] E. C. for Standardization, ‘‘En 1995-1-2: Eurocode 5: Design of timber structures - part 1-2: General - structural fire design,'' 2004.

[56] F. Wiesner, F. Randmael, W. Wan, L. Bisby, and R. M. Hadden, ‘‘Structural response of cross-laminated timber compression elements

exposed to fire,'' *Fire Safety Journal*, vol. 91, pp. 56--67, 2017. Fire Safety Science: Proceedings of the 12th International Symposium.

[57] F. Wiesner, D. Bell, L. Chaumont, L. Bisby, and S. Deeny, ‘‘Rolling shear capacity of clt at elevated temperature,'' 08 2018.

[58] F. Wiesner, L. Bisby, A. Bartlett, J. Hidalgo, S. Santamaria, S. Deeny, and R. Hadden, ‘‘Structural capacity in fire of laminated timber elements in compartments with exposed timber surfaces,'' *Engineering Structures*, vol. 179, pp. 284--295, 01 2019.

[59] F. Wiesner, D. Thomson, and L. Bisby, ‘‘The effect of adhesive type and ply number on the compressive strength retention of clt at elevated temperatures,'' *Construction and Building Materials*, vol. 266, p. 121156, 2021.

[60] S. K. Mondal, *Steel metallurgy properties, specifications, and applications*. New York, N.Y.: McGraw-Hill Education LLC, 2015.

[61] M. Hurley, D. Gottuk, H. Jr, K. Harada, E. Kuligowski, M. Puchovsky, J. Torero, W. Jr, and C. Wieczorek, *SFPE handbook of fire protection engineering, fifth edition*. 01 2016.

[62] P. D. Harvey. ASM International, 1982.

[63] J.-M. Franssen and T. Gernay, ‘‘Modeling structures in fire with safir®: Theoretical background and capabilities,'' *Journal of Structural Fire Engineering*, vol. 8, 09 2017.

[64] A. Lucherini, Q. Razzaque, and C. Maluk, ‘‘Exploring the fire behaviour of thin intumescent coatings used on timber,'' *Fire Safety Journal*, p. 102887, 09 2019.

[65] S. Bourbigot, M. Le Bras, S. Duquesne, and M. Rochery, ‘‘Recent advances for intumescent polymers,'' *Macromolecular Materials and Engineering*, vol. 289, no. 6, pp. 499--511, 2004.

[66] M. L. Bras, M. Bugajny, J.-M. Lefebvre, and S. Bourbigot, ‘‘Use of polyurethanes as char-forming agents in polypropylene intumescent formulations,’’ *Polymer International*, vol. 49, no. 10, pp. 1115--1124, 2000.

[67] M. Jimenez, S. Duquesne, and S. Bourbigot, ‘‘Characterization of the performance of an intumescent fire protective coating,’’ *Surface and Coatings Technology*, vol. 201, no. 3, pp. 979--987, 2006.

[68] M. Bartholmai, R. Schriever, and B. Schartel, ‘‘Influence of external heat flux and coating thickness on the thermal insulation properties of two different intumescent coatings using cone calorimeter and numerical analysis,’’ *Fire and Materials*, vol. 27, no. 4, pp. 151--162, 2003.

[69] I. Pope, J. P. Hidalgo, and J. L. Torero, ‘‘A correction method for thermal disturbances induced by thermocouples in a low-conductivity charring material,’’ *Fire Safety Journal*, vol. 120, p. 103077, 2021. Fire Safety Science: Proceedings of the 13th International Symposium.

[70] I. Pope, J. P. Hidalgo, R. M. Hadden, and J. L. Torero, ‘‘A simplified correction method for thermocouple disturbance errors in solids,’’ *International Journal of Thermal Sciences*, vol. 172, p. 107324, 2022.

[71] I. Pope, *Solid-phase temperature analysis and correction for multi-scale fire experimentation*. PhD thesis, The University of Queensland, Brisbane, 2022.

[72] International Organization for Standardization, ‘‘Iso 834: Fire-resistance tests - elements of building construction,’’ 1999.

[73] A. Bartlett, R. Hadden, L. Bisby, and A. Law, ‘‘Analysis of cross-laminated timber upon exposure to non-standard heating conditions,’’ 02 2015.

# Appendix A

# Temperature profile of the CLT

Appendix A contains the alternative method of presenting the results from the thermocouples readings of the CLT panels. In the graphs of the temperature profiles, the y-axis is the temperature (°C), while the x-axis is the depth of the CLT (mm). Each line represented the time during which the measurements were recorded.

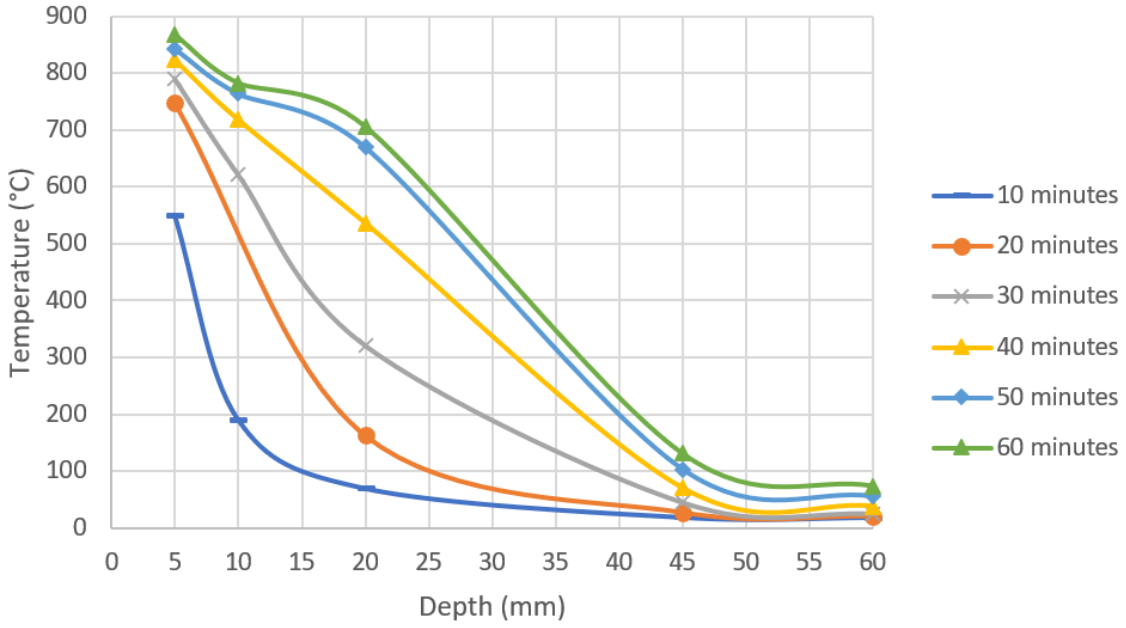


((a)) Direct exposure

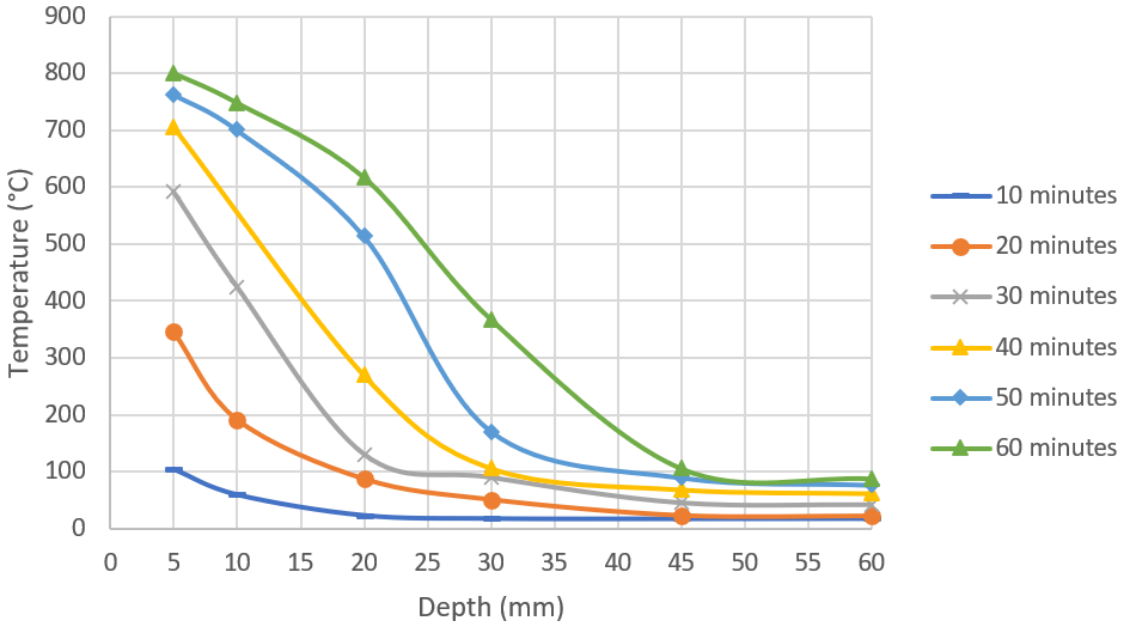


((b)) Protected by steel flange

Figure A.1: Temperature profile from test 1.A

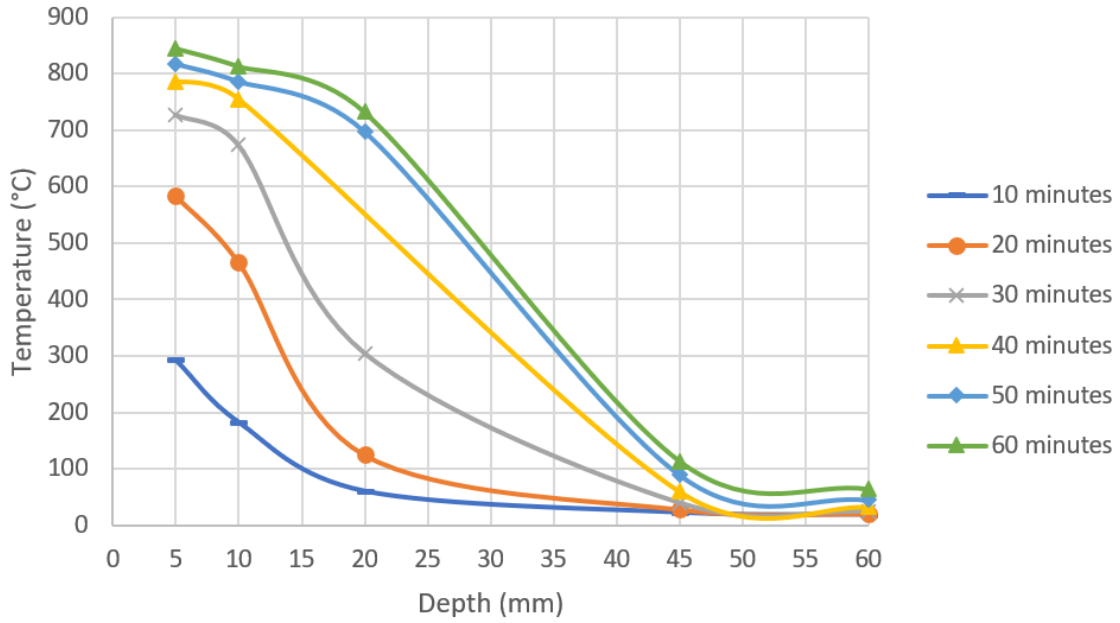


((a)) Direct exposure

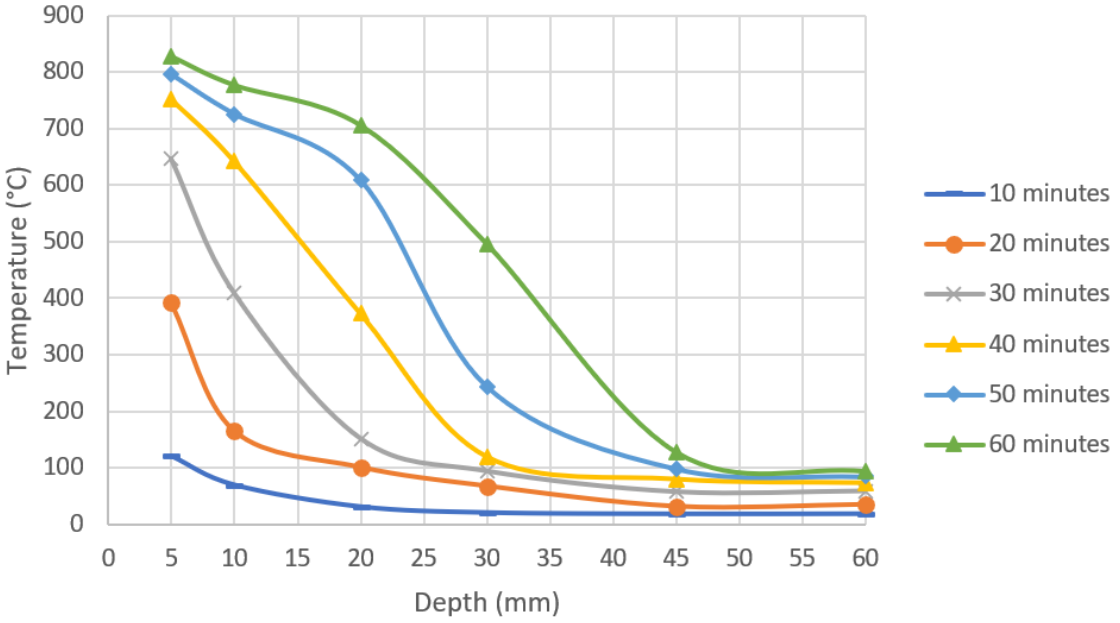


((b)) Protected by steel flange

Figure A.2: Temperature profile from test 1.B

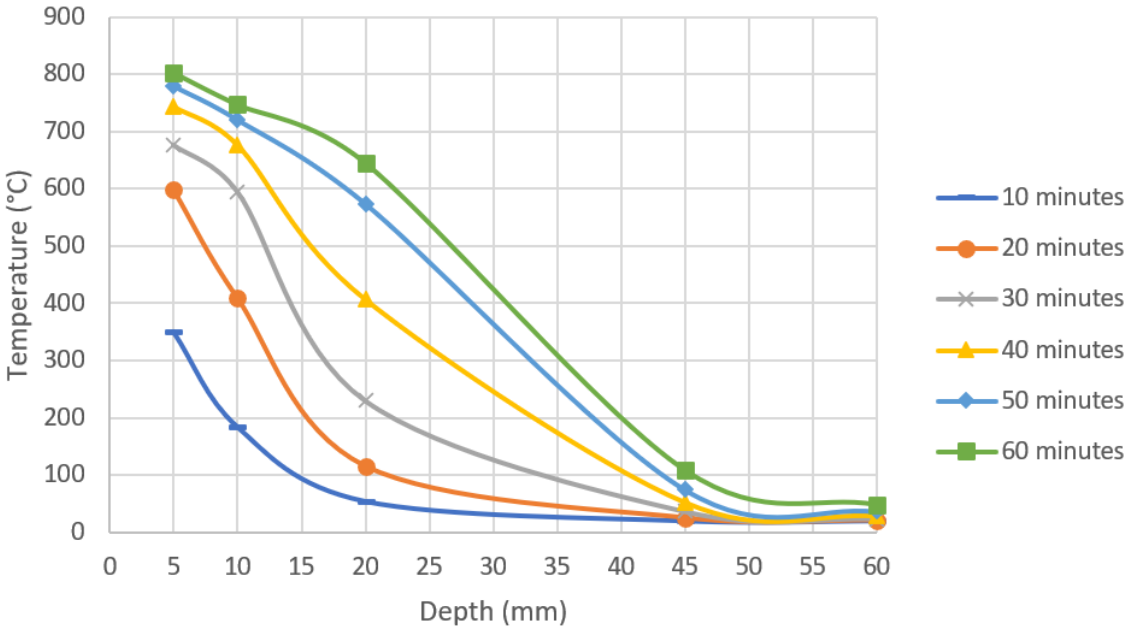


((a)) Direct exposure

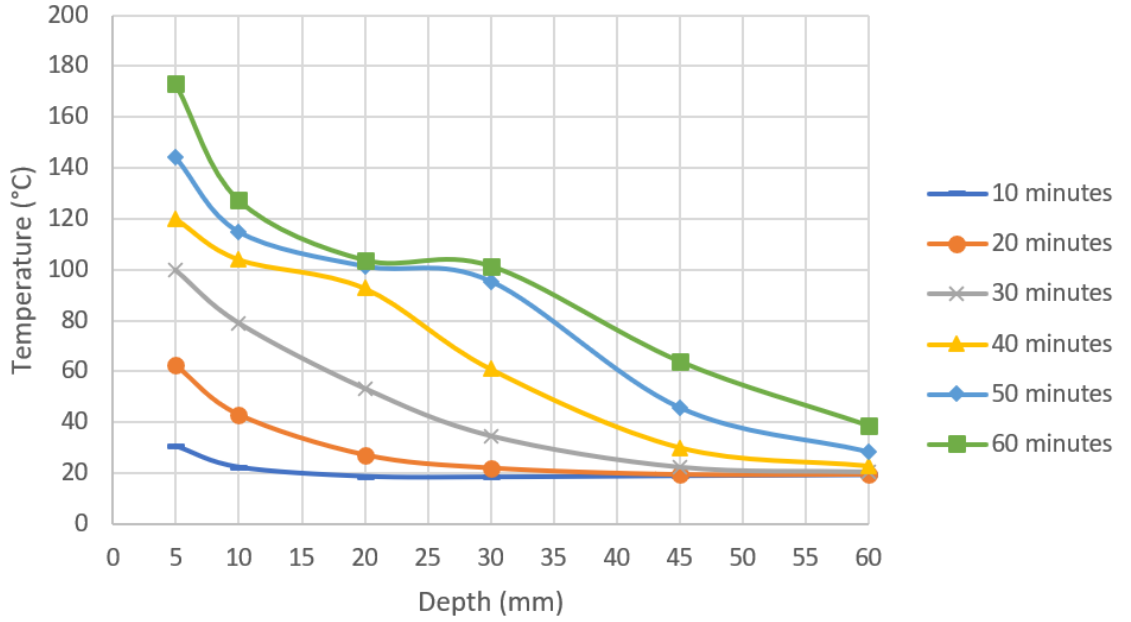


((b)) Protected by steel flange

Figure A.3: Temperature profile from test 2.A (be noted of the different boundary in the y-axis)

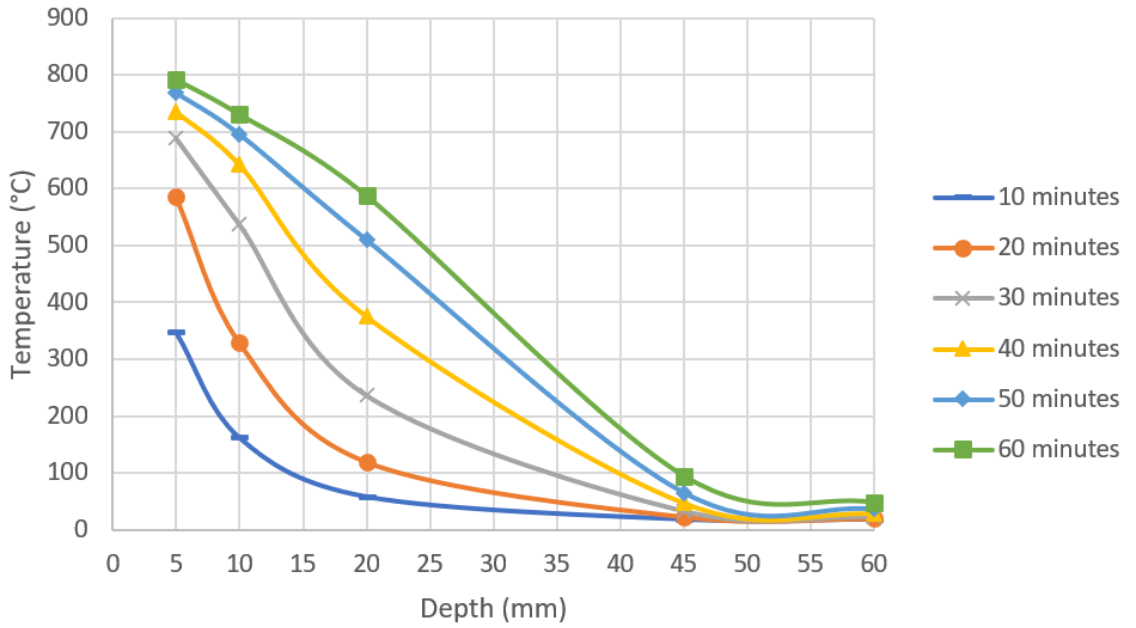


((a)) Direct exposure

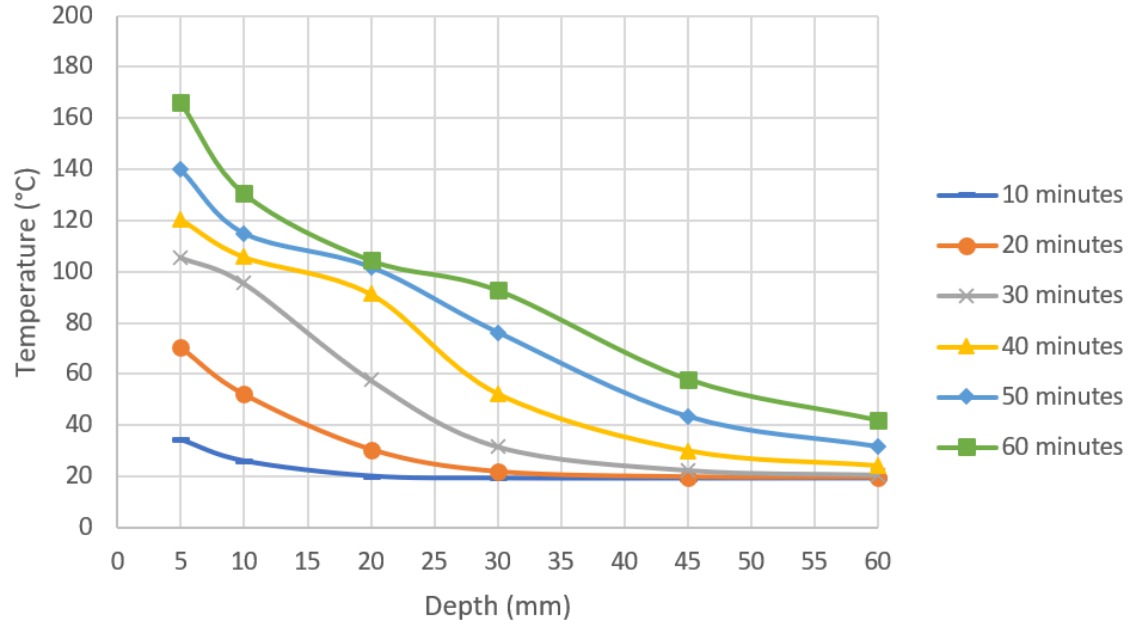


((b)) Protected by steel flange

Figure A.4: Temperature profile from test 2.B (be noted of the different boundary in the y-axis)

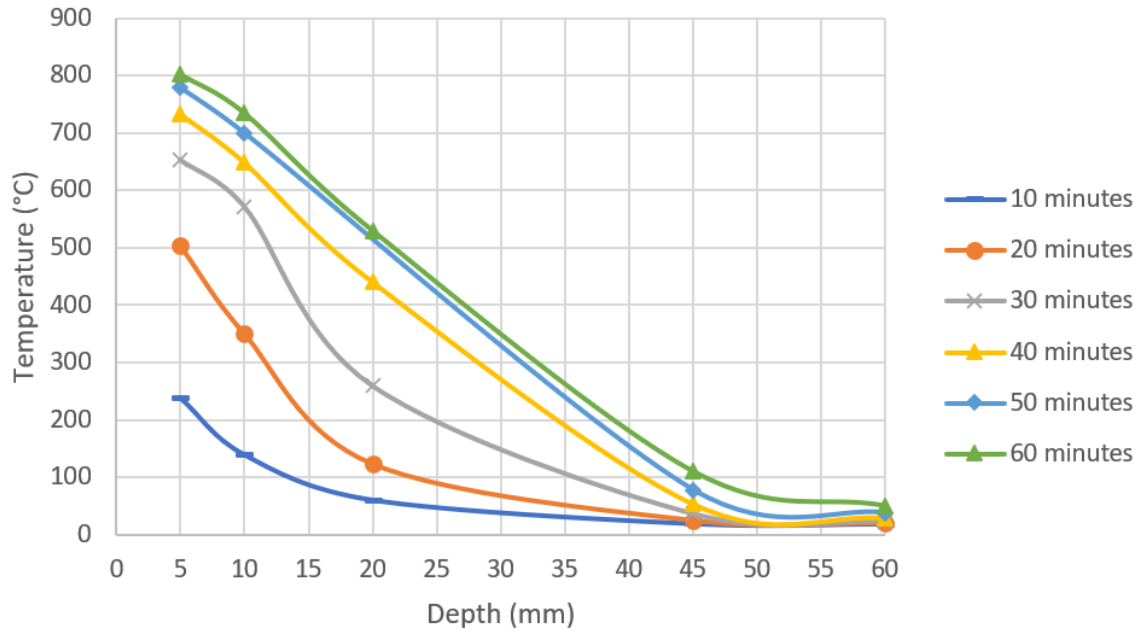


((a)) Direct exposure

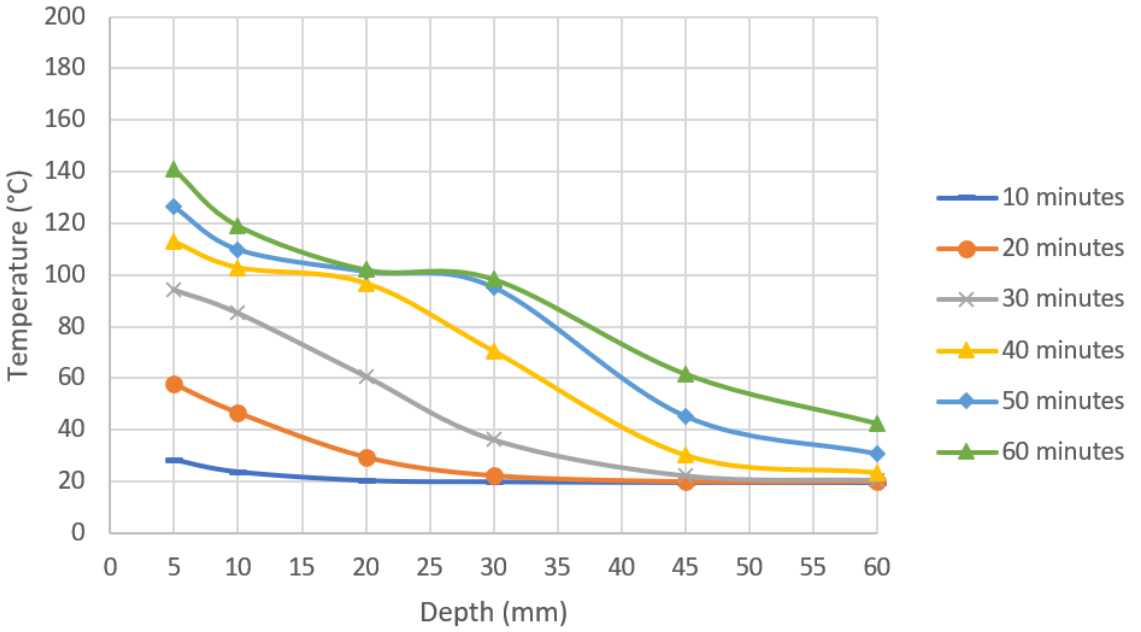


((b)) Protected by steel flange

Figure A.5: Temperature profile from test 3.A (be noted of the different boundary in the y-axis)

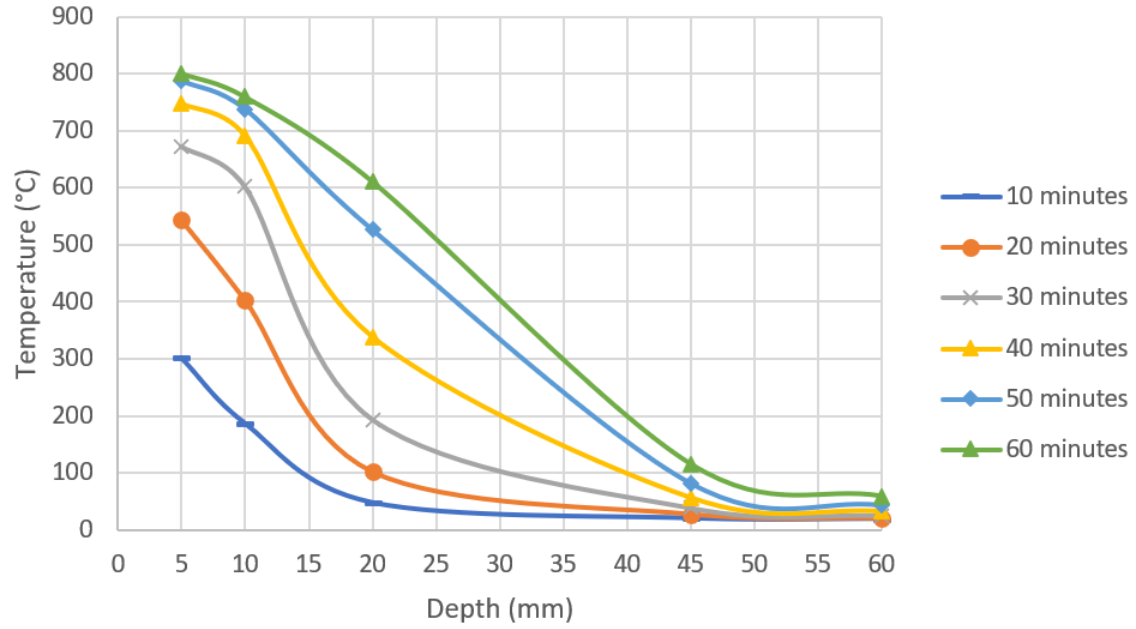


((a)) Direct exposure

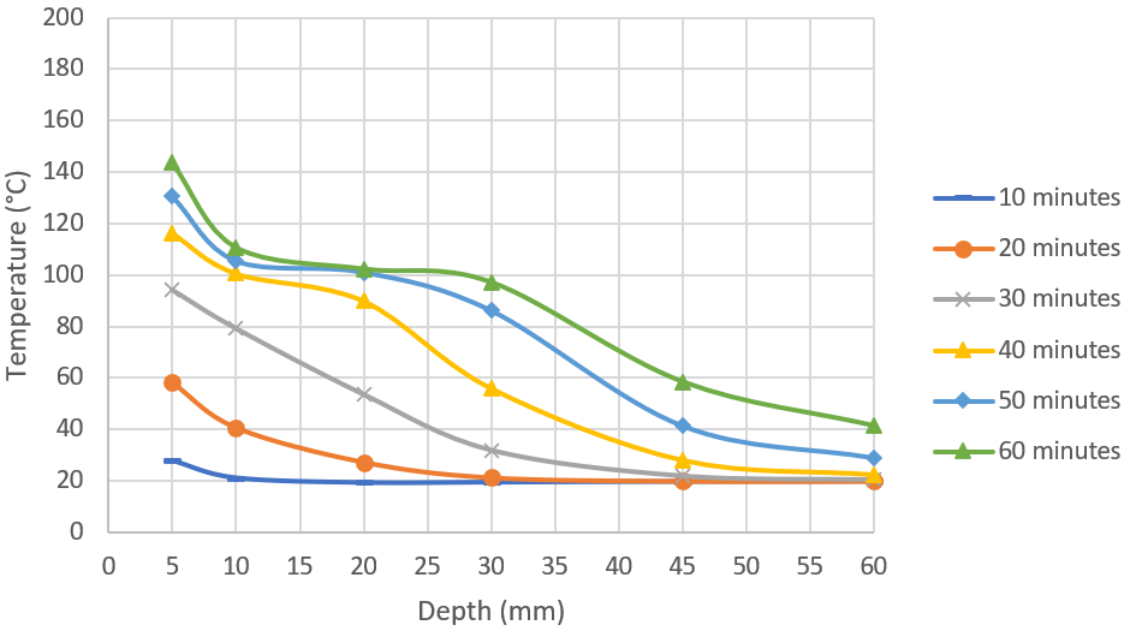


((b)) Protected by steel flange

Figure A.6: Temperature profile from test 3.B (be noted of the different boundary in the y-axis)